REACTIVE OLIGOSACCHARIDES FOR SURFACE DERIVATISATION

Thesis submitted in accordance with the requirements of the University of Liverpool for the degree of Doctor in Philosophy

By
Nina Suhaity Azmi

Acknowledgements

First and foremost, I must thank the Almighty God for the strengths and His blessings in completing this thesis. I would not have been possible to write this doctoral thesis without the help and support of the kind people around me, to only some of whom it is possible to give particular mention here. Above all, I would like to thank my beloved husband and son, Yusri and Nabil for their loves, personal supports and great patience at all times. My parents, brother, sisters and the whole family who always give me their unequivocal support throughout, as always, for which my mere expression of thanks likewise does not suffice.

This thesis would not have been possible without the help, support and patience of my main supervisor, Prof Dave Fernig. Prof Dave Fernig has been my inspiration as I hurdle all the obstacles in the completion this research work. He is always available not only for consultation, but also to solve any difficulties occurring to his students. His vast experience and erudition guided me in faltering steps. No words can adequately express my deep gratitude Prof Dave Fernig for all his guidance and kindness. The good advice, support and friendship for my second supervisor, Dr Ed Yates, has been invaluable on both academic and a personal level, for which I am extremely grateful.

My thanks and appreciation to my internal examiners, Prof Jerry Turnbull and Dr Raphael Levy for their critic's advised in my research. They were very generous in sharing their ideas during my study.

I would like to acknowledge my labmates, Alessandro, Kat, Ruoyan Xu, Dan, Katie, Chris Shaw, Thamir, Yong Li, Owain and others who are working in Lab A, C and D for their friendship.

Special thanks to Dr Noorhan Chelebi, Dr Yassir Ahmed and Dr Rebecca Miller for their generosity in helping me struggled with my labwork. Dr Noorhan, you are the real supermom. Your advice, your sincerity, your experiences makes me really proud of you. To Dr Yassir, thanks a lot for giving me a very good training in making

oligosaccharide libraries. Dr Rebecca Miller, you are the best researcher that I've ever met. It was really great experience working with you. Thank you for the best mass spect data.

Dr Igor Barsukov, Dr Mark Wilkinson and Mr Mark Prescott for their hands on training on various techniques such as ITC, HPLC and mass spect.

The staffs and support staffs of the Institute of Integrative Biology, for their untiring effort in giving supports.

The staffs at the Farfield Group (Dr Juan Wang, Dr Mohd, Dr Marcus, Dr Usha, Dr Paul and everybody in this group) for the hands on training on DPI.

I must acknowledge as well the many friends, who assisted, advised, and supported my lives, research and writing efforts over the years. I need to express my gratitude and deep appreciation to Malaysian friends at The Philharmonic Court (Jaja, Shiela, Has, Nadia Darlina and others), The Liverpool Malaysian Community, whose friendship, hospitality, knowledge and wisdom have supported, enlightened, and entertained me over the many years of our friendship. My thanks must go also to Mr Steve, the porter of Philharmonic Court who is very caring to me during my stay at the Philharmonic Court.

The dean of Faculty of Industrial Science and Technology, FIST, UMP, Prof Mashitah for her strongly support during my study. My colleagues and staff in UMP for their supports and co-operation. Last but not least, I would like to acknowledge the Malaysian government for the SLAB scholarship award.

Abstract

Polysaccharides represent a key class of biological polymers with a diverse array of functions. This is particularly true for the glycosaminoglycan heparan sulfate (HS), which has over 400 different protein partners in the extracellular space and is directly involved in regulating most aspects of cell communication. The analysis of the structure-function relationships of HS remain a major challenge, because of the diversity of structures encountered in HS, the difficulty in their analysis and in establishing the level of specificity required by biological processes of cell communication. In this thesis, heparin, an analog of heparan sulfate (HS), has been used as a proxy for HS to develop new methods of derivatising oligosaccharides that enable future functional analyses by means as diverse as surface optical techniques and single molecule optical microscopy.

To this end a strategy was developed based on the incorporation of a thiol-reactive maleimide moiety at the reducing end of oligosaccharides, which is described in **Chapter 3**. Heparin was treated with nitrous acid to specifically cleave it at $GlcNSO_3$ and unsubstituted GlcN residues to form pair-wise oligosaccharides with 2, 5 anhydromannose derivatives at the reducing end. The latter provided a site for efficient subsequent conjugation of the oligosaccharides. Initial work focussed on direct coupling of oligosaccharides to peptides, but this was not effective. Consequently, oligosaccharides were conjugated to a bifunctional hydrazide-maleimide, MPBH 4-(4-N-maleimidophenyl)butyric acid hydrazide hydrochloride). The maleimide group would then provide an efficient group for subsequent reaction of the oligosaccharides with targets. Anion-exchange chromatography (AEC) and

reverse phase HPLC were performed to identify the reaction products and mass spectrometry provided definitive evidence for the success of this approach.

Chapters 4 and 5 provide exemplars of the applications of the maleimide-derivatized oligosaccharides. In chapter 4 a set of experiments were performed on a dual polarization interferometer. The sugar-maleimide was successfully immobilized onto a thiol surface. This oligosaccharide-derivatised surfaces were then challenged with two classic HS-binding proteins, fibroblast growth factor FGF1 and FGF2. In **chapter 5**, the coupling of the maleimide-oligosaccharides to nanoparticles was attempted. This required the design and testing of a new ligand shell for nanoparticles, because hitherto it had proved a challenge to synthesise nanoparticles with a thiol function exposed to solvent. Dithiothreitol (DTT) was used to probe nanoparticle stability and so to identify the conditions for the synthesis of gold nanoparticles with a ligand shell composed of disulphide-bonded alkane ethylene glycols. These disulphide-bonded alkane ethylene glycol ligands were then used to incorporate a small mole % maleimide groups into the nanoparticle ligand shell. Reaction of the maleimide groups with DTT resulted in the incorporation of a thiol into the nanoparticles. The resulting nanoparticles were then incubated with maleimide-oligosaccharides and evidence was acquired for the first synthesis of nanoparticles with heparin oligosaccharides where the stability of the nanoparticles is independent of their functionalisation by the sugar. The results are discussed in a general conclusion that explores the future potential of the maleimide-oligosaccharide and the maleimide/thiol functionalised nanoparticles as tools to answer major questions in glycobiology.

TABLE OF CONTENTS

LIST OF TABLES

LIST OF FIGURES AND SCHEME

LIST OF ABBREVIATIONS

AEC	anion exchange chromatography
aFGF	acidic fibroblast growth factor
bFGF	basic fibroblast growth factor
BMPH	(N-[ß-maleimidopropionic acid] hydrazide, trifluoroacetic acid salt)
Bnl	branchless
Btl	breathless
CALNNGGC	Cysteine-Alanine-Leucine-Asparagine-Asparagine-Glycine-Glycine-Cysteine
COOH	carboxyl
CS	chondroitin sulfate
C-terminal	carboxyl terminal
DEAE	diethyl-amino-ethyl
Delta H	enthalpy change
Delta S	entropy change
DP	degree of polymerization
DPI	dual polarization interferometry
DTT	dithiothreitol
EXT	exostosin
FGF	fibroblast growth factor
FGFR	fibroblast growth factor receptor
GAG	glycosaminoglycan
GlcA	β-D-glucuronic acid
GlcA2S	2-O-sulfo-beta-D-glucuronate
GlcN	glucosamine
GlcN6S	2-deoxy-2-sulfamido-α-D-glucopyranosyl-6-O-sulfate
GlcNAc	2-deoxy-2-acetamido-α-D-glucopyranosyl
GlcNS	2-deoxy-2-sulfamido-α-D-glucopyranosyl
HA	hyaluronic acid
HCl	hydrocloric acid
Hep	heparin
HPLC	high performance liquid chromatography
HS	heparan sulfate
IdoA	α-L-iduronic acid
IdoA2S	2-O-sulfo-beta- α-L-iduronate
Ig	immunoglobulin
ITC	isothermal titration calorimetry
Kd	dissociation constant
KS	keratan sulfate
mAU	milli absorbance unit
MPBH	4-(4-N-maleimidophenyl)butyric acid hydrazide hydrochloride
NA	N-acetylated
NDST	N-deacetylase/N-sulfotransferase
NHS	N-hydroxysuccinamide
NS	N-sulfated

N-terminal	amino terminal
OH	hydroxyl
PBS	phosphate buffer saline
PEG	polyethylene glycol
RI	refractive index
SAM	self assembling monolayer
SAX	strong anion exchange chromatography
Std Dev	standard deviation
TE	transverse electric
TH	thickness
TM	transverse magnetic
V	Volts
VEGFR	vascular endothelial growth factor
Xyl	xylose

CHAPTER 1

Introduction

1. Introduction

1.1 Biological significance of glycosaminoglycans

Cell-cell communication is a key feature of multicellular organisms. It underlies the processes whereby a fertilised egg develops into an organism, in which cells specialise and only a minority, the germ cells, goes on to produce the next generation. A fundamental biological consequence of such pervasive cell-cell communication is that natural selection operates on the entire organism, not on the individual cell. Cell-cell communication is also the foundation of the physiological adaptations of multicellular organisms to their environment. The metazoan molecular mechanisms of cell-cell communication have presumably evolved from those of unicellular organisms, used, for example, to form biofilms, identify food sources and to reproduce sexually [1].

By definition, cell-cell communication is mediated by extracellular molecules. Three of the molecular innovations that are hallmarks of the integrated cell-cell communication of metazoans are phosphorylation of tyrosines, extracellular matrix proteins and the glycosaminoglycans heparan sulfate (HS), chondroitin sulfate (CS), keratan sulfate (KS) and hyaluronic acid (HA). Indeed, sequencing of the genome of the choanoflagellate *Monosiga brevicollis* [2], a model for the last unicellular eukaryote that evolved prior to the appearance of metazoans, demonstrates the presence of tyrosine kinases and phosphatases and of machinery for the biosynthesis of HS, albeit less complex than that found in true multicellular organisms [3].

HS and the structurally related heparin, a specialised product of the mast cell, play a crucial role in a large number of biological functions, ranging from the regulation of *in vivo* coagulation and capillary permeability, to cellular proliferation and

differentiation. These functions are mediated by the HS interactome, which comprises over 435 proteins whose functions are regulated by their interactions with HS. In spite of the numerous known biological roles of glycosaminoglycans such as HS and the recent cataloguing of its interactome [3-5] it has been challenging to decode the structure-function relationships of these interactions. The biosynthesis of glycosaminoglycans is non-template driven and a number of steps are catalysed by multiple enzyme isoforms, which are distributed in a tissue-specific manner. The complex biosynthesis and lack of proofreading machinery leads to structural heterogeneity and the expression of a large diversity of GAG structures on cells and in their surrounding extracellular matrix. The heterogeneity and diversity of GAGs have required the development of analytical techniques to define their chemical structures and the specificity of their interactions with proteins. An important step has been the development of methods to functionalise surfaces with glycosaminoglycans such as heparin and HS, and specific active fragments of these sugars. These functional surfaces have lent themselves to biophysical measurements of the interactions of the sugars with their functional protein partners. As the functions of heparin and HS have extended across many regulatory phenomena in biology, the ability to functionalise surfaces with sugars has opened-up the possibility of designing sugar surfaces to perform particular tasks.

This chapter describes first the structure of heparin and HS. It then outlines the main routes for functionalizing surfaces with intact polysaccharides and derived oligosaccharides. Finally, the aims of this thesis are described.

1.2 Heparin and heparan sulfate

Heparin, a highly sulfated polysaccharide is widely used as an anticoagulant drug. It was discovered in 1916 by Jay McLean from Johns Hopkins University [6]. A uronic acid was identified in 1928, as one of the sugars in heparin, followed by the identification of glucosamine in 1935-1936 as the second sugar component of heparin [6]. Heparan sulfate (HS) was discovered 60 years ago. Analysis of these two polysaccharides has established some of their features:

- HS and heparin are sulfated glycosaminoglycans (GAG), which are negatively charged linear polysaccharides [7].
- Whilst heparin and HS were found to contain the same sugar units, namely glucosamine and a uronic acid with various appended sulfate groups, heparin is much more sulfated, containing an average of 2.4 sulfates/disaccharide unit [8].
- Heparin and HS share a common biosynthetic pathway that starts with a monotonous heparan precursor.
- Heparin is largely restricted to mast cells. HS on the other hand has a very widespread tissue distribution.

1.2.1 Structure of heparin and HS

Heparin and HS are linear anionic sulfated polysaccharides with repeating disaccharide units of alternating uronic acid and hexosamine residues [5]. They are covalently attached to protein cores to form proteoglycans. The uronic acid can be β-D-glucuronic acid (GlcA) or its C5 epimer, α-L-iduronic acid (IdoA). Both heparin

and HS have variable substitution with *O*-sulfate, N-sulfate and N-acetyl groups [5]. The uronic acid can be found either 2-*O*-sulfated (IdoA2S, or more rarely GlcA2S) or non-sulfated (Fig.1.1). The glucosamine can be N-sulfated (GlcNS), N-acetylated (GlcNAc) or possess a free amine, as well as 6-*O*-sulfated (GlcN6S) and 3-*O* sulfated [5,9](Fig.1.1).

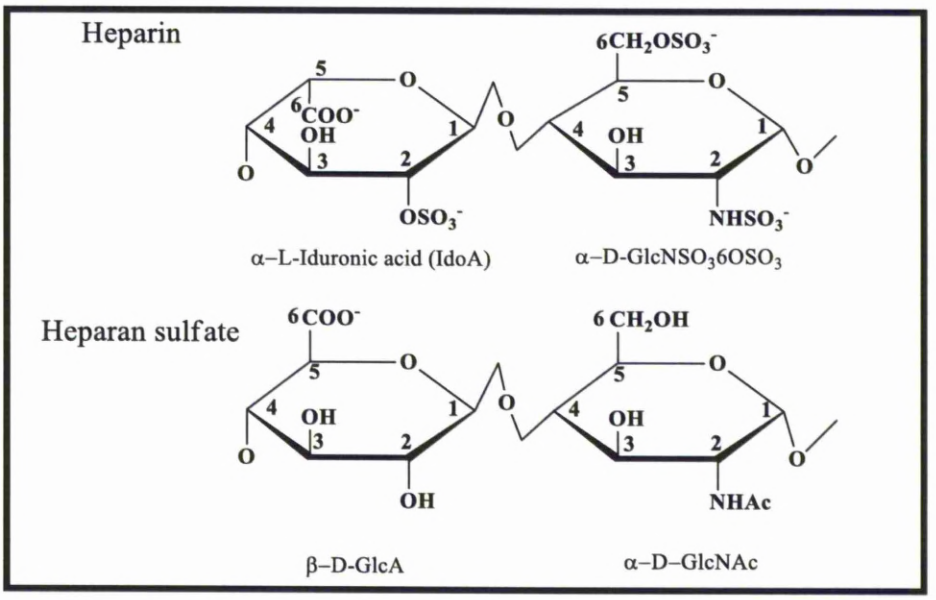

Figure 1.1: Structure of the constituent disaccharides of heparin and HS.

Top, the common trisulfated disaccharide found in heparin, in which the glucosamine is N-sulfated and the uronic acid epimerised to IdoA. Bottom, the disaccharide that is the initial product of biosynthesis in both heparin and HS, though extensive tracts of this disaccahride are only observed in the NA domains of HS. The disaccharide is not sulfated, is N-acetylated and the uronic acid is D-GlcA.

HS has the same component disaccharides as heparin, but in different and much more variable proportions. Importantly, in HS, the sulfated sugars are clustered along the chain to give a domain structure [10,11]. Heparin is richer in N-sulfated glucosamine and iduronate residues and, though it resembles the highly sulfated S-domains of HS, heparin is more sulfated. However, because of its use as an anticoagulant, heparin is easy to obtain and it binds strongly to virtually all of the proteins whose physiological ligand is cell surface HS. Thus, heparin is widely used as a proxy for HS in biochemical investigations because of its relative abundance and it exhibits high activity in processes in which HS is active.

1.2.2 Biosynthesis of HS and heparin

Investigations into the biosynthesis of heparin and HS have provided not only knowledge about this process, but also a deeper understanding of the structure of these polysaccharides and insights into the relationship between heparin and HS. Most animal cells can synthesize HS and this biosynthesis of HS occurs in the Golgi network. Biosynthesis of HS can be broken down into three steps, involving chain initiation, polymerization and modification. The first event is the synthesis of a linkage tetrasaccharide with a xylose (Xyl) linked to a serine residue of the protein, to which two galactose residues and a glucuronic acid are attached (GlcAβ1–3Galβ1–3Galβ1–4Xylβ1-)[12]. This process is known as initiation and starts with xylosyltransferase catalyzing transfer of xylose from UDP-xylose to serine residues in core protein substrates [13] and is common not just to heparin and HS, but also to CS biosynthesis. Xylosylation is an incomplete process in some proteoglycans, such that not all potential glycosylation sites are always used. This may be due to low

levels of UDP-xylose, low activity of xylosyltransferase, or, as shown in the case of thrombomodulin, the amino acid sequences surrounding the GAG attachment site [13] . The transfer of UDP-GlcNAc to the linker then directs biosynthesis to heparin/HS rather than CS [13].

The polymerization reactions that produce heparin and HS chains are carried out by the exostosin proteins, EXT1 and EXT2, which sequentially add N-acetyl glucuronic acid and glucosamine to the growing polymer, starting at the GlcNAc residue of the linker [11,14-16]. Generally, final chain length varies between 100 and 200 residues. *N*-deacetylation and *N*-sulfation of glucosamine units initiates the modification of the chain, and is carried out by the bifunctional enzyme *N*-deacetylase/*N*-sulfotransferase (NDST) of which there are four HS isoforms. The NDST enzyme removes the acetyl group from the GlcNAc residue and then a sulfate group is transferred to this position. The third state of the glucosamine residue, the unsubsituted amine is rare, but now well documented in HS. It seems likely that this is formed by the NDST failing to carry out its second reaction, sulfation. The NDSTs do not work on every GlcNAc in the polymer, but instead, having acted on one GlcNAc, then act on neighbouring residues before "skipping" a tract of residues [11,14] generating stretches of *N*-sulfated GlcN residues in the HS polymer. These act as "markers" for the other chain modification enzymes, all of which act predominantly at or near N-sulfated glucosamine. These processes result in chains with sulfated domains (NS domains) separated by acetylated regions (NA domains) (Fig. 1.2). The regions between the NS and NA domains are short mixed transition domains with alternating GlcNS and GlcNAc residues, termed NS/NA, SAS or transition domains [11,17,18]. In contrast, in heparin biosynthesis, NDST activity is more regular, so most, but not

all glucosamines are N-sulfated, and there is no obvious domain structure, with the entire sugar resembling the most sulfated NS domains of HS.

After N-sulfation, GlcA may be epimerized at C5 into IdoA [14,15]. An important consequence of this reaction is that IdoA, unlike GlcA or the adjacent glucosamine residue, exists in equilibrium between different conformations. Epimerisation thus gives the sugar chain new structural properties. The IdoA may be 2-O sulfated at the C2 position and this may also occur to a lesser extent on GlcA [14,15]. The 2-O sulfated hexuronic acids are almost always found in contiguous N-sulfated domains of the polysaccharide [14]. The 2-O sulfotransferase has been shown to form molecular complexes with the C5-epimerase, which may explain in part the greater 2-O sulfation of iduronate residues [14,15]. Three HS glucosamine 6-O-sulfotransferases have been identified, which sulfate at C6 of glucosamine residues adjacent to N-sulfated glucosamine [14]. Sulfation at C3 of glucosamine by one of the five 3-O sulfotransferases, though rare, is critical for forming structures with high anticoagulant activity [14,16] and more recently has been found important for some other activities too such as the binding of cyclophilin B [19].

Recently, a distinct biosynthetic pathway has been proposed, based on a basic disaccharide repeating structure, in which the most commonly occurring derivatives all lie on the same branch [20]. Furthermore, all of the substrates for the last enzyme step (3-O-sulfotransferase) also lie on the same major branch. The key enzyme step in this proposed scheme is the epimerase, which acts predominantly on the disaccharide GlcA-GlcNS but, has been observed to act with lower efficiency on the disaccharide GlcA-GlcNAc to yield respectively, IdoA-GlcNS and IdoA-GlcNAc [21]. This provides the junction between the two branches of the scheme.

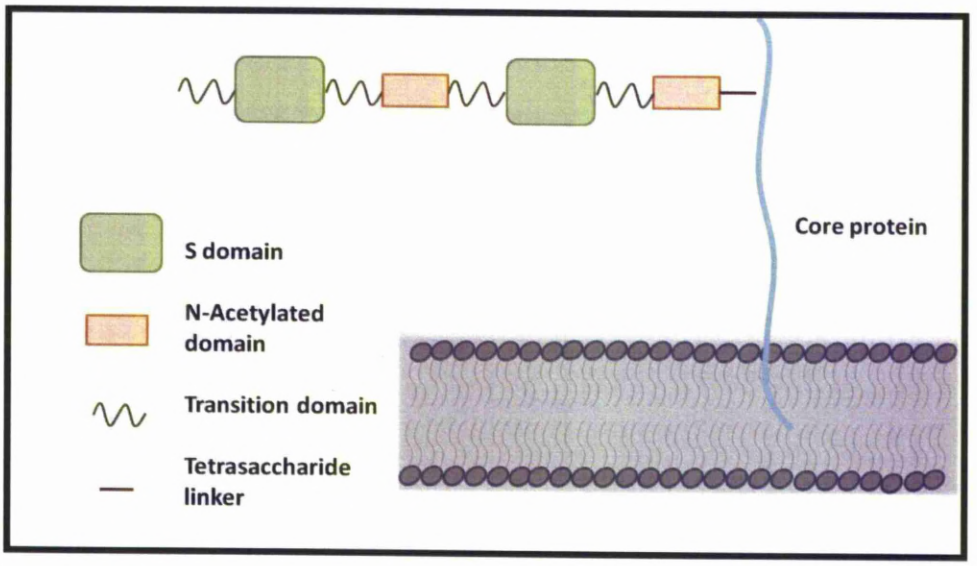

Figure 1.2: Heparan sulfate proteoglycan (HSPG).

Heparan sulfate (HS) chains are attached at specific serine residues on the core proteins through a tetrasaccharide linker to form HS proteoglycan (HSPG). The HS chains contain S-domains of various lengths and sulfation pattern, alternating with N-acetylated (NA) domains. The transition domains connect the two domains. Heparin differs from HS in being composed of higher levels of sulfation. Heparin lacks a domain structure and contains high levels of iduronate rather than glucoronate.

1.2.3 Conformation of sugars and HS chains

- *Iduronate*

Two of the three forms of uronic acid residues, IdoA2S and IdoA, possess unique conformational properties. Internal iduronates adopt an equilibrium between two principal conformers: the $^{1}C_{4}$ chair and the $^{2}S_{0}$ skew-boat[9,22] Fig. 1.3. These two forms may interconvert with little disturbance to the glycosidic linkages to adjoining residues in the polysaccharide chain. The balance of the chair to skew-boat equilibrium in internal iduronate residues depends both upon its own substitution with 2-O- sulfate and on substitution of adjacent glucosamine residues [22,23] suggesting that $^{1}C_{4}$ could most easily interchange with $^{0}S_{2}$ and $^{3}S_{1}$ forms while $^{4}C_{1}$ could interchange with $^{2}S_{0}$ and $^{1}S_{3}$ forms. In addition, the interconversion between the $^{2}S_{0}$ and other boat and skew-boat forms seemed to be less hindered than chair to skew-boat changes.

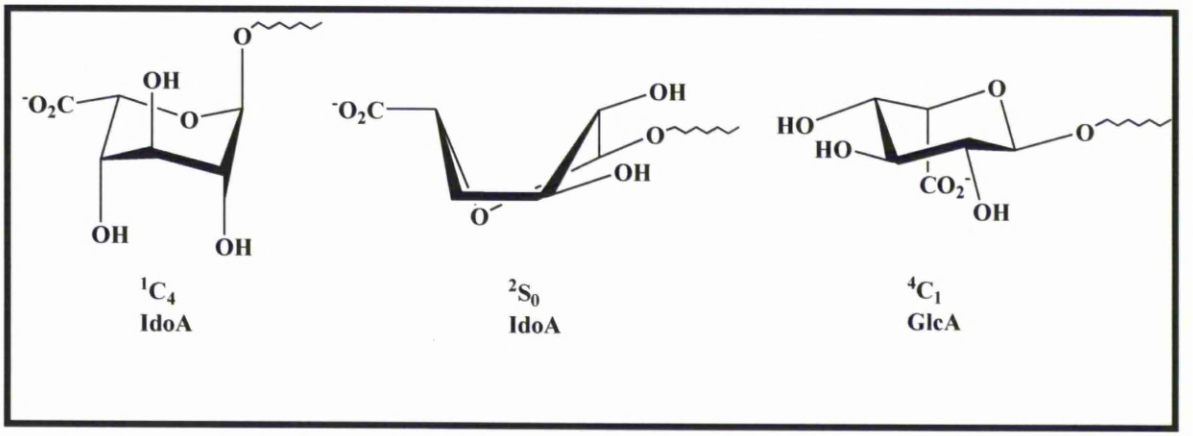

Figure 1.3: The conformations of uronic acid residues.

The internal iduronates (IdoA) can adopt an equilibrium between two conformers: The $^{1}C_4$ chair and the $^{2}S_0$ skew-boat. Unlike its C5 epimer iduronic acid, which may occur in a number of conformations, glucuronic acid (GlcA) occurs in predominantly the $^{4}C_1$ conformation.

1.2.4 Flexibility of glycosidic linkages; GlcNAc vs GlcNS

While lacking the internal flexibility generated by IdoA, the GlcA-GlcNAc sequences still maintain an ability to rotate about their glycosidic linkages. The degree of rotation occurring at GlcA linkages are greater than observed with IdoA, when the conformation of GlcA is in the $^{4}C_1$ chair form [22].

Analysis of linkage geometry as a function of substitution patterns in homogeneously modified heparin derivatives, using NMR chemical shift data as a reporter of geometric change, indicated that the geometry of glycosidic linkages were highly

redundant [20]. Thus, many sequences could potentially adopt similar overall conformations and this could be a contributory factor to the redundancy that is observed in HS and heparin interactions with proteins.

1.3 Interactions of proteins with HS

1.3.1 Protein-HS interactions

Over 435 proteins have been shown to bind to heparin/HS [3,5]. The fibroblast growth factors (FGFs) are the first growth factors to be shown to require the sugar as a co-receptor [24,25]. Many biochemical studies have investigated the structural requirements for binding of FGFs to heparin/HS. For example, FGF2 binding requires N-sulfated glucosamine and *2-O* sulfated iduronic acid [25], with tetrasaccharides being the minimal binding unit [26]. However, the formation of a complex with HS and FGFR also requires *6-O* sulfated glucosamine [27]. Tetrasaccharides cleaved from heparin will contain N-, 2-O and 6-O sulfate groups and are sufficient to enable FGF2 to engage the FGFR and activate intracellular signaling necessary for the stimulation of cell division, though octasaccharides are more efficient [28].

Another example of heparin and HS regulating growth factor activity is VEGF165. In this system, VEGF receptors (VEGFR) and neuropilin, an accessory receptor are also heparin-binding proteins. VEGF165 binding to VEGFR1 is dependent on cellular HSPGs and exogenous heparin/HS cannot fully replace cell-surface HS. VEGF165 can bind VEGFR2 in the absence of HS, but this interaction is enhanced by cellular or exogenous heparin/HS. The requirement for heparin/ HS is likely to be due to the formation of VEGF165:VEGF:HS ternary complexes. Heparin/HS also

facilitates VEGF165 interactions with neuropilin, which further promotes activation of VEGFR2 [29,30] .

In vivo studies indicate important roles for sulfation of HS in developmental processes. For example, *Drosophila* mutants in the gene *sulfateless*, show abnormalities in Wingless-mediated dorsal/ventral patterning [31]. Thus, the dependence on heparin/HS of the activity of these heparin-binding proteins is relevant *in vivo*. As well as the activity, HS has been suggested to control the transport of heparin-binding effectors. Until recently there has been no mechanistic understanding of how this may occur [32]. However, work using FGF2 stoichiometrically labelled with a gold nanoparticle probe demonstrates that the movement of FGF2 in the pericellular matrix is entirely controlled by its binding and dissociation from HS [33], again highlighting the importance of protein-HS interactions to the regulating cell activity *in vivo*.

The overall compatibility of shape and charge distribution can, at least in some cases, be simulated by several sequences from heparin and, notably, also by a number of sulfated polysaccharides with different compositions (but, not all), that are unrelated to HS and heparin. In the case of FGF-1, stabilisation of the protein in a complex with the sulfated polysaccharide followed closely the ability of this polysaccharide to support signalling through FGF-1 and FGFR1c. In contrast, with FGF-2, some of the sulfated polysaccharides could also support signalling but, in this case, it was necessary to induce a similar secondary structural change to that induced by heparin/HS [34]. This supports the notion that a major property governing HS-protein recognition is charge and shape. Furthermore, several distinct sequences in

the carbohydrate can provide this.

1.3.2 *The example of FGFs*

The human genome encodes 22 FGF proteins, of which 18 interact with cellular receptors. The amino acid sequence of FGFs comprises a core region, which binds heparin/HS and FGFR, flanked by N- and C- terminal extensions and sometimes carries an insert in the middle of the core sequence [35]. The core structure has been the subject of many structural studies using X-ray crystallography and NMR. The flanking regions are not ordered in crystals and have only been studied by NMR in FGF2. Twelve antiparallel β strands of FGF1 and FGF2 have been identified from the structural studies in the conserved core region of the protein [36]. The crystal structures of 18 kDa FGF2 (bFGF) and the closely-related FGF1 (aFGF) were the first to be determined and indicated a high degree of structural homology with the cytokine interleukin 1β [35]. The core of the FGFs form a beta trefoil structure comprising three sets of three beta strands around a pseudo axis of symmetry. In vertebrates, FGFs range in molecular weight from 17 to 34 kDa, while *Drosophila* FGF is considerably larger, 84 kDa [36].

1.3.3 *The functions of FGFs*

FGF signal transduction is regulated by HS. For example, in the absence of the HS co-receptor, FGFR2 only stimulates a transient activation of signaling through the mitogen-activated protein kinases $p42/44^{MAPK}$. This is not sufficient to stimulate cell division. In contrast, in the presence of the HS co-receptor, FGF2 stimulates sustained activation of $p42/44^{MAPK}$, which results in cell division [26]. HS also

regulates other aspects of FGF2 activity. These include its transport between and on cells, the formation of gradients, including the concentration of the growth factor on HSPGs of the cell surface [33]. Examples of these regulatory activities include the observation that FGF associated with specific HS differentially regulates proliferation versus migratory activity in breast cancer cells [31], while binding of FGF2 and FGF4 is differentially regulated by tissue-specific HS [31]. FGF signaling is important for epithelial morphogenesis in developing branching structures. The branching pattern of the tracheal tubules of *Drosophila* is established by expression of the FGF *branchless (Bnl)* in clustered cells outside the epithelium at prospective sites of budding. Bnl activates an FGFR, breathless (Btl), expressed in tracheal epithelial cells, which then migrates and elongates toward the *Bnl* expressing cells to form a bud [31].

1.3.4 FGF receptors

The tyrosine kinase receptors (FGFRs) for FGFs are encoded by four different genes. These are *fgfr-1* (*flg* or *fms-like* gene), *fgfr-2 (bek-* bacterially expressed kinase*), fgfr-3* and *fgfr-4*. They are most closely related to the platelet-derived growth factor (PDGF) family of receptor tyrosine kinases. They have three immunoglobulin-like loops in the extracellular domain compared to five in the PDGF family. FGFRs have a unique stretch of acidic residues between immunoglobulin-like loops one and two, termed the acidic box. The intracellular region of the FGFRs have a relatively long juxtamembrane domain and a tyrosine kinase domain that is split by a kinase insert [35].

1.3.5 *The models for the FGF-FGFR-heparin complex*

FGFs are among the best studied heparin-binding proteins and HSPGs regulate FGF signaling by direct molecular association with FGF and the FGFR. The identification of two crystal structures of FGF-FGFR-heparin complexes has provided new structural information regarding heparin binding to FGF and FGFR. Although these structures have similar contacts between the FGF ligand and FGFR, and between the sugar and proteins, they show distinct spatial relationships between the molecules and so lead to different models for receptor dimerization, which is thought to be the step that initiates the activation of the intracellular kinase. The symmetric model, with a stoichiometry of 2:2:2 (FGF:heparin oligosaccharide:FGFR), is far more dependent on protein-protein interactions, particularly at the level of the backbone of the FGFR [37]. It proposes two bound oligosaccharides, each occupying one half of the cleft with the non-reducing ends facing each other. As a result, it is also called the "two end model", in which the sugar stabilizes the structure. In contrast in the asymmetric model (stoichiometry 2:1:2, FGF:heparin oligosaccharide:FGFR) receptor dimerisation is driven by a single sugar chain that bridges the receptor complex. Even though the two models differ in their proposed mechanism of FGFR dimerization, it is possible to identify one FGF, one heparin molecule and the second immunoglobulin (Ig) domain, D2 of one FGFR chain, constituting what can be termed the 1:1:1 FGF-FGFR-heparin complex, in both of the proposed models.

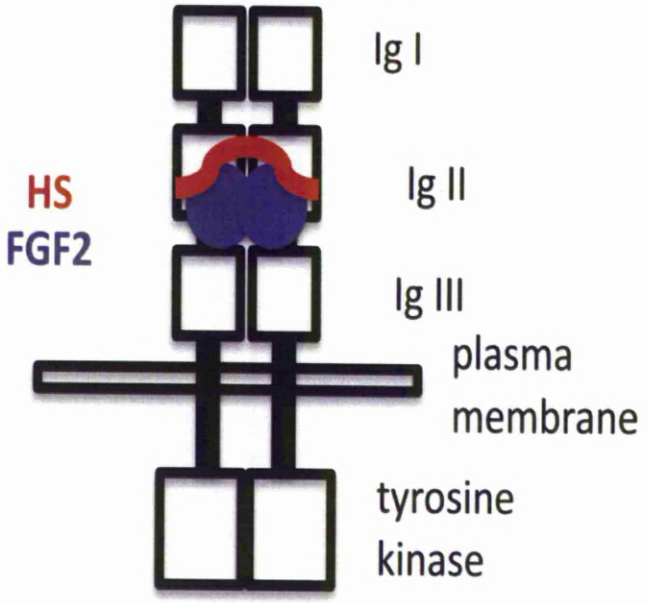

Figure 1.4: The symmetric model with a stoichiometry of 2:2:2 of FGF, FGFR heparin-derived DP6.

This model, derived from a structure solved from co-crystals of FGF-2, FGFR2 and a DP6 [37] comprises the two ligand-binding domains of FGFR2 dimerised by two FGF2 ligands and two DP6 derived from heparin. The DP6 are antiparallel, that is their non-reducing ends point at each other. Dimerisation is due to a combination of ligand-receptor contacts, whereby each ligand interacts with residues on both receptors and receptor-receptor contacts, where residues in the extracellular domain make contact. Ig I, Ig, II and Ig III, the three immunoglobin domains of the receptor; the co-crystal structure only has Ig II and Ig III, which contain the FGF and HS binding sites.

1.4 Heparin and HS-functionalised surfaces

1.4.1 General considerations

The functionalisation of surfaces with heparin and HS has become a research field in itself, driven by the scientific challenges posed by these sugars and by their biomedical potential. The use of functionalized surfaces for analytical purposes was the initial driver for the development of novel methods for the immobilisation of the sugars. The focus of much of the analytical work has been the determination of binding parameters of sugar-protein interactions. The analysis of such binding data has, however, highlighted a number of problems. Some, such as the orientation of the sugar with respect to the underlying substrate, sugar-substrate interactions, and so on, may be solved by further developments. The synthesis of a surface functionalised with heparin-derived oligosaccharides and back filled with polyethylene glycol and the analysis of the surface structure by dual polarization interferometry [38] illustrates the potential of cycles of surface design and analysis, in terms of producing robust surfaces with a low susceptibility for binding artefacts. However, there are other issues, which are inherent to the sugar. One is the so-called "parking problem" [39]. The polysaccharide, even as relatively short oligomers, often possesses multiple, overlapping binding sites for a single protein. Binding of the protein within this region would alter the kinetics of binding of a second protein to adjacent and partially overlapping sequences. A related and perhaps more fundamental issue is the meaning of such binding data. Protein binding specificity is graded, in that although a protein may have a preference for a particular disposition of sulfate groups and sugars, it will still bind other structures [34]. Even in the classic case of antithrombin III, non-canonical sequences in heparin and related

sugars can have some anticoagulant activity reference. What, therefore, is the future of the biofunctionalisation of surfaces for the analysis of protein-sugar interactions?

At one level, the future is simple. There is clearly a need for measurements of these interactions, because of the size of the heparin interactome and the low level of coverage by interaction data relating to specificity at any level [3,5]. Thus, a commercial product that consists of a 96 well plate with glycosaminoglycans, including heparins, simply adsorbed onto a carefully functionalized surface of amine groups deposited with a cold plasma is successful [40,41]. The problems associated with adsorption of the sugar are overcome by using the surface in competition assays with soluble sugars. Microarrays have yet to be commercialized, but recent progress in the chemical synthesis of oligosaccharides of heparin/HS suggests that a microarray with addressable sugar structures is not far off [40].

At another level, the future lies elsewhere, simply because the biology of heparin and HS mean that the above *in vitro* methods, which rely on pure samples and that measure the average properties of an ensemble of molecules, are wide of the mark. Many heparin-binding proteins exert their activity by engaging cellular HS and other proteins. This is exemplified by FGFs requiring HS to form complexes with their tyrosine kinase receptors capable of inducing the intracellular signals appropriate for the stimulation of cell division [5,7]. The interaction of individual proteins with HS reveals different preferences in sugar structure compared to the requirements for the formation of, for example, an active FGF ligand-receptor complex e.g., [42]. Some data indicate that highly specific and rare sequences of sugars may be required for the formation of such active complexes [43,44]. According to this view, most heparin binding proteins can interact with a broad set of structures within the

polysaccharide, but with relatively low specificity. An analogy would be the interaction of transcription factors with the sugar phosphate backbone of DNA, which is specific in the chemical, but not the biological sense. Such interactions are functionally important, since they allow the protein to "find" the highly specific binding site constituted by exocyclic groups exposed in the grooves of DNA required for its engagement of active protein partner [45]. However, they can obscure the search for binding specificity.

Thus, the enormous diversity of HS structures expressed at the cell surface and in the extracellular matrix means that ensemble measurements cannot resolve the question of specificity of protein interactions. Moreover, *in vitro,* the sugar is pure and devoid of any other protein partners. In contrast, *in vivo,* HS chains will be engaged to the substantial heparin interactome of the cell [3,5], leaving only some binding sites free. There is clear *in vivo* evidence that this is the case [46,47]. Thus, an important direction for analytical methods will be to move from *in vitro* to *in vivo* and from ensemble measurements to single molecule measurements. This transition offers substantial opportunities for surface functionalisation. Robust single molecule measurements in living animal cells rely on cutting edge probes and microscopies. Examples include fluorescence microscopy of protein-functionalised quantum dots [48] and photothermal microscopy of functionalized noble metal nanoparticles [49] . In both instances, the choice of probe is dictated by its high optical stability and would require precise functionalisation of the nano-object (quantum dot or noble metal nanoparticle) with sugar, such that the stoichiometry of probe:sugar and the orientation of the sugar relative to the probe surface are known and predictable. These will not be trivial tasks, but the rewards will be substantial. In addition to

analytical measurements, such highly sensitive probes may find applications in diagnostics and point-of-care measurements within the context of personalized medicine.

Surfaces functionalised with heparin are widely used in the clinic. Given the importance of HS and heparin-binding proteins in the regulation of cell-cell communication, which includes cell adhesion, it is surprising that the activities of sugar functionalised surfaces have not been widely explored in these contexts. Surface functionalisation chemistry is now relatively mature and libraries of natural, semi-synthetic and synthetic (though only short oligosaccharides in the latter case) are readily available. Thus, there is a clear opportunity to screen and identify sugar functionalised surfaces that possess a defined bioactivity. Obvious areas of high scientific and commercial interest would be biofouling (glycosaminoglycans are found on the non-fouling surface of many marine organisms) and the culture of stem cells and their differentiation into specific tissues.

1.4.2 Preparation of oligosaccharides and their separation.

There are two principal methods to prepare oligosaccharides from HS and heparin. The first involves the use of enzymes specific to heparin and heparan sulfate, the heparitinases, usually extracted from *Flavobacterium heparinium* or produced recombinantly, termed heparitinase I, II and III (or, alternatively, as heparinase III, II and I respectively). Each of these has distinct preferences in terms of their substrates, although the degree of specificity shown in each case, is debated. These enzymes are lyases, requiring the presence of magnesium or calcium ions to function, and act by cleaving the bond between the glycosidic linkage oxygen and C-4 of the uronic acid,

yielding an unsaturated bond between C-4 and C-5 of the uronate residue, irrespective of whether the uronate was glucuronate or iduronate [39]. The identity of this residue is therefore lost with these lyases. An advantage, however, is gained by the introduction of the double bond, which serves as a convenient chromophore, absorbing at 232 nm. The double bond has also received attention as a potential site for attachment or further derivatisation [50]. Cleavage with lyases liberates fresh reducing-end glucosamine derivatives, which can then be labelled, or serve as sites of attachment, although their identity can vary (glucosamine or N-acetylated glucosamine with a variety of additional substitutions, including N-sulfation, 6-O-sulfation and 3-O-sulfation) and also their reactivity towards nucleophiles attacking the reducing end aldehyde group [51]. The absorbance of the double bond provides one useful way of following the progress of degradation with these enzymes, for example, in the generation of medium-sized oligosaccharide fragments [52] and this can be easily terminated by heating the enzymes (100 C, 5 mins). The dimensions of the products of degradation can be followed easily by electrophoresis, with staining using Alcian Blue/Azure A revealing the oligosaccharide products.

The second method relies on the application of nitrous acid degradation which, depending on the exact conditions employed, cleaves the heparin/HS chain at glucosamine (free-amine) and/or glucosamine N-sulfate, producing an intact uronate residue at the new non-reducing end and generating an anhydromannose (formerly glucosamine) residue at the new reducing end [39]. The advantage of this method is its speed and convenience, coupled with the relatively high reactivity afforded by the presence of an aldehyde, which is not in the equilibrium involving unreactive closed ring forms of a typical reducing sugar, but is intact in anhydromannose [39]. This

means that labelling or attachment can be achieved with higher yields and more consistently than with the products of lyase enzymes but, at the cost of having no strong chromophore by which to follow the progress of degradation. The easiest way to follow this type of degradation is usually by gel chromatography although, in principle, a number of other separation techniques such as HPLC could be used.

The use of either technique to degrade heparin or heparan sulfate leads to a mixture of sizes and structures. The next challenge is to begin to separate these and this is usually done with either gel permeation chromatogrphy (GPC), or high performance strong anion exchange chromatograpy (HPAEC). The former provides fractionation through pores in the matrix of gels on the basis of the hydrodynamic volume of the products, which equates approximately with their length, but not exactly, because sulfate groups appended to the sugars are relatively bulky [39]. There is therefore, usually some mixing of sizes in GPC fractions. The latter, relies on the interaction of the anionic sugars with a positively charged surface on an HPLC support and, following attachment, samples can be eluted using a salt gradient (usually sodium chloride). Although this is the method that provides the highest resolution among commonly used techniques, allowing all disaccharides to be separated, with longer structures, overlap occurs for other lengths of oligosaccharides. These two techniques are often employed consecutively. The presence of the double bond generated by the lyase enzymes is a distinct advantage, allowing convenient monitoring and detection during chromatography. There is also a third technique, reverse-phase HPLC, which can also be employed. Although of limited resolution for separating complex mixtures, it can prove useful additional resolution, especially following further conjugation or derivatisation, and can be readily abutted to mass

spectrometer, allowing in-line monitoring of molecular mass.

1.4.3 Strategies for functionalising surfaces with HS, heparin and derived oligosaccharides

The simplest surface immobilisation approach is based on the physical adsorption of the sugars onto a surface. It is used extensively to prepare heparinised surfaces for clinical applications. For analytical applications, a variety of substrata have been used to absorb dextrans as model sugars or a variety of non-glycosaminoglycan sugars on polystyrene, nitrocellulose, polyvinylidene, glass slides coated with black polystyrene [53,54]. However, this approach has a number of drawbacks. Adsorption depends on the structure of the sugar, including its sulfation pattern and length. Physical absorption of HS or heparin will generally involve many groups along the poly- or oligosaccharide, including sulfates and carboxyls that are required for protein binding. Moreover, the surface interaction of the sugar will restrict the conformational versatility of the chain, a factor that is becoming increasingly important with respect to understanding protein binding [55,56]. Moreover, given that the sugar is not covalently attached, it can desorb. The consequences of this are the potential for disturbing the activity of the bulk phase, which in a clinical setting may include increased bleeding and thrombocytopenia. In a bioanalytical setting, this will reduce the binding of analytes to the sugar functionalised surface and/or alter the specificity of sugar recognition. More recently, surfaces with a reasonably precise charge density have been produced. These are available commercially from Iduron and are clearly proving useful in the first line analysis of protein-sugar

interactions, since they have been adopted by the research community, e.g., [57]. However, there is no doubt that in many applications it is desirable that the properties of the immobilised sugar are more predictable than is possible by simple adsorption. A number of strategies involving the direct covalent coupling of oligosaccharides and entire chains of heparin and HS have been developed. These strategies include:

- Schiff's base reaction of the reducing end of the sugar.
- Reaction of the free amines that occur on the few N-unsubstituted glucosamines in the polysaccharide chain.
- Reaction of the unsaturated bond between C4 and C5 of the non-reducing uronic acid that is formed after lyase cleavage.
- Condensation of the carboxylic acid of the uronic acid with an amine.
- Oxidation of vicinal diols by, for example, periodate, to form an aldehyde for a subsequent reaction.

The last two options are not particularly useful with heparin and HS. One sugar in two is a uronic acid, while vicinal diols occur on every non-sulfated uronic acid. Consequently, these approaches, whilst very successful in other contexts, result in substantial modification of the polysaccharide chain and a consequent change in its ability to interact with proteins. For example, a direct comparison of heparin immbolised via the reducing end, free amines and the carboxyl groups of uronic acids showed that the latter method severely affected protein binding [58].

Schiff's base reaction

The Schiff's base reaction cannot be used with entire chains of HS, since the reducing end of the polysaccharide is attached to the core protein of the proteoglycan, though it will work with heparin, since this is cleaved in the mast cell from the chains of the proteoglycan serglycin. Moreover, it is extremely inefficient with lyase cleaved oligosaccharides. With nitrous acid derived oligosaccharides, the yield of the reaction in mildly acidic anhydrous conditions can be as high as ~30%. However, oligosaccharides are reasonably, but not highly soluble in non-aqueous solvents and generally yields are ~10% to 30% of sugar and microwave enhancement allows equilibrium to be reached rapidly [51]. As a consequence, this approach consumes relatively large quantities of sugar when used in a direct reaction with a reactive surface, e.g., one possessing hydrazide groups [59]. An alternative is to perform the Schiff's base reaction with a small molecule that allows a subsequent reaction with high yield. The classic example is biotin hydrazide, which enables capture of the biotinylated sugar product on streptavidin-derivatised surfaces, e.g., [26,28,59]. The obvious advantage of this reaction is that, despite its relative inefficiency, it immobilizes the sugar in a defined orientation on a surface, that is through the reducing end, so effectively presenting binding sites in the sugar to proteins.

Free amines

The occasional free amines that are present along the polysaccharide chain provide another functional group. These can be reacted with N-hydroxysuccinamide. However, direct reaction of the polysaccharide chain with an NHS-activated surface

is extremely inefficient, perhaps because these groups are rare and/or because they are involved in extensive intrachain interactions with, for example, sulfate groups of neighbouring sugars. Consequently, it is desirable to first react these groups to form an intermediate that can then be captured or, reacted with an appropriate surface. Reaction with N-hydroxysuccinamide biotin followed by capture on streptavidin derivatised surfaces is the most common method employed [42,60]. However, a quantitative analysis has shown that this approach compromises the ability of the sugar to bind its protein partners [58], presumably because the interaction of the biotins within the sugar chain with immobilised streptavidin both sterically hinder some protein binding sites and forces the neighbouring regions of the polysaccharide chain into restricted conformations.

Reaction of the Δ 4, 5-unsaturated uronic acid derivative

The Δ 4, 5-unsaturated uronic acid derivative that arises following lyase cleavage can be reacted with Hg^{2+}. A modification of the conditions usually used to remove the unnatural Δ 4, 5-unsaturated uronic acid derivative has allowed the insertion of Hg^{2+} across the double bond. The mercury adduct of the oligosaccharide is now reactive towards thiols [50]. This reaction has the same attraction as the Schiff's base reaction in that it modifies the end of the oligosaccharide, leaving the rest of the structure free for interactions with protein partners. However, it has the significant advantage that each step is close to stoichiometric, so yields are high (>95%), allowing the analysis of smaller amounts of sugar.

1.5 Analytical tools

1.5.1 Optical and acoustic biosensors

Optical and acoustic biosensors have for over a decade been an important feature of biomolecular research. Amongst the early adopters of these techniques were glycobiologists, driven by the sheer complexity of their field to seek out new measurement methods. The examples described below include work performed with surface plasmon resonance and resonant mirror biosensors, quartz crystal microbalances and most recently with dual polarization interferometers. The examples are chosen to illustrate the approaches for immobilization of the sugars and the type of information that has been acquired.

The first studies of this type used heparin, HS peptidoglycans (released from the proteoglycan by protease treatment) or entire proteoglycans biotinylated on amine groups e.g., [60-64]. Collectively, this work demonstrated that it was possible to quantify the interaction of proteins with heparin or HS. However, it also illustrated the complexity of the interactions of proteins with the polysaccharide. Kinetic studies showed that there were multiple binding sites present on the sugar and, to enable an analysis of the data, tended to focus on the site with the highest affinity. The presence of multiple binding sites caused substantial turmoil over the following 10 years, because the field was focused on the notion of proteins recognizing individual sequences within the sugar polymer, a concept derived from the relatively high specificity of antithrombin III for its unique pentasaccharide binding site. Another important contribution of this work was the illustration that protein binding did not correlate with protein activity. A corollary was the observation that polysaccharide

chains and oligosaccharides derived from them were not equivalent in terms of biological activity [61].

The use of sized oligosaccharides derived from heparin and immobilized through a biotin at their reducing ends was an important development, since it afforded a simpler system for the analysis of binding kinetics [26]. Indeed, a comparison of amine biotinylated and reducing end biotinylated heparin demonstrated the superiority of the former [58]. A further weakness of biotinylation on amines was identified when it was discovered that cyclophilin B only bound to the sugar immobilized through its reducing end. Thus, Vanpouille and coworkers [19] found that the minimal binding unit for heparin that could interact with Cyclophilin B was a decasaccharide. Crucially, they found that different methods of immobilizing heparin onto biosensor surfaces radically affected the affinity of interaction. Cyclophilin B hardly bound heparin that had been modified via internal amines, whereas it bound both oligosaccharides that had been biotinylated at the reducing end and a heparin-bovine serum albumin conjugate synthesized by reductive amination. Further work showed that Cyclophilin B had far fewer binding sites in heparin than FGF2 and that this was likely to be due to the requirement for a rare 3-O sulfate, which is inserted onto C3 of glucosamine by a sulfotransferase requiring a free amine at C2 of its substrate [19].

Acoustic biosensors have also been used to explore the interactions of proteins with heparin and HS, though on a more limited scale [59]. Their principal application has been to demonstrate that signals observed in optical biosensors do not arise from differences in the refractive index of analytes. This is a particular problem for glycoprotein analytes when the effect of glycosylation is under scrutiny: the

assumption usually made in optical biosensors, that the refractive indices of a glycosylated and deglycosylated protein are the same, is not based on fact. Acoustic biosensors have not been fully exploited for their ability to report on the viscoelastic properties of adsorbates, though some excellent work has been done on this aspect with mucins [65].

An important issue is that in all these studies, the actual orientation of the sugar on the surface was not actually known. Thus, in the work with oligosaccharides biotinylated at their reducing ends or, heparin-bovine serum albumin conjugates, it was assumed that the sugar was completely exposed to solvent and did not interact with the underlying surface and protein(s) used to capture it.

Dual polarization interferometry (DPI) is a surface based technique that allows measurement of the changes in thickness, refractive index, mass and density of adsorbates 100 nm thick or less on the surface of a functionalized waveguide [66-68]. The advantage of this approach is that information concerning the orientation of the sugar is obtained. Indeed, in a recent study, the instrument has been used to design a surface, which allowed the covalent attachment of oligosaccharides to the sensor surface and prevented the non-specific binding of two very sticky proteins, FGF2 and lactoferrin [38]. A hydrazide surface was used to covalently couple the oligosaccharides, following which it was blocked by a short aldehyde-functionalised polyethyleneglycol. Perhaps the most challenging observation made in this work was that, despite extensive engineering of the surface, the immobilized oligosaccharides were, surprisingly, nowhere near normal to the surface, but inclined at just 30° to the surface. This indicated that the oligosaccharides probably had extensive weak interactions with the surface. Given the charge on heparin (the most anionic polymer

in nature) and HS, together with the fact that meaningful experiments must be done in water, it is perhaps inevitable that the sugar interacts with surfaces that are polar; non-polar surfaces are not useful since they bind analytes non-specifically.

1.5.2 Nanoparticles

Nanoparticles are of great scientific interest, as they are effectively a bridge between bulk materials and atomic or molecular structures and possess unique physical properties due to their size. Gold nanoparticles or colloid possess a characteristic plasmon band due to the collective oscillations of their surface plasmons [69,70]. At the plasmon frequency they are the material with the highest absorbance of light, since the absorbed photon energy is rapidly converted into phonons (vibrations). This rapid relaxation allows subsequent photon absorption. They are easily detected by eye (1 fmole in 1 ul is dark pink) and techniques such as photothermal microscopy allow individual nanoparticles to be detected. To mobilise these materials a ligand shell that is inert in biological environments is required, since gold binds to most biomolecules. In addition, for polysaccharides, a means of conjugating a defined and known number of sugars/nanoparticle is required. Peptides provide one of the best ligand shell systems for nanoparticles, because functionalisation and stabilisation are independent, yet accomplished in the same preparative step [70-74].

A new ligand shell of thiol-alkane polyethylene glycols and peptidols (peptides with a C-terminal OH rather than COOH, called mix matrices) has proved to be very effective at stabilising nanoparticles and they are not charged [71,72] [75]. This self-assembled ligand monolayer system for gold nanoparticles allows the easy introduction of a single recognition function per nanoparticle and also allows the

specific and stoichiometric labeling of proteins with gold nanoparticles. The mixed matrix-ligand system gives high stability in physical, chemical and biological terms to nanoparticles and is also simple. Besides, self-assembling monolayers impart a small hydrodynamic radius to the nanoparticle compared to polymer ligands, ~ 1 nm [76]. Therefore, they reduce the steric hindrance of the nanoparticle probe. Thus, the mix-matrices provide a useful tool for the development of nanoparticle-based quantitative bioanalytical and imaging techniques in addition to their potential in many biomedical applications.

1.5.3 Nanoparticle - surface chemistry

Gold nanoparticles are versatile materials for a broad range of applications with well-characterized electronic and physical properties due to well-developed synthetic procedures. In addition, their surface chemistry is easy to modify. These features have made gold nanoparticles one of the most widely used nanomaterials for academic research and an integral component in point-of-care medical devices and industrial products world-wide. For the nanoparticle reactions, the same techniques, size-exclusion and ion-exchange chromatography, conventionally used to separate and purify biological molecules according to their surface properties are applied. This is due to the fact that the mixed matrix-ligand shell results in the nanoparticle behaving as an inert globular protein [72].

An important feature of this work is the synthesis of stoichiometrically functionalized nanoparticles. Only in this way can the nanoparticle probe be fully exploited to elucidate the properties of the conjugated biological molecules. Stoichiometric functionalisation is achieved through knowledge of the total number

of ligands in the shell and the incorporation of a defined number of functional ligands (in published examples, ones carrying a tris nitriloacetic acid chelating group for coupling to his-tagged proteins) into the ligand shell [74] [72]. Functionalised nanoparticles can be separated from non-functionalised nanoparticles by chromatography, in this instance on a hexahistidine resin. This approach, which assumes that incorporation of the ligand carrying the function (here, a carboxylic acid) is stochastic, allows the identification of conditions that produce nanoparticles carrying just one function [74]. Nanoparticle technology is one technique that can be used as an alternative way to study surface chemistry. Instead of using the optical biosensor, which is expensive, nanoparticles promise the same surface chemistry, and can be used to verify findings.

1.5.4 Optical properties

Gold nanoparticles have been extensively used for applications in biology, owing to their unique optical properties. These properties arise from the interaction of light with electrons on the gold nanoparticle surface. At a specific wavelength of light, the collective oscillation of electrons on the gold nanoparticle surface cause a phenomenon called surface plasmon resonance resulting in the strong absorption of light. The particular wavelength, or frequency, of light where this occurs is strongly dependent on the gold nanoparticle size, shape, surface and agglomeration state [77]. Plasmon resonances of the nanoparticle, which determines the optical absorption and scattering properties of the nanoparticle, may be tuned by changing the ratio of the nanoparticle's core size to its shell thickness [78].

1.6 Aims

It is clear from just the few examples described in Sections 1.3.2, 1.3.3 and 1.4.1 that the diversity of structures in cellular HS presents a major challenge with respect to understanding the specificity and function of protein-HS interactions. The importance of this challenge is underlined by a recent systems biology analysis of the functional significance of the protein-protein interactions of the 435 known heparin-binding proteins: the network described by these interactions forms the heart of the extracellular network of proteins that control cell fate [20]. The use of surface-based analytical tools presents many advantages for the analysis of protein-sugar interactions (Sections 1.4 and 1.5). Generally, two approaches have been used for functionalising surfaces: biotinylation of the reducing end of oligosaccharides followed by their capture on streptavidin surfaces, e.g., [26] and direct covalent coupling of oligosaccharides to a reactive surface, e.g., [38,79]. However, these have advantages and disadvantages related directly to the sugar-surface coupling strategy.

Biotinylation provides what can be termed a "reactive" sugar, i.e., a sugar that readily couples to a streptavidin surface. This approach allows for efficient functionalisation of multiple surfaces for the analysis of specificity of multiple protein-sugar interactions. However, the biotin-streptavidin bound is not covalent, so the fouling of the surface cannot be prevented: effective cleaning would need denaturing agents (SDS, urea and so on), which would break the biotin-streptavidin linkage. Moreover, streptavidin has a diameter of ~ 5.5 nm and is tetravalent, so it would not be suited for functionalising nanoparticles with sugars. Stoichiometric coupling of sugars (1 sugar: 1 nanoparticle) might be difficult and the increased distance between nanoparticle and sugar would reduce the efficiency of detection of

optical coupling caused by the binding of a protein-nanoparticle conjugate to the sugar.

Direct covalent coupling of the reducing end of the sugar to a reactive surface overcomes the disadvantages noted above for the biotin-streptavidin strategy. However, it presents its own problems, related to the inefficiency of the reaction of the sugar's reducing end. The consequence is that high concentrations of sugar and of reactive groups on the surface are required. This consumes relatively large amounts of sugar for functionalising just one surface. Furthermore, this would be unlikely to be effective with nanoparticles, since only one reactive group per nanoparticle would be present (to achieve 1 sugar; 1 nanoparticle) and concentrations high than ~ μM are difficult to achieve with nanoparticles.

The aim of this thesis is to devise an alternative approach, which possesses the advantages of these strategies, but not their disadvantages. This will be achieved by producing a sugar with a reducing end with greatly enhanced reactivity. In this way the reactants can be at high concentrations in a solution phase reaction and subsequently a short covalent bond would be formed between the reactive sugar and the surface. An attractive strategy would be to incorporate a thiol or thiol reactive entity onto the sugar's reducing end, since the consequent coupling reaction with a surface would be orthogonal to the groups present on the sugar (carboxyl, amine, hydroxyl). The implementation of this approach will involve a series of preparative and analytical steps (Scheme 1.1). Successful production of reactive sugars would then be followed by their use in functionalising surfaces suitable for the analysis of protein-sugar interactions.

Scheme 1.1: Flow diagram summarising the strategy for producing a reactive sugar that may be used to functionalise biosensor surface and nanoparticles.

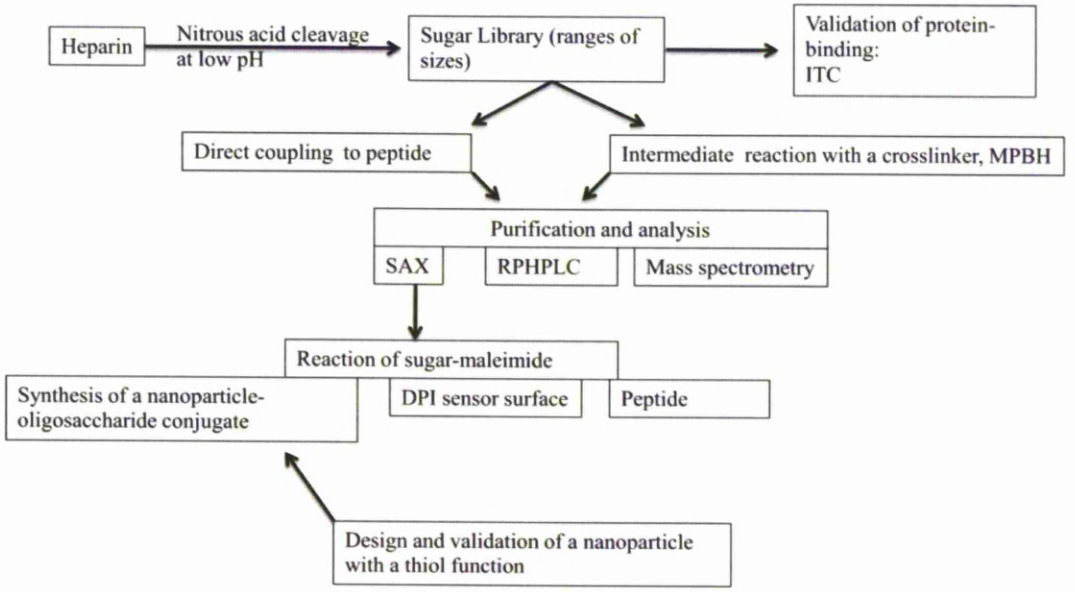

CHAPTER 2

Materials and Methods

2. Materials and methods

2.1. Chemicals and solutions

All chemicals used were of highest purity available commercially and are listed in Appendix (i).

2.1.1 MPBH solution

MPBH (4-(4-N-maleimidophenyl)butyric acid hydrazide hydrochloride) was purchased from Thermo Scientific, Rockford, U.S.A. This crosslinker was dissolved in formamide at 15 mg/mL.

2.1.2 Peptides and alkane thiol etheylene glycols

The peptide C(Acm)-Ala-Leu-Asn-Asn-Gly-Gly-Cys-OH was purchased from Bachem, Bubendorf, Switzerland. This peptide was dissolved in N,N-Dimethylformamide, 99% at 10 mg/mL. The peptidol CVVVT(ol) and peptide CALNN were purchased from Peptide Protein Research, Fereham, UK and dissolved in DMSO : H_2O as 25:75 (v/v) to 4 mM. The alkane thiol ethylene glycol SH-$(CH_2)_{11}EG_4$ (Prochimia, Poland), hereafter referred to as "HS-PEG" was dissolved in methanol to 4 mM. The disulphide bonding ligands EG_4 -$(CH_2)_{11}EG_4$ S-S-$(CH_2)_{11}EG_4$ and EG_4 -$(CH_2)_{11}EG_4$ S-S-$(CH_2)_{11}EG_4$-Mal, where Mal is a maleimide (both Prochimia) were dissolved at 4 mM in ethanol.

2.1.3 *Buffers for reverse phase HPLC*

HPLC water was used as a mobile phase in buffer A. Buffer B contained 80% (v/v) methanol. Both solutions were filtered and degassed before used.

2.2 Oligosaccharide libraries

2.2.1 *Nitrous acid cleavage at low pH*

Nitrous acid digestion at pH 1.5 was used to cleave glycosidic bonds of N-sulfated GlcN residues at room temperature to yield oligosaccharides. A freshly made nitrous acid solution, a mixture of 0.5 M sodium nitrite and 0.5 M hydrocloric acid), 5 mL was added to 5 mL heparin solution (500 mg/mL) and incubated at room temperature. At intervals, 2 mL of this mixture was removed and added to 250 μL ammonium bicarbonate (1 M) to quench the reaction.

2.2.2 *Polyacrylamide gel electrophoresis*

A 33% acrylamide (w/v) resolving gel was prepared containing 3.15 mL glycomap buffer, 3.85 mL acrylamide (60% w/v 19:1), 20 μL 10% (w/v) ammonium persulfate and 15 μL N,N,N',N'-tetramethylethylenediamine. Glycomap buffer is: 200 mL of 895 mM Tris acetate, adjusted to pH 7.0 and then added to 350 mL ethylene glycol and 350 mL water. The overlay buffer was 3.15 mL glycomap buffer plus 3.85 mL water. To prepare a loading gel, 0.9 mL glycomap buffer, 0.3 mL (60% w/v 49:1) acrylamide, 0.8 mL water, 10 μL 10% (w/v) ammonium persulfate and 5 μL N,N,N',N'-tetramethylethylenediamine were used. Ten times running buffer consisted of 36.3 g Tris, 40 g MES in 1 L water.

The samples were loaded onto the gel (0.5 μL each lane). For molecular weight

calibration, BLH (bovine lung heparin), which had been enzyme digested and of known degree of polymerization (DP) from DP4 to DP16 was used.

The gel was run at 200 V until the dye front had migrated 1 to 5 mm from the bottom of the gel normally in 2 hours. The potential was reduced to 110 V and the gel was then run overnight. After the gel was agitated for 5-10 minutes on a slow rotary shaker in water. About 50 mL of staining solution (Azure A dye, 0.08% w/v) was poured on the gel and left for 1 hour and then the gel was rinsed with a few changes of water for 1 hour. Bands were visualized on a light box.

2.2.3 Gel filtration

A Superdex 30 XKx2 column (15 mm x 200 cm) was equilibrated with 500 mL 0.5 M ammonium bicarbonate at a flow rate 0.5 mL/min. Samples of Enoxaparin and nitrous acid digested heparin (1 mL at 100 mg/mL) were applied to the column and 1.0 mL fractions were collected; the absorbance of the effluent was monitored at 232 nm.

2.2.4 Removal of ammonium bicarbonate

To remove ammonium bicarbonate in oligosaccharide samples, fractions were subjected to at least four freeze drying cycles; after freeze drying, samples were dissolved in 3 mL water and freeze dried again.

2.3 Coupling reactions of oligosaccharides

2.3.1 Reaction of oligosaccharides with MPBH

The reaction of the reducing end of oligosaccharides with the hydrazide moiety of MPBH (Section 2.1.1) and peptides (Section 2.1.2) was performed in different conditions, specified in the text. Different sizes of oligosaccharides (1 mg) were reacted with 100 µl, 15 mg/mL MPBH. Acetic acid (2.5 µL) was added to the reaction to allow protonation. All reactions were incubated at temperatures specified in the text (generally 20°C or 40°C) for overnight to a week before analysis and purification. All oligosaccharides in the reactions were lyophilized prior to use.

2.3.2 Reaction of maleimide sugar conjugate with peptides

The sugar-maleimide purified by SAX was then reacted with peptide at 10 mg/mL, where the peptide was in 10 times molar excess. The buffer used in this reaction was 20 mM sodium phosphate, pH 7. The samples were incubated at room temperature overnight before anion exchange chromatography.

2.3.3 Strong anion-exchange chromatography (SAX) of reaction products

The HiTrap™ Q HP column is a strong anion-exchanger with a bed volume of approximately 1 mL. The column was connected to a Shimadzu liquid chromatography system. The mobile phase was HPLC grade water and 2 M NaCl in HPLC grade water. A 500 µL sample (102.5 µL sample plus 397.5 µL water) was centrifuged before injection and loading onto the Q column at 1.0 ml per minute.

Fractions (21 ml) were collected and the absorbance of the effluent was monitored at 230 nm. The peaks representing the reaction product were pooled and lyophilized before being used in further experiments.

2.3.4 Detection of oligosaccharide reaction products by reverse-phase HPLC (RPHPLC)

A C18 column (Supelco) was connected to reversed-phase HPLC (Shimadzu) with a 580A, UVD 170S variable wavelength detector and online DG-2410 degasser. The mobile phases were HPLC grade water for buffer A and 80% methanol (v/v) in water for buffer B. The products of the MPBH reaction, which bound to the SAX column were injected onto the C18 column. Fractions were collected, and the absorbance of the effluent was monitored at 214 nm. The peaks representing the reaction products were pooled and lyophilized before being used in other experiments.

2.4 Synthesis of sugar functionalized surfaces

2.4.1 Oligosaccharide preparation

The sugar-maleimide conjugate from HPLC fractions (Section 2.3.3) were collected, lyophilized and used to functionalize sensor surfaces. The samples were dissolved with PBS 1x, the same buffer used in dual polarization interferometry (DPI) (Section 2.5).

2.5 Dual polarization interferometry (DPI)

The objective of this experiment is to measure changes in thickness, refractive index (RI) and mass of materials ≤ 100 nm thick at the surface of a silicon nitride waveguide in real-time. The DPI system was illuminated with laser light of alternating polarizations at one end. A classic interference pattern is produced when the light exits the two waveguides at the other end, in the Farfield. The waveguide structure is integrated with a fluidic system permitting the continuous flow of material over the upper waveguide. When material absorbs or desorbs from the surface of the waveguide, the interference pattern in the farfield moves. These changes in the position of the interference pattern can be resolved into changes in thickness, RI and mass of the material on the waveguide.

All DPI measurements were performed on an Analight® Bio200 (Farfield Group, Crewe, UK) equipped with a 632.8 nm laser. The instrument is a dual-channel system, with each 2 μL cell maintained at 20°C unless otherwise stated. Following calibration steps to measure the refractive index of the waveguide and running buffer, stepwise injections of materials over the waveguide to formulate the oligosaccharide surface were undertaken.

2.5.1 In situ formation of oligosaccharide surfaces

A silicon nitride waveguide whose surface was covalently functionalized with thiol groups was used in the dual polarization interferometer instrument, and PBS was allowed to flow over the waveguide surface at rate 50 μl min^{-1}.

Once the baseline sensor response had stabilized, the sensor was calibrated. Ethanol/water (80%, w/w) was injected over the sensor for 90 s, followed by PBS and then pure water was injected for 90 s. Since the refractive index of the ethanol/water and water are known, these injections allowed calibration of the optical structure of the waveguide and the refractive index of the buffer solution to be determined; the instrument response was used to calculate the thickness and refractive index of the waveguide and the refractive index of the buffer solution (bulk refractive index) to be used in subsequent layer calculations.

Sugar-maleimide conjugates (200 μL) from 2.3.4 were dissolved in PBS, degassed before injected into channel 1. The flow rate was reduced to 17 μl min^{-1} and was run for 10 minutes. BMPH (5mg/mL) was dissolved in PBS just prior to injection then was allowed to flow over the sensor for 30 minutes.

2.5.2 Blocking the hydrazide surfaces

Unreacted hydrazide groups were blocked by the addition of CH_3O-$(EG)_{17}$-NH-CO-C_4H_8-CHO (PEG-CHO) (20 mg/mL) dissolved in PBS. Thus, each of the glycochips described in the following sections was composed of two parts, one flow cell containing the BMPH linker, an oligo-maleimide and the PEG blocker, whilst the control flow cell was identical except for the absence of oligosaccharide, thereby creating side-by-side active (carbohydrate-containing) and control surfaces.

2.5.3 *Protein injection*

A series of different concentration of proteins (3-464 nM of fibroblast growth factors) were injected over the surfaces at a flow rate of 50 μl min^{-1}. The protein solution was dissolved with PBS at pH 7. The flow cell temperature was set at 20°C.

2.6 Nanoparticle synthesis

2.6.1 *Preparation of mixed matrix stabilised nanoparticles*

The concentration of ligands added in the synthesis of the ligand shell was 2 mM. Stock solutions of ligands were diluted to 2 mM with H2O and then mixed at a ratio of 7 CVVVT(ol) : 3 HS-PEG. Mixed matrix capped nanoparticles were prepared exactly as described [72] by adding 9 volumes of colloidal gold solution to 1 volume of the matrix ligands, CVVVT-ol and HS-PEG at a ratio of 70:30 (v/v). After addition of the ligands, 1 volume equivalent to the ligands of PBS 10X was added. Matrix ligands and nanoparticles were left to react overnight at room temperature. Excess ligands were removed by using a Nanosep centrifugal ultrafiltration device (30 kDa cut off) and size-exclusion chromatography on a 10 mL column of Sephadex G25, equilibrated in PBS-Tween-20 (0.02% v/v). Nanoparticles were loaded and the excluded volume, containing the nanoparticles was collected. The amount of nanoparticles in each fraction was quantified by the measurement of their absorbance spectrum between 450-750 nm. In some experiments, the peptide CALNN, which has a C-terminal carboxyl group was incorporated into the ligand shell at 2% (mole/mole) of total ligand.

2.6.2 Condensation of nanoparticles by using cysteamine hydrochloride and EDC

Nanoparticles were added to 110 µl 10 mM of cysteamine hydrochloride and 110 µl of 100 mM 1-ethyl-3-(3-dimethylaminopropyl)-carboiimide (EDC). The reaction was left for two hours prior to the separation of products and reactants on a G25 column. The eluates were monitored by measuring their spectrum between 400-750 nm. All the samples were then buffer exchanged into water with 10 mM citrate by five centrifugations on a 30 kDa cut-off nanosep ultrafiltration device.

2.6.3 Anion-exchange chromatography of nanoparticles on DEAE Sepharose

Columns of DEAE Sepharose (volume specified in the text) were equlibrated with 20 column volumes of PBS followed by 10 column volumes of water. The samples were concentrated by centrifugation in a nanosep device (cut off 10 kDa) at 10,000 rpm for 7 minutes until the final volume was 100 µl. After loading the column, samples were collected following a water wash and an elution with 2 M NaCl in 10 mM phosphate buffer, pH 7.2.

2.6.4 *Synthesis of nanoparticles with a thiol function*

To synthesise nanoparticles with a thiol function ligands with a disulphide, rather than a free thiol were used: EG_4 -$(CH_2)_{11}EG_4$ S-S-$(CH_2)_{11}EG_4$ and EG_4 -$(CH_2)_{11}EG_4$ S-S-$(CH_2)_{11}EG_4$-Mal,. Since these ligands have disulphides, they do not react with the maleimide function. Ligands were dissolved in ethanol to 4 mM and then added a 1 mM final concentration, because the ligand is less soluble in water and it is effectively equivalent to two HS-PEG ligands, to nanoparticles, as described in Section 2.5.1. After the separation of nanoparticles from free ligand on Sephadex G25, ligand was added again for a further 24 h, followed by gel filtration to purify the nanoparticles. This was necessary, because in pilot experiments, the ligand shell resulting from the first 24 h reaction were not sufficinetly stable and prone to some non-specific binding to Sephadex G25 (result not shown).

2.6.5 *Nanoparticle stability to ligand exchange*

A 1 M DTT stock solution was prepared by dissolving the powder in milliQ H_2O and kept at -4 °C. The stock solution was further diluted to give concentrations ranging from 0.05 mM to 500 mM. Purified ligand capped nanoparticles (57 µL), 33 µL PBS 10X and 10 µL DTT solution at different concentrations (or milliQ water when the required concentration of DTT was 0 mM) were added to a 384 well plate. A blank well, which only contained 100 µL milliQ H_2O, was used as reference. All samples were in duplicate. Absorption spectra of the nanoparticles were recorded after incubation with DTT for times indicated in the figure legends at room temperature between 400 nm and 700 nm.

2.6.6 *Calculation of a stability parameter for nanoparticles*

The surface plasmon absorption peak of 8.8 nm diameter gold nanoparticles is around 520 nm [72,73]. When nanoparticles are aggregated, their surface plasmons couple, causing a red shift in their plasmon absorbance to ~ 650 nm. Therefore, a stability parameter was calculated to allow different experiments to be compared. The stability parameter (SP) was defined as $(A_{650nm}-A_{ref650nm})/(A_{520nm}-A_{ref520nm})$, where A_{650nm} and A_{520nm} are the absorbance of nanoparticles in different concentrations of DTT at 650 nm and 520 nm, respectively. $A_{ref650nm}$ and $A_{ref520nm}$ are the absorbance of reference water at 650 nm and 520 nm. For comparison of the results, this primary stability parameter was normalized by dividing the SP value of same ligand capped nanoparticles measured in 0 mM DTT.

CHAPTER 3

Synthesis of oligosaccharide conjugates suitable for incorporating into functional surfaces

3.0 Synthesis of oligosaccharide conjugates suitable for incorporating into functional surfaces

3.1 Strategy

The ability of heparin to interact with many proteins in biological systems, led to investigation of its characteristics with the aim of providing insights into the structure-activity relationship of these complex and subtle polysaccharides. Structure-function relationships that underpin the formation of FGF receptor-ligand complexes are not at all clear. A possibility is that there are in fact several different complexes that may co-exist and have different biological functions [80] [37]. One way to resolve this is to make measurements on individual molecules rather than averaging across a population. The different sulfation patterns of HS leads to its heterogeneity and makes the molecules extremely challenging to characterize. Analysis of HS preparations obtained by enzymatic and chemical degradation reveals heterogeneity in the sugar composition between different samples [81]. Thus, a study of single entities is very important in order to determine the specificity of the FGF system and the association of receptors, protein and ligands in signalling complexes. To facilitate a biological function of heparin with proteins, a conjugation method for chemically defined heparin and substrates involved in the reaction is important. The initial strategy was to conjugate oligosaccharides with peptides, which could then be incorporated into the ligand shells of nanoparticles.

Consequently, the first part of this project will aim to produce a range of oligosaccharides, and conjugate these stoichiometrically with nanoparticles. Alongside, fundamental biophysical data, using conventional averaging techniques,

of the interactions of FGFs with these oligosaccharides will be acquired. This will allow direct comparison of averaged data on, e.g. stoichiometry, with many individual measurements. Averaging the latter should give the same result as the conventional data.

3.1.1 Conjugation reactions

Oligosaccharides often occur as glycoconjugates attached to proteins known as glycoproteins or lipid (glycolipids) on the cell surface. Chemical and chemoenzymatic methods have been developed to facilitate the synthesis of the oligosaccharides to gain a better understanding of their biological effects and function. A number of strategies involving the direct covalent coupling of oligosaccharides and entire chains of heparin and HS have been developed. These strategies include:

(i) Schiff's base reaction of the reducing end. .

(ii) Reaction of free amines along the polysaccharide chain.

(iii) Reaction of the unsaturated C4, C5 bond between in the non-reducing uronic acid formed during lyase cleavage.

(iv) Condensation of the carboxylate with an amine.

(v) Oxidation of vicinal diols by, for example, using periodate, to form aldehydes for subsequent reaction.

The last two options are not particularly useful with heparin and HS for the applications proposed here. One sugar in two is a uronic acid containing a carboxylate, while vicinal diols occur on every non-sulfated uronic acid.

Consequently, these approaches, whilst very successful in other contexts, result in substantial modification of the polysaccharide chain and a consequent change in its ability to interact with proteins. For example, a direct comparison of heparin immobilised *via* the reducing end free amines and the carboxyl groups of uronic acids showed that the latter method severely affected protein binding [58]. The condensation reaction between the reducing end aldehyde group of the sugar and an amine to form a Schiff's base (imine) (Fig 3.1), is widely exploited. The modification of unsubstituted glucosamine or GlcNS residues by nitrous acid (HNO_2) forms pair-wise oligosaccharides with 2,5-anhydro-D-mannose derivatives at the reducing end [39]. The Schiff's base reaction cannot be used with entire chains of HS, since the reducing end of the polysaccharide is attached to the core protein of the proteoglycan, although it will work with heparin, since this is cleaved in the mast cell from the chains of the proteoglycan serglycin, as long as the reducing end survives the heparin isolation procedure. Moreover, as described above, the reaction is extremely inefficient with lyase cleaved oligosaccharides because only a small fraction of the reducing end sugars are in the reactive aldehyde form and are, in any case, in equilibrium with unreactive, closed-ring forms and these latter predominate. With nitrous acid derived oligosaccharides, the yield of the reaction in mildly acidic, anhydrous conditions can be as high as ~30%. However, charged oligosaccharides are not highly, soluble in non-aqueous solvents and generally yields are ~10% to 30%, while microwave enhancement allows equilibrium to be reached rapidly [51]. As a consequence, this approach consumes relatively large quantities of sugar when used in a direct reaction with a reactive surface, e.g., one possessing hydrazide groups [59] and, in effect, there is insufficient nucleophile available to drive the reaction towards a satisfactory yield. An alternative is to perform the Schiff's base

reaction with a small molecule that allows a subsequent reaction with high yield. The classic example is biotin hydrazide, which enables subsequent capture of the biotinylated sugar product on streptavidin-derivatised surfaces, e.g., [26,28,59]. The obvious advantage of this approach is that, despite its relative inefficiency, it immobilizes the sugar in a defined orientation on a surface through the reducing end, so effectively presents binding sites in the sugar to proteins.

The Δ 4, 5-unsaturated uronic acid derivative that arises following lyase cleavage can be reacted with Hg^{2+}. A modification of the conditions usually used to remove the unnatural Δ 4, 5-unsaturated uronic acid derivative has allowed the insertion of Hg^{2+} across the double bond. The mercury adduct of the oligosaccharide is now reactive towards thiols[50]. This reaction has the same attraction as the Schiff's base reaction, in that it modifies the end of the oligosaccharide, leaving the rest of the structure free for interactions with protein partners. However, it has the significant advantage that each step is close to stoichiometric, so yields are high (>95%), allowing the analysis of smaller amounts of sugar. In addition, the variable yield of reducing end glucosamine units, of which there are potentially several, is eliminated, providing just 2 non-reducing units; a 4,5, unsaturated uronic acid either with, or without, a 2-O-sulfate group. It would also be conceivable, by prior treatment with an enodosulfatase, to remove the 2-O-sulfate group prior to Hg reaction, thereby providing a uniform non-reducing end unit which would eliminate the problem entirely.

Occasional free amines that are present along the polysaccharide chain provide another relatively unique functional group. These can be reacted with N-

hydroxysuccinamide. However, direct reaction of the polysaccharide chain with an NHS-activated surface is extremely inefficient, perhaps because these groups are rare and/or because they are involved in extensive intra-chain interactions with, for example, sufate groups of neighbouring sugars. Consequently, it is desirable to first react these groups to form an intermediate that can then be captured or reacted with an appropriate surface. Reaction with N-hydroxysuccinamide biotin followed by capture on streptavidin derivatised surfaces is the most common method employed [42,60]. However, quantitative analysis has shown that this approach does compromise somewhat the ability of the sugar to bind its protein partners [58], presumably because the interaction of the biotin within the sugar chain with immobilised streptavidin both sterically hinder some protein binding sites and forces the neighbouring regions of the polysaccharide chain into restricted conformations.

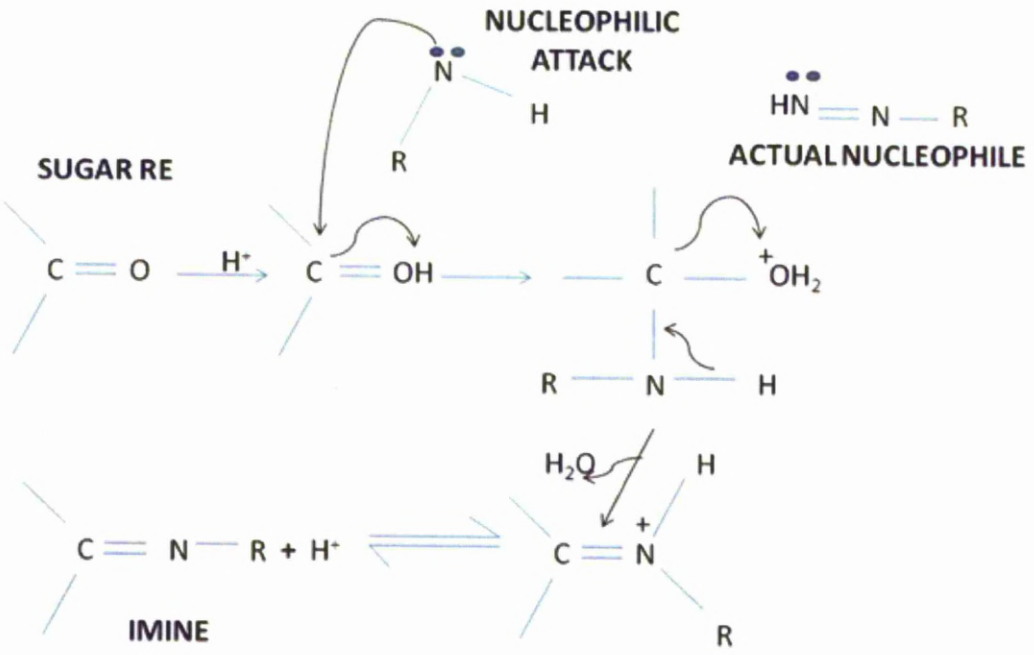

Figure 3.1: General Schiff Base reaction

Mechanistically, the formation of an imine involves two steps. First, the carboxyl group is protonated (the reaction is therefore catalysed by mild acidity) , then the amine nitrogen acts as a nucleophile, attacking the carbonyl carbon. Then, the nitrogen is deprotonated, and the electrons from this N-H bond 'push' the oxygen off of the carbon liberating water (the reaction is a condensation), leaving a C=N double bond (an imine). The key points are the acid catalysis and the desirability of excess amine to drive the reaction, but this is not possible on surfaces.

3.1.2 *Types of surface*

The functionalisation of surfaces with heparin and HS began as a means of preventing the induction of thrombosis in various clinical interventions, such as lines into the bloodstream during dialysis, blood transfusion and surgery. The advent of new tools for the analysis of molecular interactions and the growth of the heparin interactome stimulated a search for more controlled routes to surface functionalisation. The success of this work and the drive provided by fundamental problems in biomolecular research has resulted in the development of a substantial new research field. It is clear that there are major opportunities for the biofunctionalisation of surfaces with these sugars, particularly at the very small (nanoparticle) and the very large (surfaces for cell culture) scale.

3.1.3 *Possible routes*

There are several applications for the attachment of sugars to surfaces; one is the biosensor. Dual polarization interferometry (DPI) is a surface-based technique that allows measurement of the changes in thickness, refractive index, mass and density of adsorbates 100 nm thick or less on the surface of a functionalized waveguide [38]. The advantage of this approach (compared to, for example, using biotin-straptavidin capture) is that the sugar is covalently attached to a hydrazide-functionalized surface *via* the reducing end and regeneration of the surface is not a problem, allowing protein denaturants to be used. The unreacted hydrazide was blocked with aldehyde-functionalized surface poly(ethylene glycol) (PEG-CHO).

Nanoparticles are of great scientific interest, as they are effectively a bridge between

bulk materials and atomic or molecular structures, and possess unique physical properties due to their size. Gold nanoparticles or colloids possess a characteristic plasmon band arising from the collective oscillations of their surface plasmons [74]. At the plasmon frequency they are the material with the highest absorbance of light, since the absorbed photon energy is rapidly converted into phonons (vibrations). This rapid relaxation allows subsequent photon absorption. They are easily detected by eye (1 fmole in 1 ul appears dark pink) and techniques such as photothermal microscopy allow individual nanoparticles to be detected. To mobilise these materials, a ligand shell that is inert in biological environments is required, since gold binds to most biomolecules. In addition, for polysaccharides, a means of conjugating a defined and known number of sugars/nanoparticle is necessary. Peptides provide one of the best ligand shell systems for nanoparticles, because functionalisation and stabilisation are independent, yet accomplished in the same preparative step.

A new ligand shell of thiol-alkane polyethylene glycols and peptidols (peptides with a C-terminal OH rather than COOH, called mix matrices has proved to be very effective at stabilising nanoparticles and they are not charged [72]. This self-assembled ligand monolayer system for gold nanoparticles allows the easy introduction of a single recognition function per nanoparticle and also permits the specific and stoichiometric labeling of proteins with gold nanoparticles. The mix matrix ligand system provides high stability in physical, chemical and biological terms to nanoparticles and is also simple. Besides, self-assembling monolayers impart a small hydrodynamic radius to the nanoparticle compared to polymer ligands. Therefore, they reduce steric hindrance of the nanoparticle probe. Thus,

mix-matrices provide a useful tool for the development of nanoparticle-based quantitative bioanalytical and imaging techniques in addition to their potential in many biomedical applications.

3.2 Production of the oligosaccharide library

Oligosaccharide samples that had been treated with nitrous acid at low pH were fractionated on a Superdex ™ 30 SEC chromatography (16 mm I.D. x 200 cm length). The column was calibrated with different sized oligosaccharides obtained by heparinase digestion from heparin. Treatment with nitrous acid specifically cleaves heparin at $GlcNSO_3$ and unsubstituted GlcN residues to form pair-wise oligosaccharides with 2, 5 anhydromannose derivatives at the reducing end, providing a site for efficient subsequent conjugation of the oligosaccharides (Fig. 3.2).

Figure 3.3 shows application of 2 mL 100 mg/mL heparin-derived oligosaccharides from nitrous acid digestion at low pH to a gel filtration column of Superdex ™ 30 SEC chromatography (16 mm I.D. x 200 cm length) , which allows the separation of fragments from DP 4 to DP 16. DP 16 is eluted at 200 mL, followed by a succession of peaks representing oligosaccharides of decreasing size. In addition, DP 10 eluted at 368 mL. The remaining pooled fractions for sugar digestion at 40 and 60 minutes (1mL) were applied to a gel filtration column. The DP 16 fraction eluted at 300 mL while DP 4 eluted at 450 mL. The largest oligosaccharides eluted earlier. The highest peak in the chromatogram at 600 mL is the salt peak.

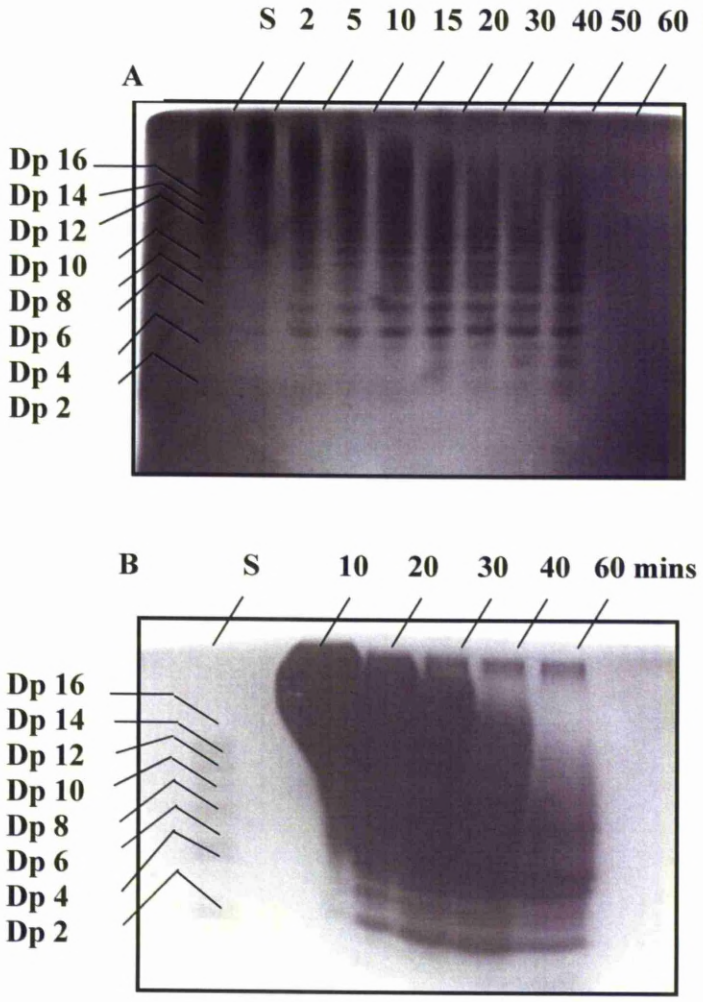

Figure 3.2: Polyacrylamide gel electrophoresis analysis of nitrous acid cleaved heparin-derived oligosaccharides at low pH.

Heparin (100 mg/mL) was digested with 0.5 M, pH 1.5 nitrous acid, as described in Section 2.2.1 for various times (minutes). The reaction was neutralized by adding 250 µL 1 M ammonium bicarbonate and the products were analyzed by polyacrylamide gel electrophoresis (Section 2.2.3). Bovine lung heparin digested enzymatically was used as a standard (S) encompassing sizes corresponding to DP 4 to DP 16. A. The samples were incubated from 2 to 60 minutes on ice. Ten µL samples were removed and quenched with ammonium bicarbonate and 0.5 µl was loaded onto the polyacrylamide gel. Ten microlitre samples were loaded onto each lane. B. Digestion of sugar of a preparative scale. Two µL samples were removed at different times, and 0.5 µL was loaded onto the polyacrylamide gel. The gel was run at 200 V for two hours at which point the potential was reduced to 110V and the gel was then run overnight. The gel is heavily loaded but clear that progressive

degradation has occurred.

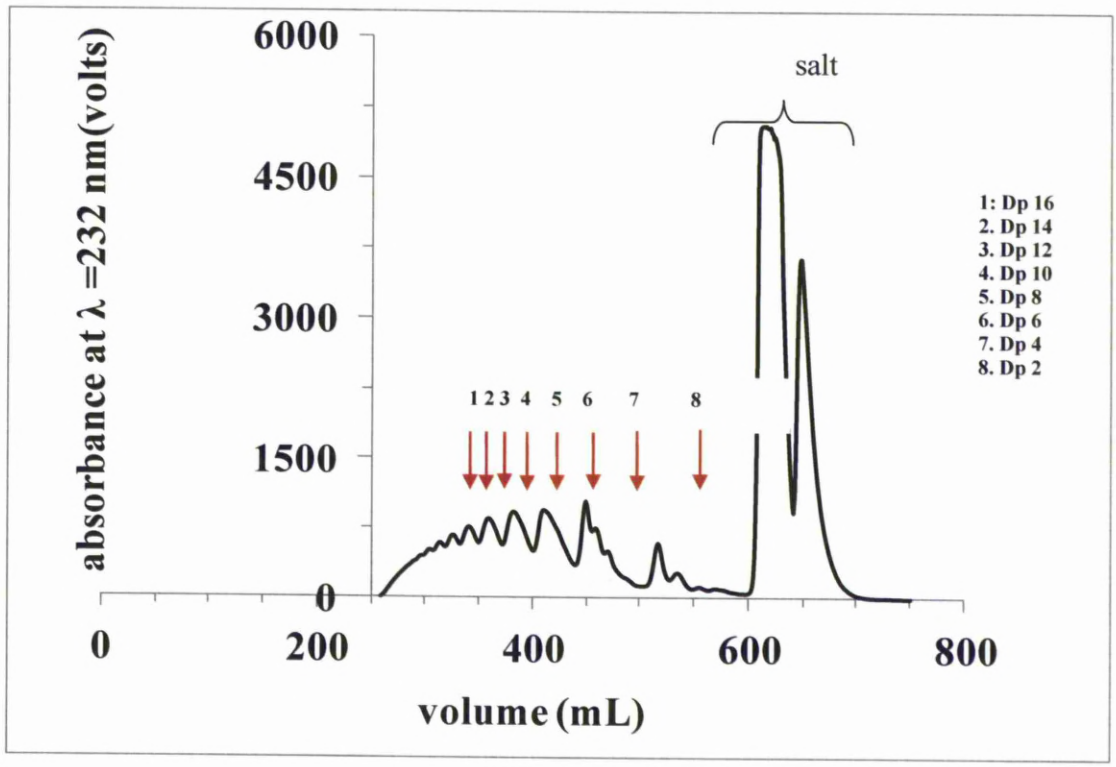

Figure 3.3: Fractionation of oligosaccharides produced by nitrous acid cleavage of heparin by gel filtration.

Samples were separated by running buffer (0.5 M ammonium bicarbonate) at 0.5 ml/min and 1.0 ml fractions were collected. The effluent was monitored at 232 nm. Heparin cleaved with nitrous acid pH 1.5 at a preparative scale (Section 2.2.1 and Fig 3.2) was subjected to gel filtration on a Superdex ™ 30 SEC chromatography (16 mm I.D. x 200 cm length) using an AKTA purifier 10. The pooled samples 20 and 30 minutes from heparin-nitrous acid cleavage were freeze dried and further dissolved with 2 ml of water. Then, each ml of the samples was fractionated over Superdex ™ 30 SEC chromatography (16 mm I.D. x 200 cm length). The samples were run at a flow rate of 0.5 ml/min and 1.0 ml fractions were collected. Sizes of oligosaccharides are shown as DP 2, DP 4, DP 6, DP 8, DP 10, DP 12, DP 14 and DP 16.

	Yield (%)							
DP	**4**	**6**	**8**	**10**	**12**	**14**	**16**	**Total**
HNO_2-hep1	7.86	6.40	4.60	2.60	0.86	0.07	0.27	22.65
HNO2-hep2	8.00	7.60	8.60	3.40	2.60	1.60	2.60	34.40
HNO2-hep3	6.20	14.2	11.00	7.40	5.60	2.40	2.60	47.40

Table 1.1: The percentage yield for oligosaccharides.

The percentage yield for oligosaccharides after heparin-HNO_2 digestion, following separation by gel filtration on a Superdex ™ 30 SEC chromatography (16 mm I.D. x 200 cm length) and freeze-drying to remove water and ammonium bicarbonate. The yield as a percentage of starting mass is shown.

Oligosaccharide fractions collected from gel filtration columns were freeze dried and lyophilised from aqueous solution several times to remove ammonium bicarbonate remaining from the chromatography step. Then, the samples were weighed and total amounts of oligosaccharides of each size were recorded. The selection of fractions was based on the separation of sugar by gel filtration chromatography. The percentage yield of oligosaccharides in each size fraction was equal to the amount of oligosaccharides in each peak divided by the starting amount of heparin-digested injected onto the column. HNO_2-hep 1 shows oligosaccharides richer in smaller sizes (Table 1.1). The percentage of DP 4 olgosaccharides is 7.86%, followed by 6.40%, 4.6% and 2.6% of DP 6, DP 8 and DP 10 oligosaccharides. The DP 16 fraction contained the least. DP 10 and DP 12 were separated moderately, providing 2.6% and 0.86%. The total yield for HNO_2-hep 2 is 34.40%. Conversely, there is increased mass for each size in HNO_2-hep 2 preparation. In this sample, DP 8 provides the most material from the separation on Superdex ™ 30 SEC chromatography, followed by DP 4, Dp 6, DP 10 and DP 12. The least material in this sample was for DP 16. The yield increased to 47.40% for all sizes of oligosaccharides in the sample HNO_2-hep 3. DP 6 showed the most oligosaccharide (14.2%), followed by DP 8 (11.0%), DP 10 (7.4%), DP 4 (6.2%), DP 12 (5.6%) and DP 16 (2.6%). All preparations provided the most abundant yields for the smaller size fractions (DP4-DP8). To prepare oligosaccharide libraries, there are several steps and these may result in the loss of some oligosaccharides during the procedure. To prevent mixing of sizes, one should avoid collecting the lower regions of peaks and because of this, yields of sugars are low due to some losses and some variations in yield during the process of gel filtration.

3.3 Summary of results from early conjugation strategy

The initial strategy was to conjugate oligosaccharides to peptides, which could then be incorporated into the ligand shell of nanoparticles. Thin layer chromatography (TLC), anion-exchange (AEC) and reverse phase chromatography were tested as a means of identifying the successful reaction product. Thin layer chromatography did not produce a clear result. Indeed, it was difficult to identify reactants and products reproducibly. AEC and reverse phase were found to be more reliable for detecting the conjugation of peptide-sugar. Thus, on AEC the product, which had good absorbance at 215 nm from the peptide bond, was strongly anionic, due to the conjugated oligosaccharide. On reverse phase, only the conjugate and the free peptide chromatographed; free oligosaccharide did not bind to the column. However, yields were low. It is possible that, as a result of deprotection of the first peptide after conjugation (the peptide was protected to prevent oligosaccharide reacting with the free amine) led to the loss of detectable conjugate. An unprotected peptide of reverse sequence (GGGTVVC-amide) did not yield a conjugate. This may be due to the amine group in the peptide, which is probably less reactive towards the sugar compared to the hydrazide group in the first peptide. An alternative peptide was then tried; (hydrazide)GGGTVVVCa (Hydrazide)GGGTVVVC/amide). However, yields were still low and this wasprobably simply the result of the inefficiency of the reaction with the reducing end of heparin-derived oligosaccharides with any type of amine (refer to Fig. 3.1) in labelling procedures, for instance with fluorescent end-labels, the amine is in very large excess to force the reaction over to the right hand side of the equilibrium but, in this instance, the peptide could not be dissolved in polar solvents at concentrations much greater than the oligosaccharide.

3.3.1 Maleimide reaction scheme

The reaction of oligosaccharides with the bifunctional hydrazide-maleimide MPBH was carried out as an alternative route to conjugate the peptide and sugar. The idea was that by conjugating MPBH 4-(4-N-Maleimidophenyl)butyric acid hydrazide hydrochloride with heparin-derived oligosaccharides, the reaction could be pushed towards the products more easily, since MPBH is very soluble. The sugar was produced by partial digestion with nitrous acid, which ensured that it possessed a reducing (aldehyde) function. The reducing (aldehyde) function was then reacted with MPBH (4-(4-N-Maleimidophenyl)butyric acid hydrazide hydrochloride; the hydrazide moiety of the latter reacts through a Schiff's base reaction with the reducing end of the sugar (Fig 3.4). The MPBH modified oligosaccharide would then possess a maleimide function at the reducing end, which will react stoichiometrically with thiols. This reaction is also orthogonal to the reactivity of groups present on the sugar or the nanoparticles, allowing highly specific coupling between the two. MPBH was preferred over BMPH, another bifunctional hydrazide-maleimide cross linker, because it possesses an aromatic ring, whose absorbance is in the range of standard hplc uv-vis detectors (Fig. 3.5).

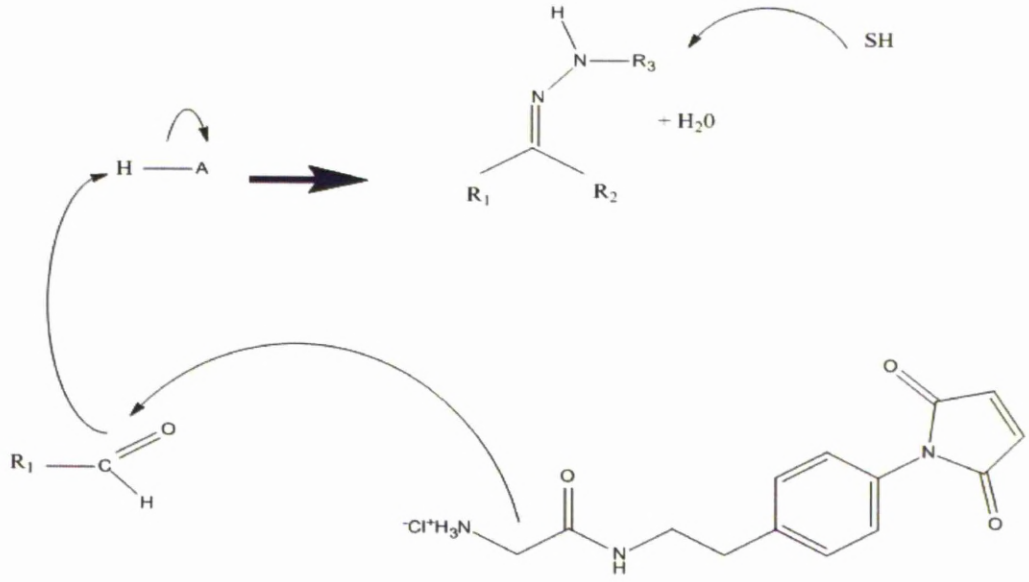

Figure 3.4: Mechanism of sugar-maleimide reaction.

MPBH is heterobifunctional, containing hydrazide and maleimide groups, which reacts with aldehydes and thiols. Formation of a sugar-maleimide conjugate involves several steps similar to the formation of the Schiff base with aldehydes and amines. The electrophilic carbon atoms of oligosaccharides are attacked by nucleophilic nitrogen atoms in the hydrazide group in MPBH. In this step, nitrogen is deprotonated and the electrons from the N-H bond push the oxygen off the carbon, leaving a C=N double bond (an imine) and a displaced water molecule.

3.3.2 *MPBH UV-vis absorbtion*

To identify a suitable wavelength for the detection of MPBH, its UV-vis spectrum was measured (Fig.3.5). MPBH powder was dissolved in water 0.016 μg/μl and the absorbance spectrum was measured between 200-700 nm. The spectrum showed a strong absorbance between 200-230 nm. The absorbance at 230 nm was therefore used to follow the MPBH during chromatography. However, the intensity of the absorbance could not be used to quantify the reaction products because the absorption in the UV of MPBH consists of contributions not just from its aromatic ring, but also from the maleimide and hydrazide groups.

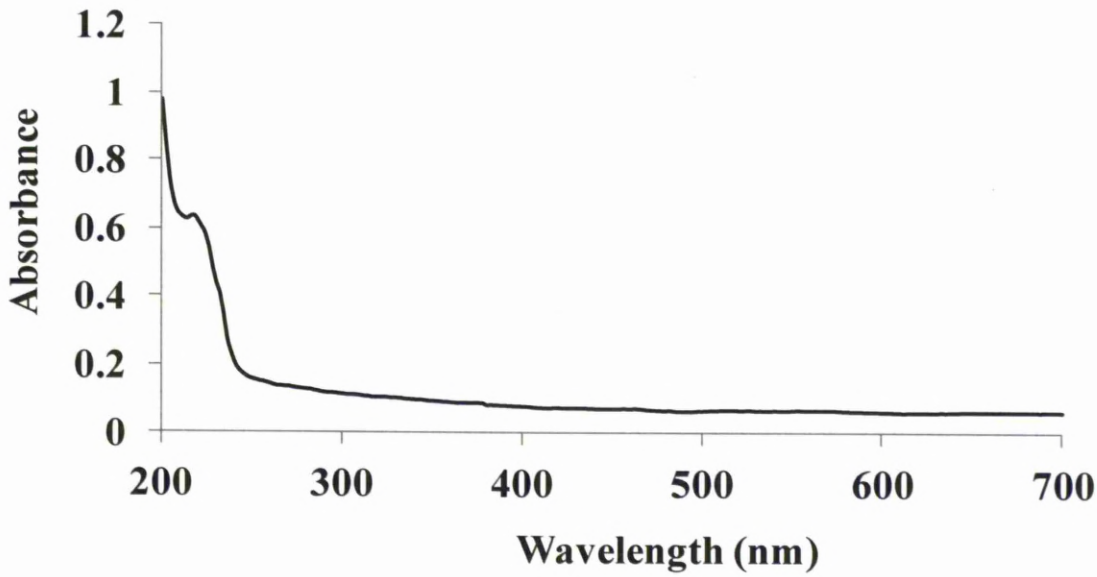

Figure 3.5: UV Vis absorption of MPBH.

MPBH powder was dissolved with water at 0.016 μg/μl and its absorption measured between 200 nm and 700 nm.

3.3.3 Anion exchange chromatography for products of conjugated sugar-maleimide

In this experiment, MPBH was used as a crosslinker, to enable coupling to carbohydrates and thiol containing proteins *via* their reactive hydrazide and maleimide moieties. These two stable nucleophile/electrophile pairs were separated by a 4-phenylbutanoyl spacer. The advantage of using this type of spacer is its ability to limit the possibility of steric hindrance between the crosslinked compounds [82]. The compounds do not react with each other spontaneously and this avoids self-polymerization. Heparin-derived oligosaccharides were reacted with the hydrazide group in MPBH. However, the maleimide group will react with a peptide to form a stable thioether linkage with thiols. These 'bioconjugate products' could be incorporated further onto gold nanoparticles for development into single molecule detection systems, which promise to be useful tools in glycobiology research.

To identify the 'products', a chromatography technique was used, which provides reliable data. Strongly anionic molecules such as heparin-derived oligosaccharides are well separated by anion-exchange at pH values above their PI. In this experiment, a Hitrap Q column (1mL) was used to ascertain the separation of the product of the reaction of three sizes of sugars (DP 4, DP 8 and DP 12) with MPBH from free MPBH and free sugars. The high resolution and the short separation times achieved with this support makes it ideal for such analyses. The sugar control, in which DP 4, DP 8 and DP 12 were chromatographed, gave very little signal (Fig 3.6 A, B and C). This oligosaccharide lacks a strong chromophore since it was produced using nitrous acid (Section 2.2.1). Very small peaks are apparent at ~15% and 100% 2M NaCl

with the larger early peak (0-2 minutes) due to the sample injection (Fig 3.6 A). MPBH control, 100 µl 15 mg/mL MPBH in formamide, diluted with 400 µl (buffer A) prior to injection produced a large peak at the beginning (0-2 minutes), which is due to MPBH not binding to the positively charged column. The absorbance of the peak is more than 400 000 µ volts at 230 nm. After starting the NaCl gradient, peaks appeared at 12-18 minutes, suggesting MPBH or, a contaminant weakly bound to the column. When the conjugation reaction of sugar-MPBH was loaded, there was an early peak, corresponding to the unreacted free MPBH. Several peaks were eluted at the beginning of the NaCl gradient (12-18 minutes), with absorbances of more than 400 000 µ volts at 230 nm. After 20 minutes, there were also several peaks corresponding to elution at 30-50% 2 M sodium chloride. After 38 minutes, the absorbance decreased rapidly to the base line. Overall, these results suggested that sugar and MPBH had reacted to form a new product, the absorbance value for the 'expected conjugate' was 10 times higher than that of the sugar and MPBH control. It should be noted that these fractions, which were eluted with 2 M salt, were a mixture of the expected conjugate and some free sugar (sugar which has not reacted with MPBH).

Similar data were obtained for octasaccharides (DP8) (Fig 3.6, panel B). These do not possess chromophores that are particularly active in the range of the detector, but nonetheless, a small peak was observed at ~ 16 minutes, after injection of DP 8 control onto the column. This corresponds to 0.25 M NaCl and represents an anionic species, which may be the low sulfated oligosaccharides. The second peak at ~ 35 minutes of MPBH again, will correspond with that mainly eluted early with some small peaks at 12-18 minutes (Fig. 3.6 B). Separation of the MPBH-sugar reaction

mixture (Fig 3.6 B) indicated that some free MPBH eluted in the flow through. A highly absorbing species eluted, starting at 12.5 minutes. The area of the peak was more than 400 000 μ volts and corresponded to a small peak in the sugar control. Further peaks at ~ 25 min and 30 to 38 min were also observed. The latter corresponded to a peak in the sugar control. These are considerably larger than those observed with the unreacted sugar, which is likely to be due to the presence of the aromatic ring of the MPBH. This reaction was carried out at 40°C, with 1 mg of freeze-dried DP 8 in formamide and acetic acid, a source of protons to promote the Schiff's base reaction. The reactions were left for 7 days to ensure they attained equilibrium. These experiments established circumstantial evidence for the successful reaction of sugar with MPBH in the form of increased absorbance of material eluting at the position of the oligosaccharide. To prove that the sugar-maleimide was successfully conjugated, putative samples from anion exchange were further analyze on mass spectrometry.

Analysis of the reaction of DP 12 and MPBH by anion exchange chromatography (Fig 3.6, panel C) showed that MPBH did not bind to the AEC column and eluted in the flow through, whilst peaks corresponding to the sugar eluted with 8% of 2 M sodium chloride, with retention times ~13, ~ 25 min and 35 min, a profile very similar to that of DP 8 (Fig. 3.6 B) and DP 4 (Fig 3.6 A). Several peaks appeared after the salt gradient, which is several times higher compared to the result of MPBH control and DP 12 control (Fig 3.6 C). The small peak that appeared at the beginning of the injection of the DP 12 alone may be due to some salt remaining from the purification of the oligosaccharides by gel filtration column. Figure 3.6 C shows the separation of the conjugation reaction of DP 12 and MPBH. As for previous samples

(Figs 3.6 A and Fig 3.6 B), MPBH (100 μl of 15 mg/ml) injected as a control eluted at the beginning ~4 minutes of retention time. There were also several small peaks after 20 minutes elution. However, for the sample of 'conjugate sugar-maleimide' collected from anion exchange chromatography, a much higher set of peaks was observed at a gradient position corresponding to 28% of methanol 80%. All fractions were collected and kept in -80°C before prior to further analysis. Clearly, the next step was to determine in a series of experiments, whether, in fact, this product had been formed.

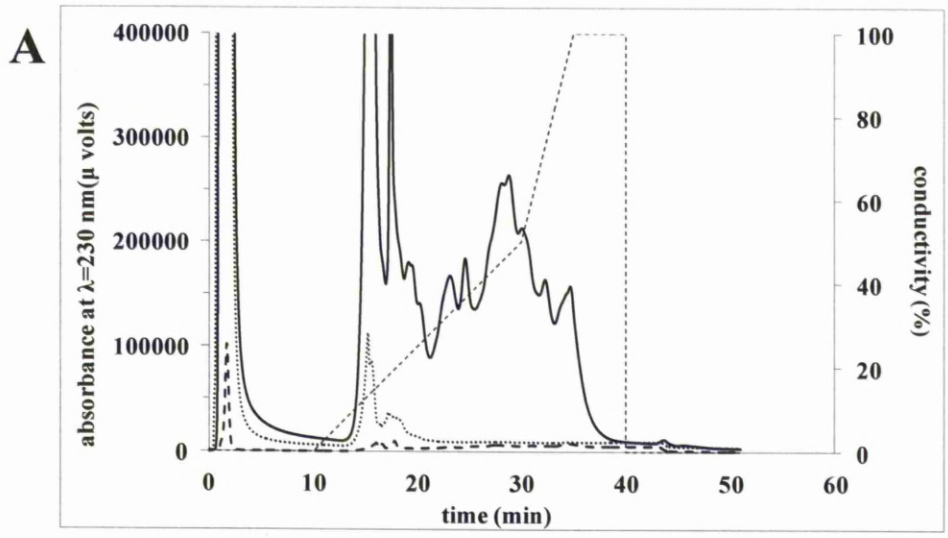
A
400000
300000
200000
100000
0
absorbance at λ=230 nm(μ volts)
0
10
20
30
40
50
60
time (min)
100
80
60
40
20
0
conductivity (%)
DP 4 control
MPBH control
DP 4-MPBH reaction
conductivity

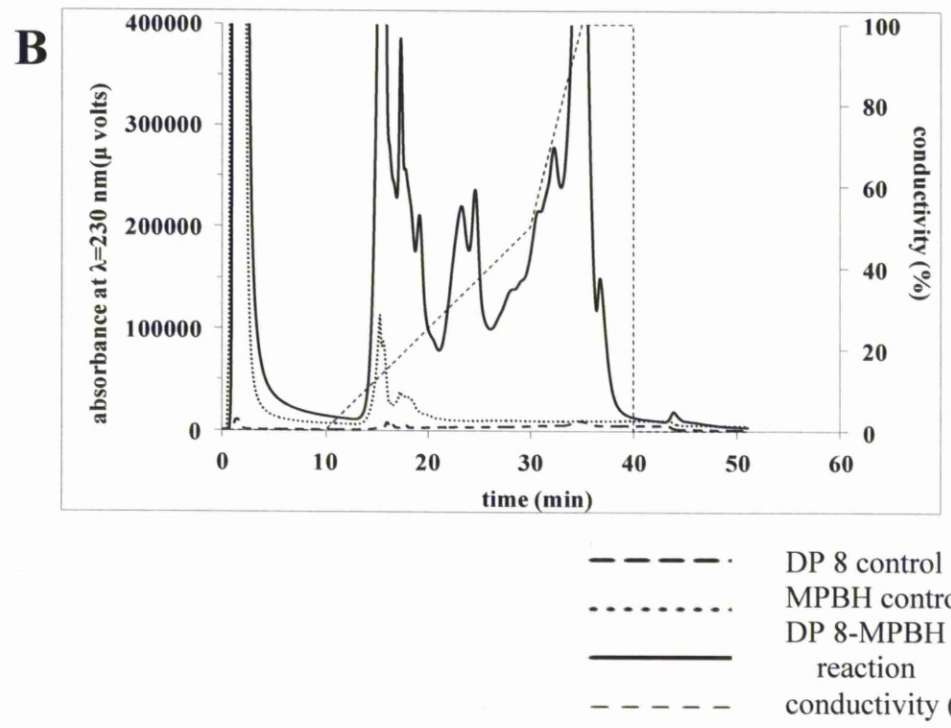
B
400000
300000
200000
100000
0
absorbance at λ=230 nm(μ volts)
0
10
20
30
40
50
60
time (min)
100
80
60
40
20
0
conductivity (%)
DP 8 control
MPBH control
DP 8-MPBH reaction
conductivity (%)

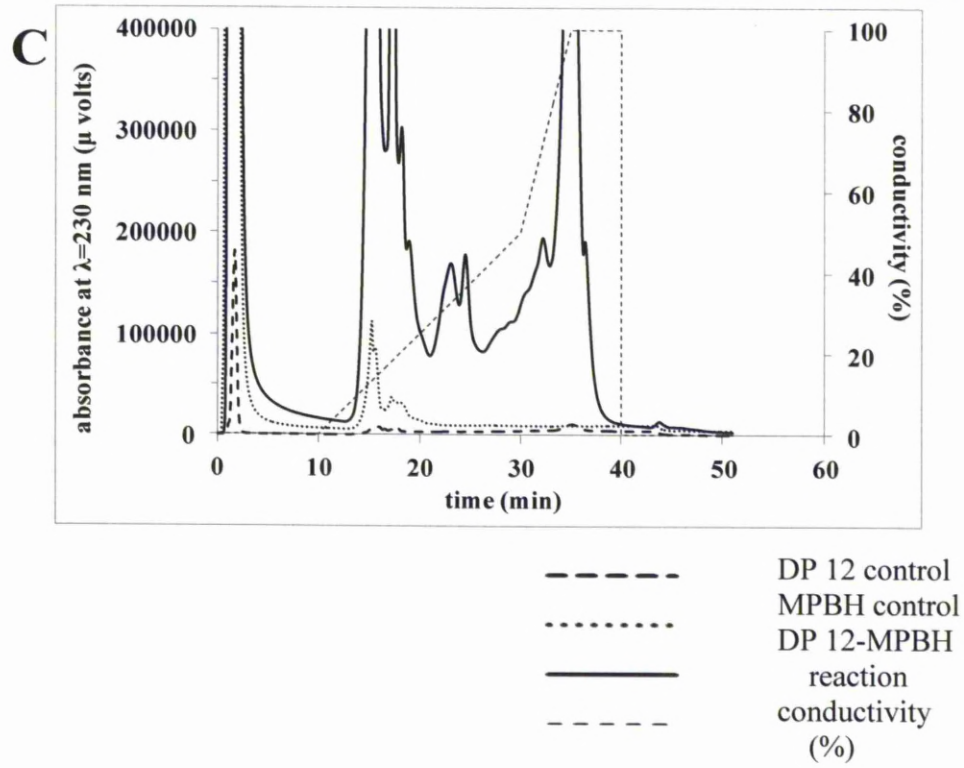

Figure 3.6: Anion-exchange chromatography of the products of reaction of MPBH and heparin-derived oligosaccharides (DP 4, DP 8 and Dp 12) in formamide.

Analysis of the products of the reaction of MPBH (15 mg/ml and a heparin-derived oligosaccharide, DP 4 **(panel A)**, DP 8 **(panel B)** and DP 12 **(panel C)** (1 mg) in formamide using anion-exchange chromatography (230 nm). A Hitrap Q column (1 mL) was equilibrated in HPLC grade water. After application of the sample, the column was developed with a gradient of increasing 2 M NaCl in the same buffer at a flow rate of 1 mL/min, as described in Section 2.3.3. Sugar control: 100 μl of 1mg freeze-dried sugar in buffer A. MPBH control: 100 μL of 15 mg/mL MPBH was dissolved in formamide and was added, with 2.5 μL acetic acid to 400 μL buffer A. Sugar-maleimide reaction: 1 mg of freeze dried sugar was reacted with 100 μL of 15 mg/mL MPBH in formamide, 2.5 μL acetic acid added and incubated for 7 days at 40°C. The sample of sugar-maleimide reaction was dissolved in buffer A (400 μL) prior to injection.

3.3.4 Reverse phase chromatography for products of conjugated sugar-maleimide

Peaks collected from anion exchange chromatography were then analyzed by reverse phase HPLC on a C18 column. This technique was chosen since it may allow separation of free sugar and electrolytes from the product of the sugar-maleimide conjugate. After sample application, the elution was performed by reducing the polarity of the mobile phase. MPBH (100 µl of 15 mg/ml) was injected as a control (Fig 3.7). The result showed that at ~4 mins, a peak was eluted corresponding to material that did not bind to the column. The absorbance reading for the peak was ~ 140 000 µ volts. After 10 minutes, several peaks were eluted. For the sample of 'conjugate sugar-maleimide' from anion-exchange chromatography, a peak appeared at retention time 4 to 8 minutes. Fractions collected between these intervals contained salt and free oligosaccharides. After 10 mins, some peaks appeared and increased after 20 mins eluting at ~22% elution of 80% methanol. The highest absorbance reading was about 200 000 µ volts 214 nm.

Samples of reaction (sugars and MPBH) collected from anion exchange chromatography (Fig 3.6), were injected into a C18 column on reverse phase HPLC chromatography. Free MPBH again eluted at the beginning of the injection, ~4 mins. For the sample of 'conjugate sugar-maleimide' collected from anion exchange chromatography, an unbound sample came off the column, suggesting free oligosaccharide and electrolyte in the sample reaction. However, after starting the gradient, several peaks appeared after 20 minutes of injection or at 28% of 80% methanol. The absorbance reading of the main peak at 22 minutes was about 200 000

μ volts at 214 nm (Figure 3.7). The fractions were freeze dried and lyophilised from water several times to remove excess methanol in the samples before further analysis.

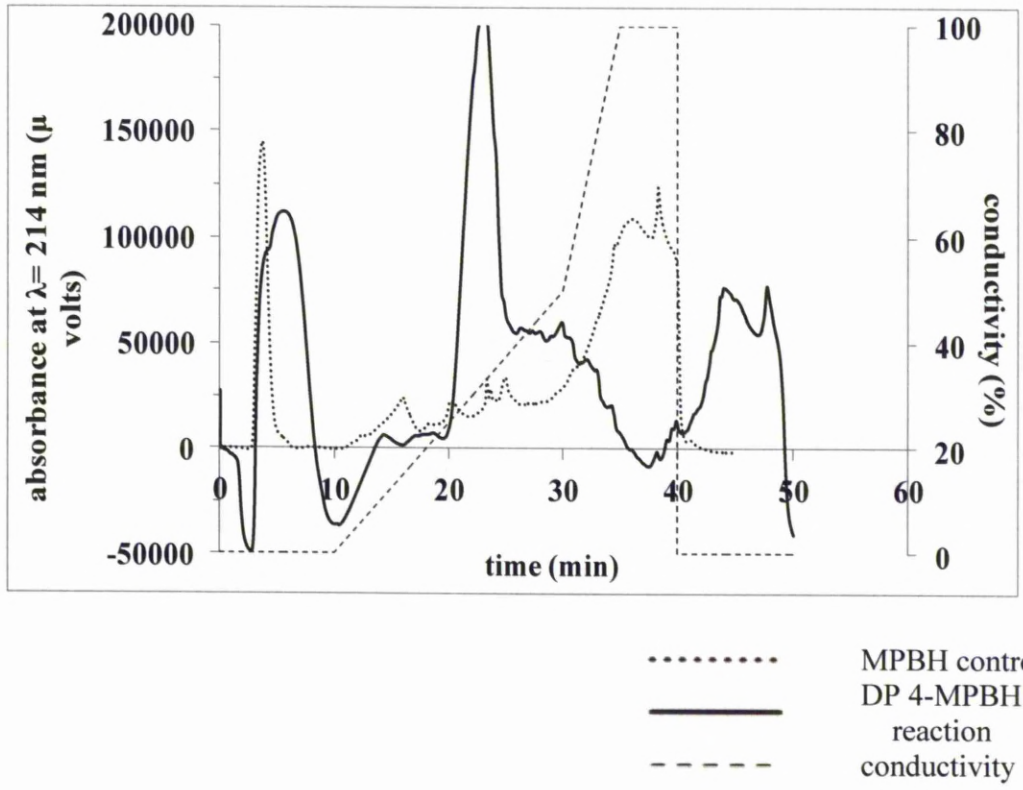

Figure 3.7: RPHPLC separation of putative sugar (DP 4)-maleimide from anion-exchange chromatography.

The products of the reaction of MPBH (15 mg/ml) a heparin-derived oligosaccharide, DP 4 (1 mg), in formamide were collected from anion-exchange chromatography. Freeze dried samples were dissolved with 5 ml buffer A. A C18 column (250 mm×4.6 mm, 5 μm particle size) was equilibrated in HPLC grade water and applied to the column, which was developed with a gradient of increasing 80% methanol in the same buffer at a flow rate of 1 mL/min, as described in Section 2.3.4. MPBH control: Samples corresponding to anion exchange chromatography fractions 0-10 minutes. Sugar-maleimide reaction: Samples from anion exchange chromatography fractions were collected and pooled at retention time 12-32 minutes.

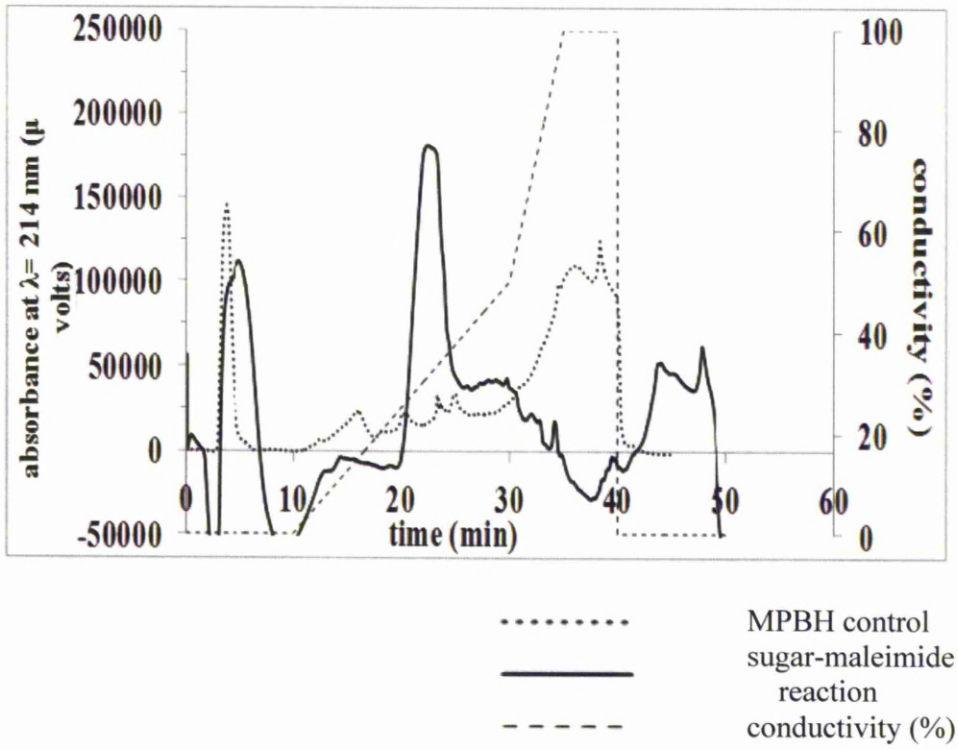

Figure 3.8: RPHPLC separation of putative sugar (DP 8)-maleimide from anion-exchange chromatography.

The products of the reaction of MPBH (15 mg/ml) and a heparin-derived oligosaccharide, DP 8 (1 mg), in formamide were collected from anion-exchange chromatography. Freeze dried samples were dissolved in 5 ml buffer A. A C18 column (250 mm×4.6 mm, 5 μm particle size) was equilibrated in HPLC grade water and the sample was applied to the column, which was developed with a gradient of increasing 80% methanol in the same buffer at a flow rate of 1 mL/min, as described in Section 2.3.4. MPBH control: Samples corresponding to anion exchange chromatography fractions 0-10 minutes. Sugar-maleimide reaction: Samples from anion exchange chromatography fractions were collected and pooled at 12-32 minutes.

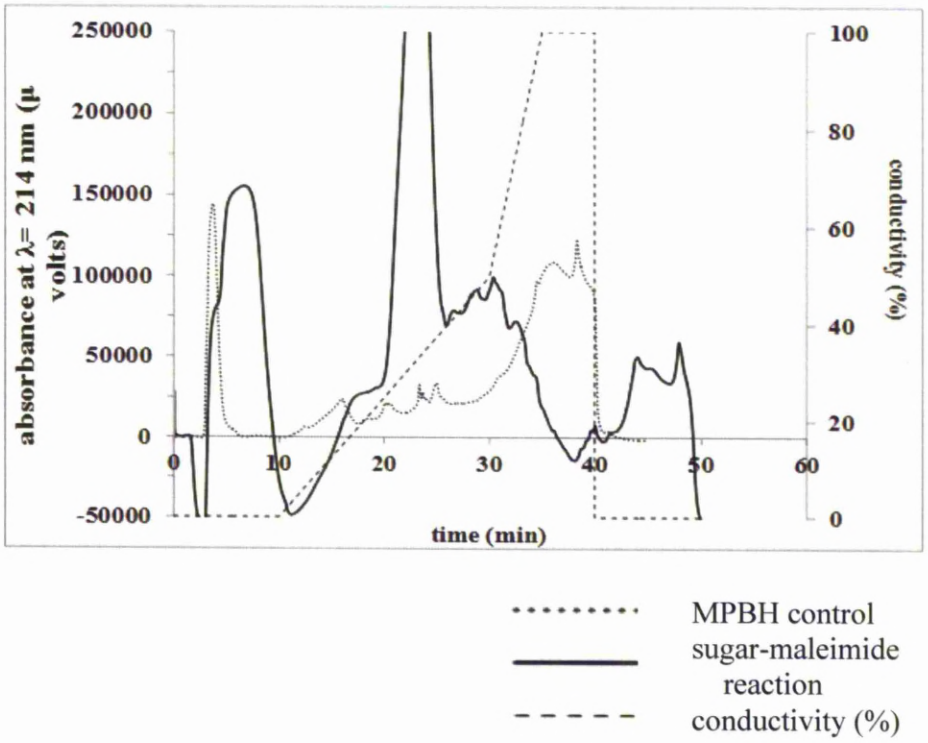

Figure 3.9: RPHPLC separation of putative sugar (DP 12)-maleimide from anion-exchange chromatography.

The products of the reaction of MPBH (15 mg/ml) and a heparin-derived oligosaccharide, DP 12 (1 mg), in formamide were collected from anion-exchange chromatography. Freeze dried samples were dissolved in 5 ml buffer A. A C18 column (250 mm×4.6 mm, 5 μm particle size) was equilibrated in HPLC grade water and the sample was applied to the column, which was developed with a gradient of increasing 80% methanol in the same buffer at a flow rate of 1 mL/min, as described in Section 2.3.4. MPBH control: Samples corresponding to anion exchange chromatography fractions 0-10 minutes originate from the sugar-maleimide reaction, while samples from 12-32 minutes were collected.

3.3.5 Anion exchange chromatography for products of conjugation of sugar-maleimide after separation by reverse phase chromatography

Products of conjugation of sugar-maleimide using different sizes of oligosaccharides from RPHPLC were freeze-dried and reacted with 10 mg/mL of peptide (C(Acm)-Ala-Leu-Asn-Gly-Gly-Cys-OH) in N-methyl formamide at 10 times higher molar concentration of peptide and the reaction left at room temperature overnight. Peptide control (10 mg/ml) in N-methyl formamide was dissolved in buffer A before injecting onto the Hitrap Q column. The result showed that a peak appeared at the front in the chromatogram (1-8 minutes), which should correspond to the unbound peptide (Fig 3.10, Fig 3.11 and Fig 3.12). However, after 12 minutes, at ~ 8% elution of 80% methanol, there was a peak, which may have been due to the positive charge of peptide associating weakly with the column or, to contaminants. The areas of the peaks were around 150 000 s (μ volts) at 230 nm (Fig. 3.10). Similar results were obtained with the other sizes of sugars, DP 8 and DP 12 used in the reaction (Fig 3.11 and Fig 3.12). The area for reaction of DP 8-maleimide with peptide gave an absorbance reading at 200 000 μ volts (Fig 3.11), while synthesis of DP 12-maleimide-peptide gave an absorbance reading of ~250 000 μ volts. It showed the same peak at the beginning of the chromatogram, which is consistent with unbound peptide (free peptide). After 12 minutes, several peaks also appeared, giving an absorbance reading ~ 400 000 μ volts at 230 nm. Fractions were collected (from 12-31 minutes), which would be expected to contain the product of conjugation (sugar-maleimide-peptide), some free peptide (unbound peptide) and free sugar-maleimide (unreacted sugar-maleimide). Those fractions were freeze dried for further analysis.

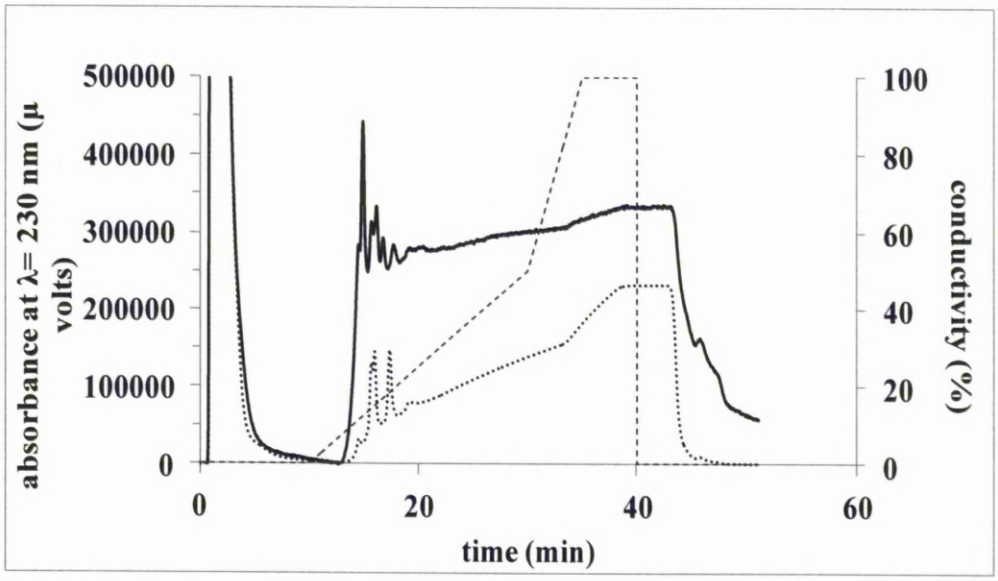

Figure 3.10: Anion-exchange chromatography of the products of the reaction of sugar-maleimide (DP 4) and peptide in N-methyl formamide.

Analysis of the products of the reaction of sugar-maleimide by reverse phase HPLC was made using anion exchange chromatography (230 nm). Sugar (DP 4)- maleimide and peptide were reacted at room temperature overnight. A Hitrap Q column (1 mL) was equilibrated in HPLC grade water. After application of the sample, the column was developed with a gradient of increasing 2 M NaCl in the same buffer at a flow rate of 1 mL/min, as described in Section 2.4.2. Peptide control: 10 mg/mL peptide was dissolved in N-methyl formamide and was added to 400 μL of buffer A. Sugar-maleimide reaction: Sugar-maleimide conjugate (from reverse phase HPLC), fractions 13-36 minutes were reacted with peptide C(Acm)-Ala-Le-Asn-Asn-Gly-Gly-Cys-OH (10 mg/ml) in N-methyl formamide at room temperature overnight. Each sample was dissolved in 500 μl buffer A prior to injection. Fractions 14 mins-41 mins corresponding to the elution of oligosaccharide were collected.

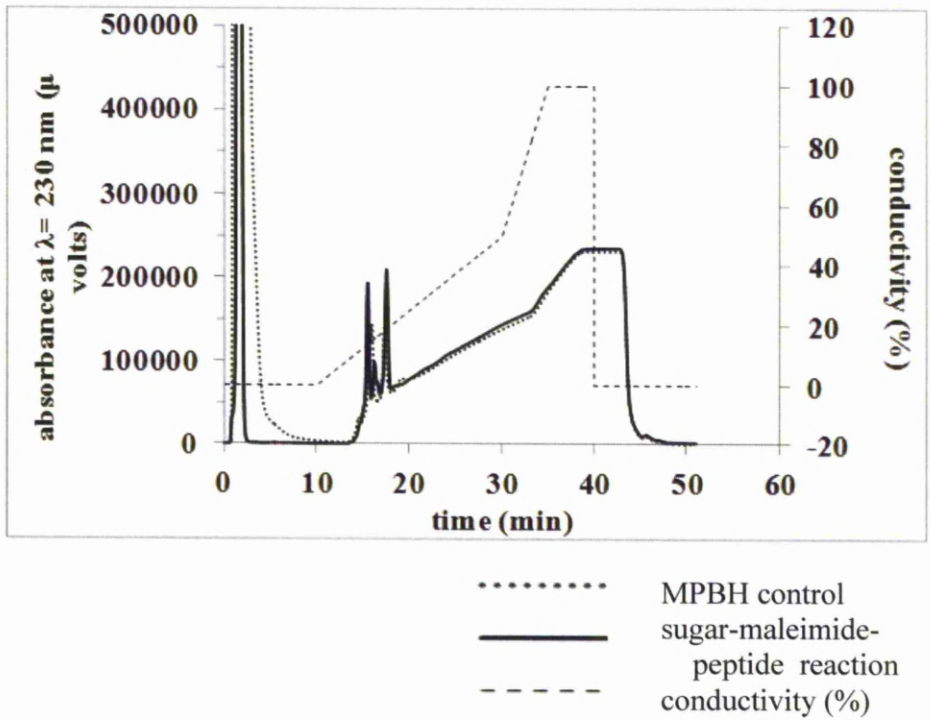

Figure 3.11: Anion-exchange chromatography of the products of reaction of sugar-maleimide (DP 8) and peptide in N-methyl formamide.

Analysis of the products of the reaction of sugar-maleimide from reverse phase HPLC fractions were made using anion exchange chromatography (230 nm). Sugar (DP 8)- maleimide and peptide were reacted in room temperature overnight. A Hitrap Q column (1 mL) was equilibrated in HPLC grade water. After application of the sample, the column was developed with a gradient of increasing 2 M NaCl in the same buffer at a flow rate of 1 mL/min, as described in Section 2.4.2. Peptide control: 10 mg/mL peptide was dissolved in N-methyl formamide and was added to 400 μL buffer A. Sugar-maleimide reaction: Sugar-maleimide conjugate (from reverse phase HPLC), fractions 13-36 minutes were reacted with peptide C(Acm)-Ala-Le-Asn-Asn-Gly-Gly-Cys-OH (10 mg/ml) in N-methyl formamide at room temperature overnight. Each sample was dissolved in 500 μl buffer A prior to injection. Fractions corresponding to the elution of oligosaccharide between 14 mins-41 mins were collected.

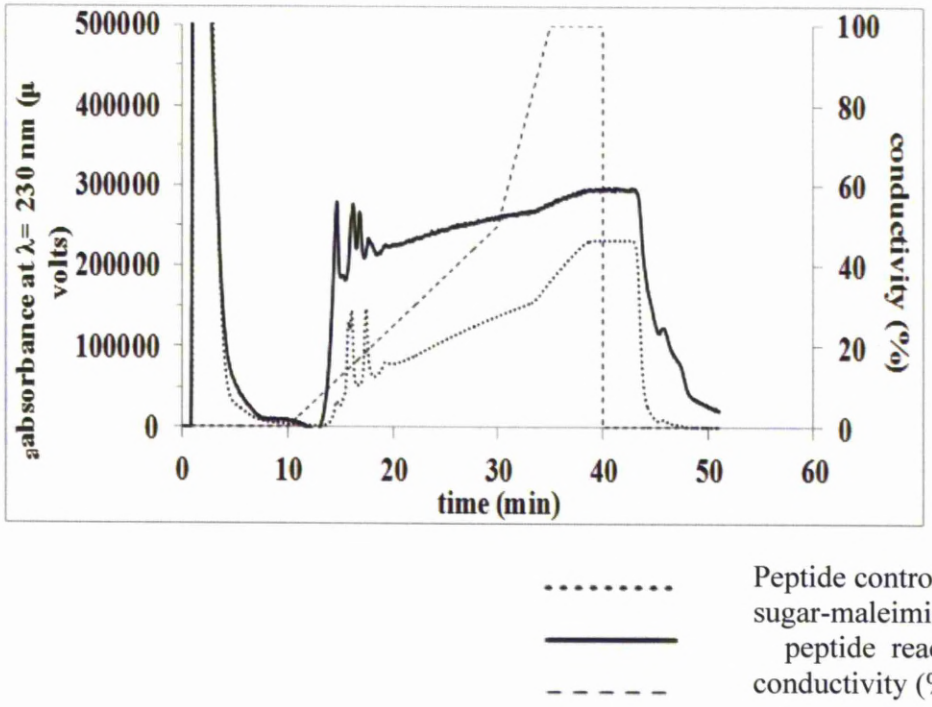

Figure 3.12: Anion-exchange chromatography of the products of reaction of sugar-maleimide (DP 12) and peptide in N-methyl formamide.

Analysis of the products of the reaction of sugar-maleimide from reverse phase HPLC fractions with peptide, using anion exchange chromatography (230 nm) was undertaken. Sugar (DP 12) maleimide and peptide was reacted in room temperature overnight. A Hitrap Q column (1 mL) was equilibrated in HPLC grade water. After application of the sample, the column was developed with a gradient of increasing 2 M NaCl in the same buffer at a flow rate of 1 mL/min, as described in Section 2.4.2. Peptide control: 10 mg/mL peptide was dissolved in N-methyl formamide and was added to 400 μL buffer A. Sugar-maleimide reaction: Sugar-maleimide conjugate (from reverse phase HPLC), fractions 13-36 minutes were reacted with peptide C(Acm)-Ala-Le-Asn-Asn-Gly-Gly-Cys-OH (10 mg/ml) in N-methyl formamide at room temperature overnight. Each sample was dissolved in 500 μl buffer A prior to injection. Fractions corresponding to the elution of oligosaccharide were collected between 14 mins-41 mins.

3.3.6 Reverse phase HPLC for products of sugar-maleimide-peptide conjugation

Samples of the reaction of sugar-maleimide with peptide for different sized oligosaccharides were analyzed on HPLC, using a C18 column (Fig 3.10 and Fig 3.11). The peptide controls were injected into the column. After 2 minutes, unbound peptide eluted from the column. The area of the peak was high, more than 500 000 μ volts at 214 nm for both chromatograms. After 10 minutes, ~10% of 80% methanol, peaks consistent with weakly bound peptide were eluted. The absorbance dropped to the base line after 20 minutes (Fig 3.13 and Fig 3.14). The samples of sugar-maleimide-peptide for both reactions (Fig 3.10) and (Fig 3.11) for both sizes of oligosaccharides, DP 4 and DP 8, were injected onto the column. Peaks eluting early (1-2 minutes) refer to the unbound peptide, where they elute from the C18 column. Hence, after elution with more than 10% of 80% methanol, several peaks appeared, consistent with sugar-maleimide-peptide and sugar-maleimide products. The relatively hydrophobic methanol permitted the retention of the hydrophilic oligosaccharides on the column. Although RPHPLC has been shown to be effective for the separation of depolymerised heparin, it did not provide adequate retention of intact heparin, which eluted in the column void. Those positive fractions were freeze dried for further experiment.

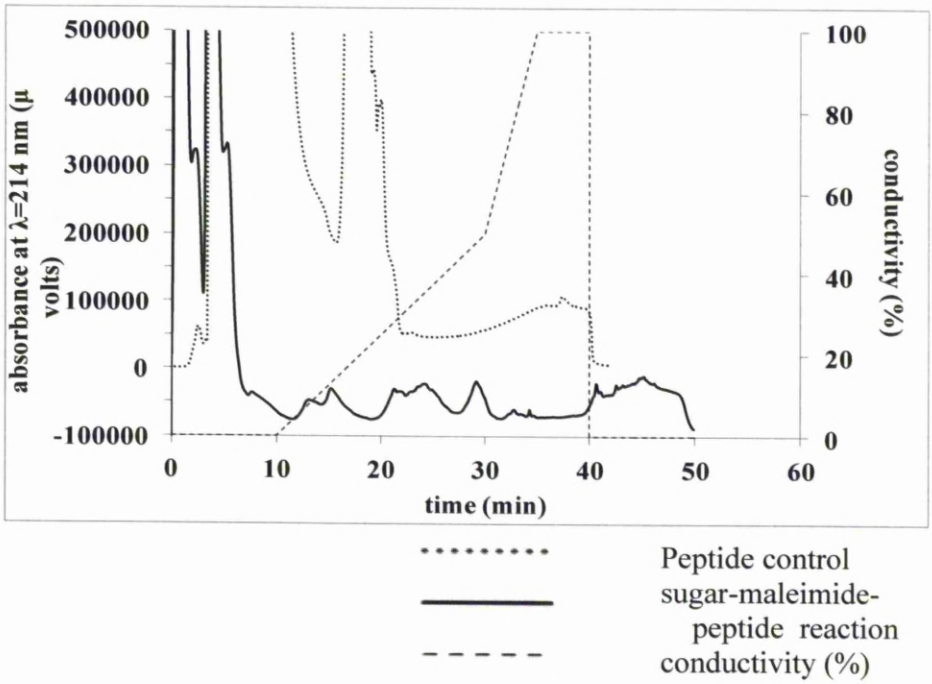

Figure 3.13: RPHPLC separation of sugar (DP 4)-maleimide-peptide on a 0-50% gradient over 20 minutes with 80% methanol elution buffer.

Analysis and separation of the products of reaction of sugar (DP 4)-maleimide collected from anion-exchange chromatography with peptide. A C18 column (250 mm×4.6 mm, 5μm particle size) was equilibrated in HPLC grade water. After application of the sample, the column was developed with a gradient of increasing of 80% methanol in the same buffer at a flow rate of 1 mL/min, as described in Section 2.4.2. Peptide control: Samples of peptide control collected from anion exchange chromatography fractions at retention time 0-12 minutes. Sugar-maleimide reaction: Samples from anion exchange chromatography fractions were collected and pooled at retention time 14-41 minutes.

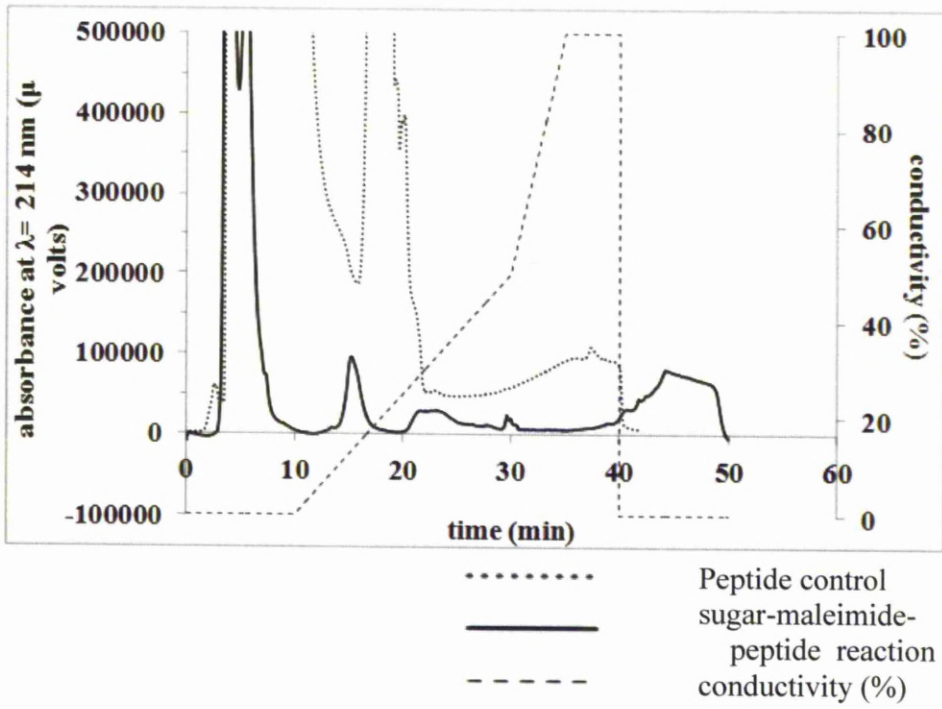

Figure 3.14: RPHPLC separation of sugar (DP 8)-maleimide-peptide on a 0-50% gradient over 20 minutes of 80% methanol elution buffer.

Analysis and separation of the products of reaction of sugar (DP 8)-maleimide peptide collected from anion-exchange chromatography. A C18 column (250 mm×4.6 mm, 5 μm particle size) was equilibrated in HPLC grade water. After application of the sample, the column was developed with a gradient of increasing of 80% methanol in the same buffer at a flow rate of 1 mL/min, as described in Section 2.4.2. Peptide control: Samples of peptide control were collected from anion exchange chromatography fractions at 0-12 minutes. Sugar-maleimide reaction: Samples from anion exchange chromatography fractions were collected and pooled at retention time 14-41 minutes.

3.3.7 *Mass spectrometry*

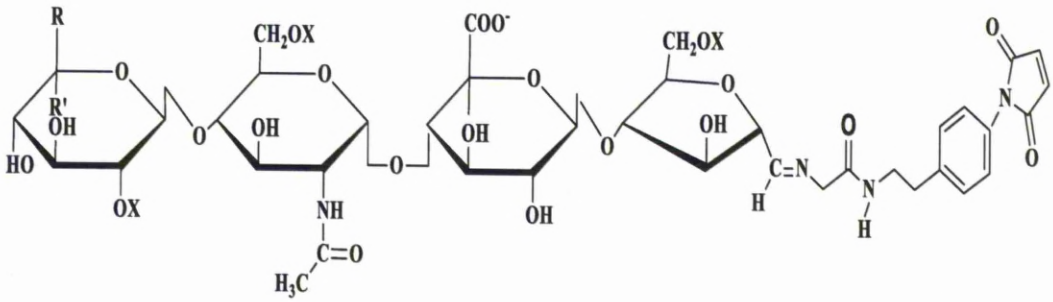

DP 4 oligosaccharide **MPBH**

Figure 3.15: The structure of DP 4 oligosaccharide conjugated with MPBH at the reducing end.

The structure of DP 4 oligosaccharide with 2,5-anhydromannose at the reducing end reacted with MPBH (maleimide-tag) analyzed by mass spectrometry. The result of successful product has been analysed in the mass spectrometry chromatogram in Fig. 3.16.

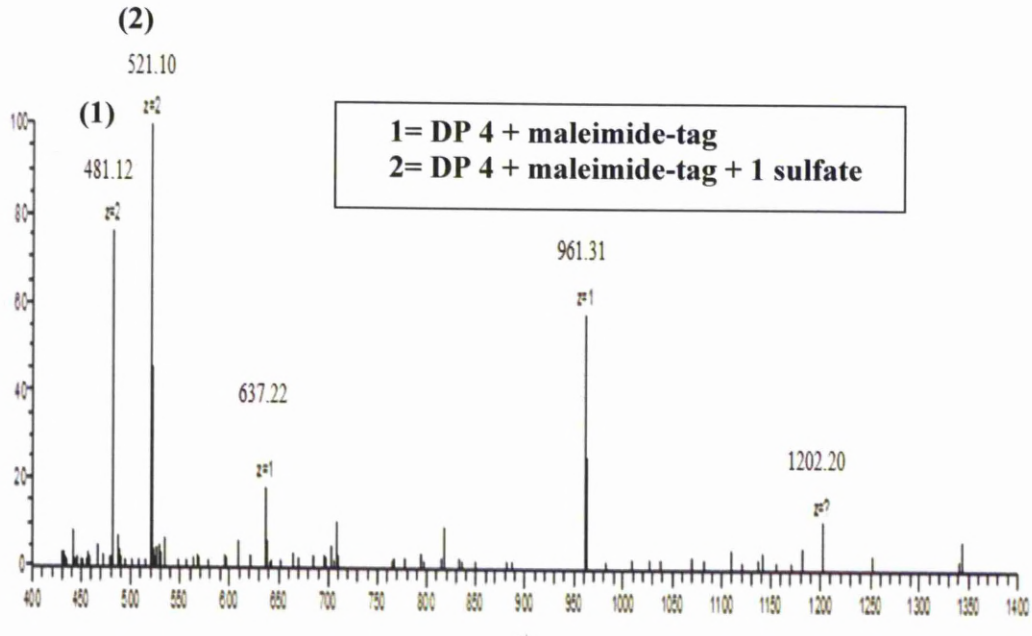

Figure 3.16: Mass spectrometry analysis.

ESI MS was performed by Rebecca Miller (University of Liverpool) on a sample, DP 4-tag a sample of which was taken and subjected to LCMS. A peak (19-20 minustes) was taken and analysed. The spectrum shows two clear ions at z=2, 481.12 and 521.10 (Fig 3.16). If a tetrasaccharide with the maleimide tag at the reducing end is considered, it has a mass of 942 or 1022, if there is one sulphate (Fig 3.16). Since the present compound is a sodium adduct, the ions will be $481[M+1Na-3H\}^{-2}$ and $521[M+1Na-3H\}^{-2}$ (Miller, 2011). The clear conclusion from this analysis is that reaction of the DP 4 with the maleimide tag conjugate has been successful. This interpretation is consistent with a mass of 272 associated with the tag.

3.4 Conclusion

Oligosaccharides produced by nitrous acid cleavage of heparin at low pH were analyzed by gel electrophoresis. Reaction times greater than 10 minutes yielded oligosaccharides of DP 4 to DP 16 and were pooled. Fractionation of these samples on a Superdex ™ 30 SEC chromatography (16 mm I.D. x 200 cm length) allowed the separation of the different size classes of oligosaccharides. These purified oligosaccharides represent the starting point for the remainder of the project. Nitrous acid digestion cuts the heparin chain at N-sulfated glucosamine to produce a reducing end anhydromannose, which is in the reactive aldehyde form. This is a better reactant for amines than enzyme-cleaved heparin, which has a reducing end N-sulfate glucosamine in equilibrium between the closed ring, (which predominates) and the open reducing form.

Several batches of sugar-maleimide were successfully made by reacting the reducing (aldehyde) function with MPBH (4-(4-N-Maleimidophenyl)butyric acid hydrazide hydrochloride; the hydrazide moiety of the latter reacts through a Schiff's base with the reducing end of the sugar. Analysis by FPLC shows successful reaction and clearly identifies MPBH modified oligosaccharide with a maleimide function at the reducing end. This will react stoichiometrically with thiols. The products of conjugation were separated by using anion exchange and reverse phase chromatography. Mass spectrometry has been used to measure mass to charge ratio of the samples. The successive products of conjugation are clearly shown in the mass spectrogram.

CHAPTER 4

Functionalization of a DPI sensor surface

4.0 Functionalization of a DPI sensor surface

4.1 Introduction

Measurement of the interactions of proteins with sugars at surfaces using optical techniques has provided much valuable information. However, it is also clear that the immobilisation of the sugar can interfere with subsequent protein binding, e.g., [58]. Dual polarization interferometry (DPI) is a surface-based technique, which uniquely allows real-time measurement of the changes in thickness, refractive index and the mass of adsorbed material, 100 nm thick, or less, on the surface of a functionalized waveguide [83]. As a consequence, DPI may provide information concerning the orientation of sugars on a functionalized surface before their interaction with selected proteins. Thus, in principle, the engineering of a sugar functionalised surface using DPI would allow the interaction of the sugar with proteins to mimic that occurring at the cell surface. Moreover, DPI is far more sensitive than suface plasmon resonance, which means that small oligosaccharides are readily detected.

In a DPI instrument, the sensor chip has three waveguides or channels. Channels 1 and 3 are exposed to the flow and so are used to bind molecules, while channel 2 is buried and is used as the reference. The instrument measures changes in both the magnetic and electrical polarisations of light, Transverse Magnetic (T_M) and Transverse Electric (T_E), respectively. These two measurements enable the response of the instrument to be converted directly into changes in refractive index, the thickness of the bound molecules, the mass of the bound molecules and their density. These calculations are performed using the instrument software and the initial calibration of the refractive index of the sensor chip using 20% (v/v) ethanol in

water, and water with PBS running buffer (Section 2.3.3). A set of experiments were performed on a dual polarization interferometer with two aims. One aim was to test the reactivity of the maleimide-sugar described in Section 3.1. The second aim was to determine whether such sugars would provide a new means of producing a functionalised surface where the saccharides were not engaged in substantial interactions with the underlying surface, i.e., in which they were fully exposed to the solvent rather than lying down.

Previous work has included immobilised, nitrous acid-cleaved oligosaccharides linked directly to a hydrazide functionalised surface [38]. However, this approach consumed a large amount of oligosaccharide, since the reaction is inefficient (Chapter 3). Moreover, evidence suggested that the immobilised oligosaccharide were lying down and so probably associated on one side with the underlying surface. This may be the consequence of unreacted hydrazide goups interacting with sulfate and carboxyl groups on the oligosaccharides. The present approach sought to avoid these issues, by reacting the oligosacchairdes *ex-situ* with MPBH and then employing a thiol surface.

Before attempting to make oligosaccharide-functionalised surfaces, the interactions of FGF1 with DP6 and DP12 were characterised by isothermal titration calorimetry. This aimed to provide a baseline reference for any subsequent quantification of binding parameters achieved on the DPI with an immobilised oligosaccharide.

4.2 Isothermal titration calorimetry

For ITC, the concentration of protein in the cell should be around 5 times the value of the equilibrium dissociation constant (Kd), while a concentration of sugar in the injection syringe ligand should be ten times higher than that of the protein, to ensure saturation of the binding reaction. The syringe containing a sugar was titrated (injected) into the cell containing a solution of the protein. For an exothermic reaction, an injection of the binding partner (sugar in this instance) results in the evolution of heat, which causes the feedback power to the sample cell to be decreased in so that an equivalent temperature can be maintained in the two cells. In an endothermic reaction, the opposite occurs; the feedback circuit increases the power in order to maintain an equal temperature. When the protein in the cell becomes saturated with added sugar, the heat signal diminishes until only the background heat of dilution is observed (Fig. 4.1). Data were plotted as the power in μcal/sec required to maintain the reference and the sample cell at identical temperatures and is expressed as a function of time in seconds. As a result, the raw data for an experiment consisted of a series of spikes of heat flow (power), where every spike corresponds to a ligand injection (Fig. 4.1 A, B, upper panels). These heat flow spikes/pulses were integrated with respect to time, giving the total heat effect per injection (Fig. 4.1 A, B lower panels). The pattern of these heat effects as a function of the molar ratio [ligand]/[macromolecule] was then be analysed to provide the thermodynamic parameters of the interactions. It should be noted that degassing samples is necessary in order to minimize interference arising from the presence of air bubbles. In the top panel in Figure 4.1, the peaks indicate the heat absorbed after each addition of heparin. Figure 4.1A shows the data for a FGF1-DP 6 interaction. These do not reach saturation level, in all likelihood, because the concentrations of

protein and oligosaccharide are insufficient. The stoichiomoetry for this reaction was calculated to be 1.2±0.05. The interaction of FGF1-DP 12 was approximately sigmoidal (Figure 4.1B), yielding a stoichiometry of 0.63±0.02. The calculated affinities (Kd) for protein-sugar binding for FGF1 and DP 6 was 14 ± 3.6 μM and for FGF1 and DP 12 was 23 ± 17 μM at 25°C (Figure 4.1). While these measurements were not optimal, because the concentrations of FGF1 and oligosaccharides needed to be higher, they clearly demonstrate that the oligosaccharides prepared by partial nitrous acid degradation bind FGF1. Moreover, they highlight an important difference between such solution measurements and those conducted on sensor surfaces; the affinity measured here for FGF1 and DP6 and DP12 is far lower than that measured by others for FGF1 and HS using surface techniques [42]. This is discussed in Section 4.4.

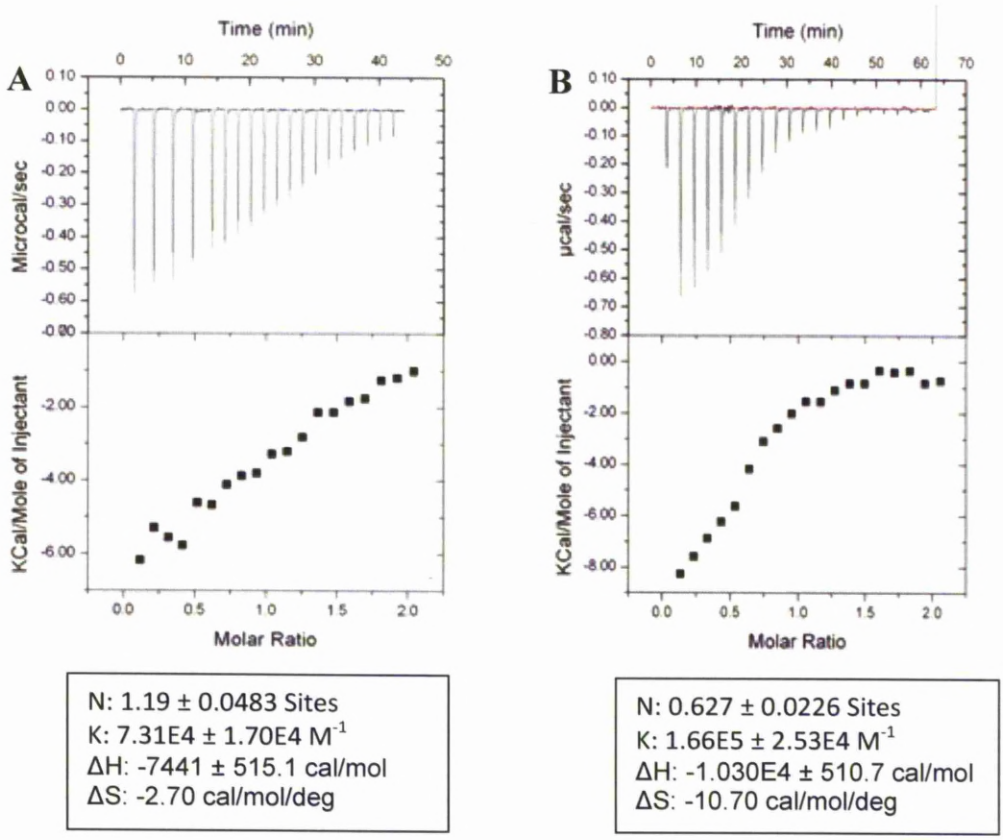

Figure 4.1: Isothermal calorimetry of protein-ligand interactions (FGF1 with DP 6 and DP 12).

Protein-oligosaccharide interactions were measured in an ITC_{200}^{TM} (Microcal, LLCEurope, Milton Keynes) with a cell dimension: 16.5 x 33 x 26.7 cm and a cell volume of 0.2 mL. A, DP6; B, DP12. FGF1 was placed in the cell separately while the ligand (DP 6 and DP 12) was maintained in a syringe at 500 µM. The total injection time was 30 min and the gap between injections was 180 sec. The experiment was carried out at 25°C.

4.3 Strategy of the DPI experiment

Figure 4.2 shows a schematic of the functionalisation and blocking of a channel surface. The thiol surface is prone to non-specific binding, so a blocking step, comprising hydrazide derivatisation of the thiols remaining on the surface after reaction with oligosaccharide and then reaction with the aldehyde-PEG.

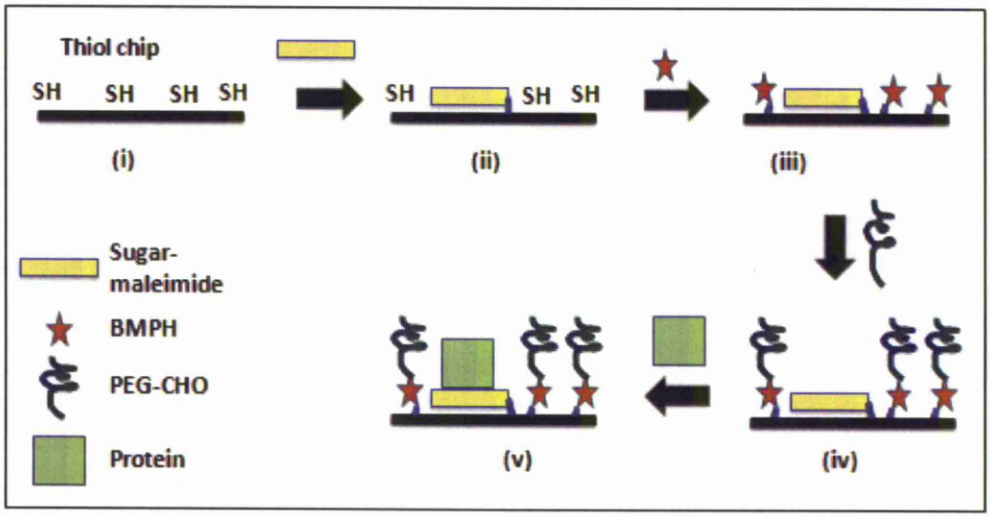

Figure 4.2: Schematic of dual polarization interferometry experiment on a working channel.

Material from fractions containing putative oligosaccharides-MPBH conjugate from AEC analysis were reacted with a thiol on a DPI surface in channel 1 (working channel), as shown in (ii). The unreacted thiols were then reacted with a linker, BMPH (*N*-[ß-maleimidopropionic acid] hydrazide, trifluoroacetic acid salt), (iii). PEG-aldehyde blocking agent was then applied to the hydrazide sites of BMPH to prevent non-specific binding, (iv). Different proteins were then injected to measure binding to the sugar-maleimide surface, (v).

4.3.1 Immobilization of sugar-maleimide onto a thiol surface

Material from fractions containing the putative oligosaccharides-MPBH conjugate from AEC analysis were injected onto a thiol DPI surface. With the instrument running in PBS, the sugar-maleimide DP 8, (30 µl 10 mg/ml in 400 µl PBS) was injected onto the surface of the working channel at 17 uL/min (arrow 1, Fig. 4.3). This was the second of three injections of sugar-maleimide and resulted in a gradual increase in T_M and T_E (Fig 4.3 A). At the end of the injection the surface was washed with PBS (arrow 2 Fig 4.3 A). This caused a decrease in

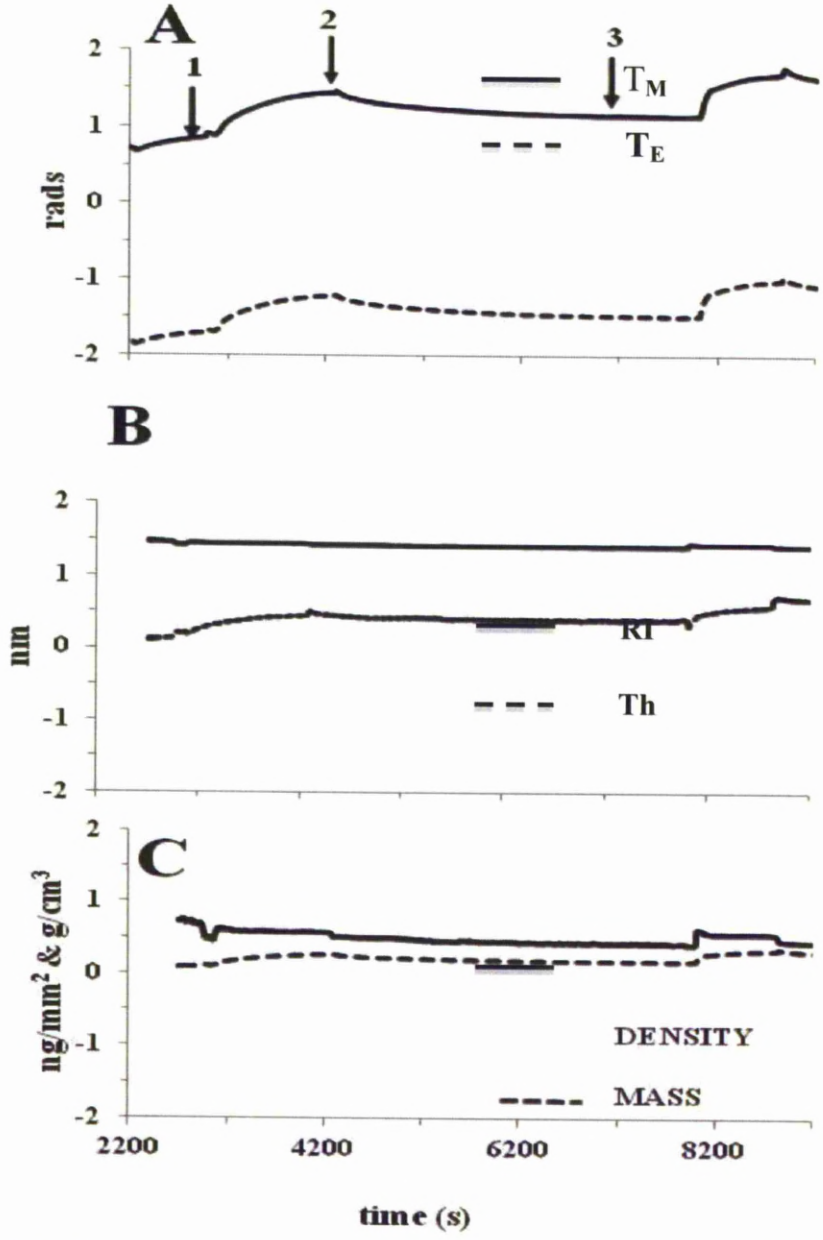

Figure 4.3: Coupling of putative oligosaccharides-MPBH from AEC analysis onto a DPI surface.

Changes in T_M and T_E upon immobilization of sugar-maleimide onto a thiol chip surface. (A) change in T_M and T_E in radians. (B) Change in refractive index (RI) and thickness (Th) calculated from the changes in in T_M and T_E. (C) =Associated changes in density and mass. Arrow 1, 2 and 3 indicate injection of sugars.

T_M and T_E (arrow 3 Fig 4.3 A), due to the difference in the refractive index of the solutions (PBS + DP 8 *versus* PBS) and to desorption of non-covalently bound DP8, but not to baseline. Thus, the difference in refractive index before the injection of DP 8 and after the PBS wash demonstrates that the sugar-maleimide has bound to the thiol surface. From the T_M and T_E values the refractive index (RI), thickness (Th) and mass [83] were calculated, showing that 0.292 ng/mm^2 of the sugar was bound to the surface with a thickness of 0.668 nm to give a density of 0.436 g/cm^3 (values compared to the original, unreacted thiol surface) (Table 4.1). The thickness was considerably lower than that expected for a DP 8, which would have approximate dimensions of 1 nm x 1 nm x 4 nm. Thus, if the sugar was lying down on the surface, then its thickness would be of the order of 1 nm. A number of factors are likely to contribute to these discrepancies. The analysis assumes an optically homogenous layer [83]. This assumption is met with a surface coverage of 16% or higher. It should be noted that this figure represents a percentage of close packing, not the physical coverage. Close packing will always be less than 100% for charged oligosaccharides possessing both flexibility and a high aspect ratio. Above 16% surface coverage, the thickness of the adsorbed layer is calculated to the extremity of the bound molecules and the gaps between the molecules do not affect the calculation. However, below 16% coverage, the average thickness of the absorbed molecules, including the gaps, which have a thickness of zero, is calculated. The lower level of oligosaccharide immobilised in the present work may be below that required to give 16% coverage.

These data show clearly that the sugar-maleimide has indeed reacted with the surface. This provides direct evidence for the successful conversion of at least some reducing ends of the oligosaccharide to a maleimide. However, comparison with a previous approach, where comparable oligosaccharides derived from heparin by nitrous acid cleavage were reacted directly with a hydrazide surface [38] indicates that approximately one third of the oligosaccharide was immobilised in the present case. Why less maleimide-sugar was immobilised is a puzzle. The maleimide-thiol reaction is known to be extremely efficient and, even if only a small fraction of the reducing ends of the total reacted oligosaccharide was in fact successfully converted to a maleimide, a far greater level of reaction would be expected. The low thickness indicates that the sugar is lying down on the thiol surface. Two possible explanations for the relatively low coverage of oligosaccharide observed in the present experiments may relate to the different ways that the sugar may interact with the underlying surface. The first is that on the thiol surface, the oligosaccharide blocks more potential positions of reaction than it does on the corresponding hydrazide surface, simply because of charge neutralisation of sulfates and carboxyl groups in the sugar by the hydrazide groups. A second is that through these charge interactions, a high local concentration of oligosaccharide is achieved at the surface, which increases the number of reactions.

4.3.2 Coupling of linker (BMPH) and blocking with PEG-CHO

BMPH (5 mg/mL in buffer) was injected onto both channels (working and control channel) for 30 min. After washing with PBS, PEG-CHO was injected for 120 min. The reaction of this surface with BMPH resulted in a slight decrease in RI to 1.409 compared to the RI value of the sugar-maleimide surface, which was 1.414. The

value for thickness, mass and density of the layer after the addition of BMPH were 0.799 nm, 0.327 ng/mm^2 (values compared to the original surface, so DP8-MPBH plus BMPH), 0.63 g/cm^3 respectively. This indicates that the BMPH (dimensions ~0.5 nm) has been incorporated into the thiol-DP 8 substructure, which would be expected. To block the surface and thereby reduce non-specific binding of proteins, PEG-CHO was reacted with free hydrazide groups. The values for RI, thickness, mass and density show that some PEG-CHO reacted with the surface (Table 1). However, the amount of PEG-CHO was low compared to that obtained previously [38]. In the case of the working channel previously reacted with sugar-maleimide, this could be explained by the presence of the oligosaccharide, but why the level of reaction was also lower in the control channel is not clear.

	RI	Thickness, th (nm)	Mass (ng/mm^{-2})	Density (g/cm^3)	Mean ± Std Dev for RI	Mean ± Std dev for th	Mean ± Std Dev for mass	Mean ± Std Dev for density
				Working channel				
Sugar-maleimide	1.414	0.668	0.292	0.436	1.432 ± 0.02	0.606 ± 0.07	0.393 ± 0.04	0.618 ± 0.16
BMPH	1.409	0.799	0.327	0.41	1.422 ± 0.02	0.751± 0.08	0.436 ± 0.05	0.550 ± 0.10
PEG-CHO	1.409	2.299	0.939	0.408	1.434 ± 0.03	1.920 ± 0.58	1.236 ± 0.2	0.643 ± 0.29
				Control channel				
BMPH	1.341	2.563	0.088	0.034	1.372 ± 0.04	3.073 ± 4.04	0.137 ± 0.07	0.228 ± 0.24
PEG-CHO	1.419	1.75	0.811	0.463	1.429 ± 0.02	1.702 ± 0.63	0.950 ± 0.23	0.609 ± 0.21

Table 4.1: Surface measurement using Dual Polarization Interferometry (DPI).

DPI with immobilization of sugar-maleimide onto a thiol chip surface, addition of BMPH linker, and blocking with PEG-CHO. Measurement of changes in refractive index (RI), thickness (Th), mass and density of each DPI experiment are followed by the corresponding mean values ± standard error of four independent experiments.

4.3.3 Protein injections

The thiol-DP 8 surfaces blocked with PEG (Section 4.3.2) were used to study the interactions of two fibroblast growth factors, FGF1 and FGF2 with the immobilised sugar. These FGFs were chosen because their interactions with heparin and HS is well characterised and FGF2 has been used previously in an analogous surface made by direct reaction of the reducing end of heparin oligosaccharides with a hydrazide surface [38]. The FGFs were injected over a range of concentrations at 50 μL/min in PBS; FGF 2 between 3 nM and 464 nM (Fig. 4.4), and FGF 1 between 5.7 nM and 229 nM (Fig. 4.4). In both cases, as the concentration of the FGF increased, the level of binding increased, indicating that binding was concentration dependent (Figs 4.4 and 4.5). Importantly, after the surface was returned to PBS, washing the surface with 2 M NaCl was found to remove all bound FGF, since the response returned to the baseline observed prior to injection of protein. Thus, this wash was sufficient to regenerate the surface, and so allow multiple cycles of protein binding. This also suggested that the interaction of the FGF with the surface was driven by charge and so was likely to reflect and interaction with the immobilised DP 8.

The thickness of the layer also increased as the concentration of FGF was increased, though this effect was more marked for FGF-1 than FGF-2 (Tables 4.2 and 4.3). However, changes in mass were much more modest. This suggested that the capacity of the surface for binding FGF-1 and -2 was low, which is in agreement with the low level of DP 8 immobilised (Section 4.3.1). In each case, the control channel (thiol surface reacted with hydrazide and then blocked with CHO-PEG) was also challenged with the same concentration of FGF1 or FGF2. The response of the

control channel was almost identical in terms of the refractive index changes (Tables 4.2 and 4.3). However, this does not mean that the two responses are due to the same binding events. This is because the presence of DP 8 may reduce or even prevent non-specific binding to the underlying thiol/hydrazide surface. The Analight uniquely allows the "position" of the bound species to be determined. Thus, although the increases in mass are very similar for control and experiment, a comparison of the density and thickness values (Tables 4.3 and 4.4) provides direct information as to where the FGFs are binding. The DP 8 layer was around 0.6 nm thick (Table 4.1). The PEG layer extended beyond this, to around 1.9 nm (Table 4.1). The increase in thickness observed upon FGF-2 binding to the DP 8 derivatised channel was consistently higher than in the corresponding control channel (Table 4.2; between ~0.5 nm and 0.7 nm greater). Similarly for FGF-1, where binding to the DP 8 surface resulted in a ~ 0.4 to 0.7 nm increase in layer thickness compared to the non-specific binding (Table 4.3). The consequence is that the density of the layer of non-specifically bound FGF-2 and FGF-1 was higher (by around 20%) that the layer formed on the DP 8 surface. This demonstrates that the FGFs are bound at different heights on the two surfaces; the differences are consistent with the height of the DP 8 (6 nm, Table 4.1). Thus, these data argue that on the DP 8 derivatised surface, the FGFs are largely bound to the sugar, rather than to the underlying surface. That is much of the binding is actually specific. However, it is not possible to quantify the relative levels of specific and non-specific binding in the DP 8 surface. Allied to the low levels of DP 8 immobilied, which reduce confidence in the absolute values of the calculated thicknesses this means that the binding of FGF2 and FGF-1 to the DP 8 surface could not be used to calculate affinities or stoichiometries.

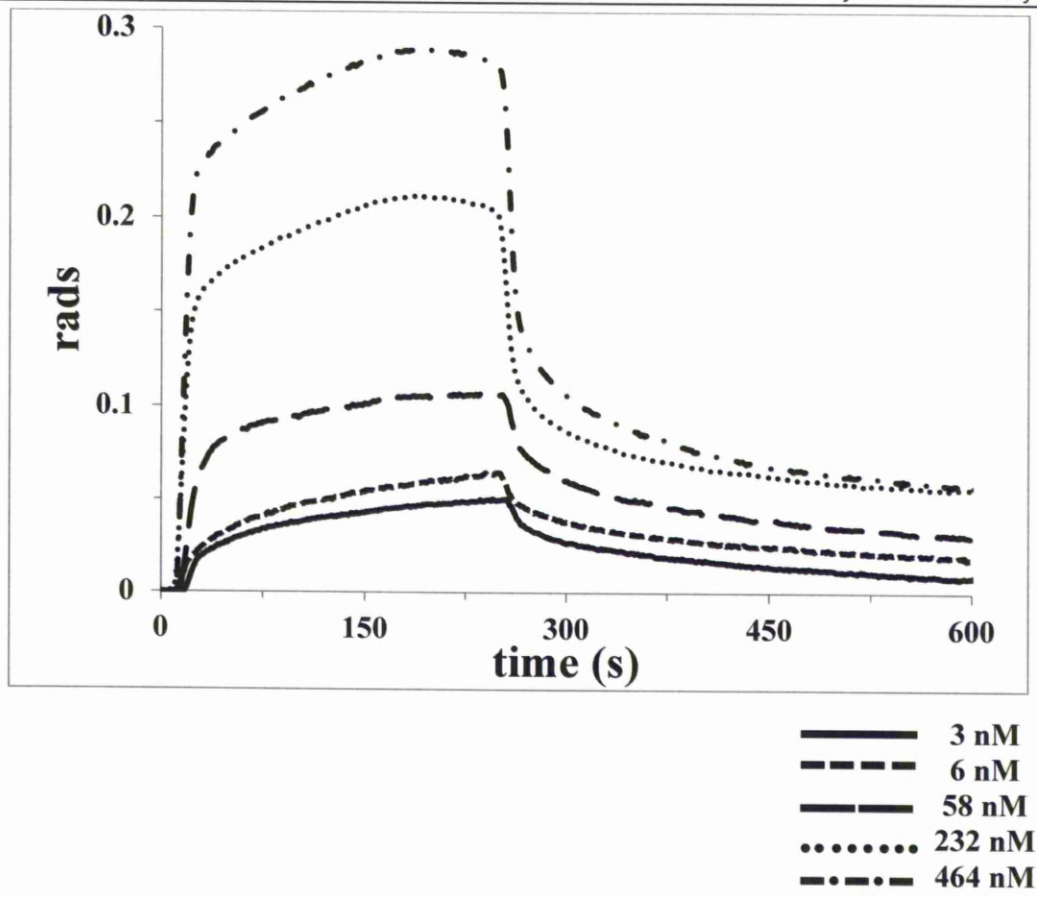

Figure 4.4: Binding of FGF 2 to immobilized sugar-maleimide.

FGF 2 at different concentrations was added to the sugar functionalised surface and the response in Tm and were Te measured by DPI. For clarity, only the response of Tm is shown (radians). Surfaces were regenerated by injection of 2 M NaCl.

Name	RI	Th (nm)	Mass (ng/mm^{-2})	Density (g/cm^3)
		Working channel		
FGF2 (3 nM)	1.414	2.211	0.960	0.434
FGF2 (6 nM)	1.413	2.250	0.965	0.429
FGF2 (58 nM)	1.411	2.329	0.970	0.416
FGF2 (232 nM)	1.413	2.300	0.983	0.427
FGF2 (464 nM)	1.412	2.365	0.997	0.422
		Control channel		
FGF2 (3 nM)	1.419	1.658	0.769	0.464
FGF2 (6 nM)	1.424	1.612	0.791	0.491
FGF2 (58 nM)	1.422	1.661	0.792	0.477
FGF2 (232 nM)	1.422	1.661	0.792	0.477
FGF2 (464 nM)	1.421	1.738	0.822	0.473

Table 4.2: Changes in refractive index, thickness, mass and density of surface layer after injection of FGF2.

Refractive index (RI), thickness (Th) of the bound layer of proteins, the mass of bound protein and the density were calculated using the Analight analytical software package.

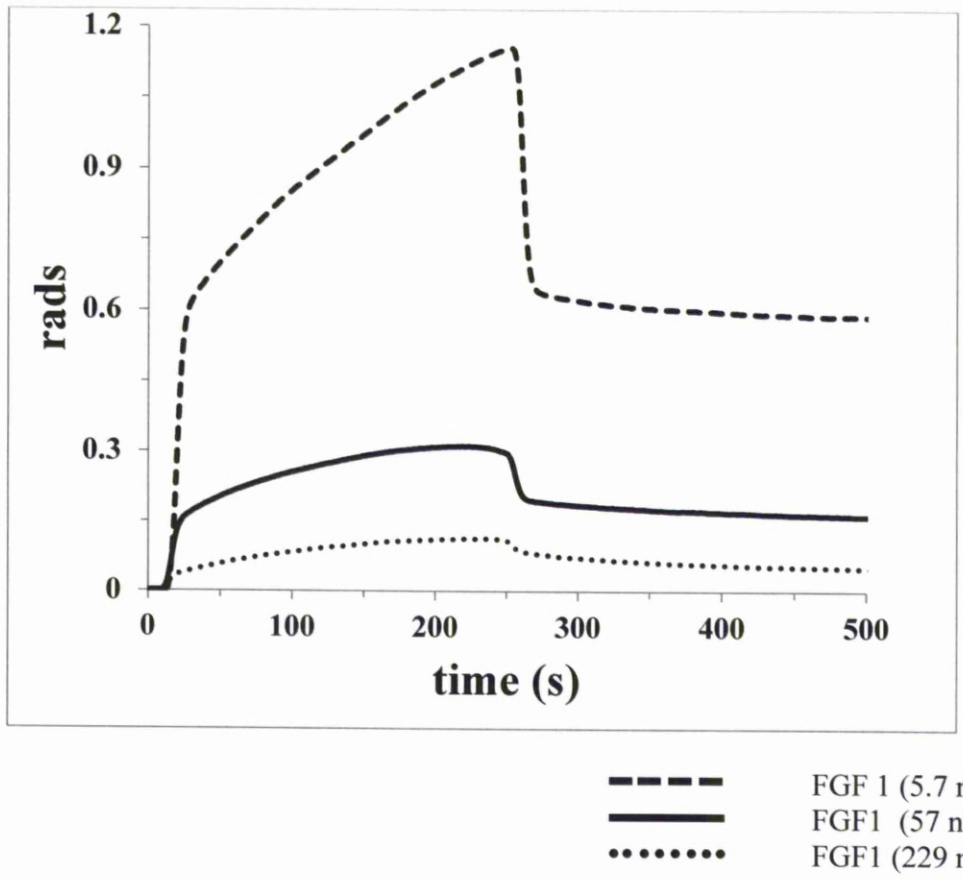

Figure 4.5: Binding of FGF1 to immobilized sugar-maleimide.

FGF1 at different concentrations was added to the sugar functionalised surface and the response in Tm and Te measured by DPI. For clarity, only the response of Tm is shown (radians). Surfaces were regenerated by injection of 2 M NaCl.

Name	RI	Th (nm)	Mass (ng/mm^{-2})	Density (g/cm^3)
		Working channel		
FGF1 (5.7 nM)	1.405	2.389	0.927	0.388
FGF1 (57 nM)	1.405	2.522	0.968	0.384
FGF1 (229 nM)	1.402	3.049	1.126	0.369
		Control channel		
FGF1 (5.7 nM)	1.414	1.906	0.826	0.433
FGF1 (57 nM)	1.411	2.047	0.859	0.420
FGF1 (229 nM)	1.409	2.355	0.961	0.408

Table 4.3: Changes in refractive index, thickness, mass and density of surface layer after injection of FGF1.

Refractive index (RI), the thickness (Th) of the bound layer of proteins, the mass of bound protein and its density were calculated using the Analight analytical software package.

4.4 Conclusion

Previous work [38] showed that nitrous acid derived oligosaccharides do not react with this thiol surface. Thus, the present DPI experiments demonstrate that the oligosaccharide-maleimide retained its reactivity, since it was successfully immobilised on the thiol surface. However, the amount of sugar-maleimide immobilised was consistently lower than that achieved previously involving the reaction of the oligosaccharide reducing ends with a hydazide surface [38]. Moreover, it seems likely that the oligosaccharides were lying down on the thiol surface. This is suggested by the thickness of the sugar layer. Blocking of the thiol surfaces with PEG was not as efficient as in previously published work [38]. The low efficiency of blocking was reproducible and a variety of strategies (overnight incubation of surfaces in PEG-CHO following BMPH reaction with the flow stopped and/or repeated injections of PEG-CHO) failed to increase the amount of PEG on the surface. The result was considerable non-specific binding to the control channel (Tables 4.2 and 4.3). The response of the control channel was only a little lower than that of the working channel, but it is clear from the analysis of the thickness and density data that the non-specifically bond FGF2 and FGF1 are interacting with the underlying surface. In contrast, in the working channel the FGFs are interacting with something above the surface, at a height consistent with the thickness of the immobilised DP 8. However, because of the uncertainty as to the contribution of non-specific binding observed in the working channel and of affinity and stoichiometry was not performed.

Technique	Protein & sugar	KD (μM)	ΔH (cal/mol)	ΔS (cal/mol/deg)	N (sites)
ITC	FGF1 & DP6	14 ± 3.6	-74000 ± 520	-2.70	1.2 ± 0.05
	FGF1 & DP12	23 ± 17	-10000 ± 510	-10.7	0.63 ± 0.02
OPTICAL BIOSENSOR (Rahmoune *et al*, 1998)	FGF1 & HS	0.49	-	-	-

Table 4.4: ITC results.

Comparison of ITC results and those from measurements of the interaction of FGF1 with HS measured in an optical biosensor. In the latter experiments, the binding kinetics were measured and used to derive the Kd. Consequently, these experiments only measured the highest affinity binding site on the HS, since they depend on measuring monophasic kinetics.

In the ITC measurements, the affinity of the FGF1-DP6 and the FGF1-DP12 interactions was around 40-fold lower than that measured for FGF1 binding HS in an optical biosensor (Table 4.4 and [42]. One explanation is that in ITC all binding sites are saturated. Even with heparin-derived oligosaccharides there is considerable heterogeneity of structure. Thus, the affinity measured by ITC would reflect the average affinity of FGF1 for all these structures. In optical biosensor experiments, where kinetics are measured, it is the interaction with the highest affinity sites that is measured. However, this may not be the entire explanation. For example, in experiments where saturation was reached, the Kd measured by DPI for FGF2 binding to a DP10 from heparin [38] was similar to that determined in kinetic experiments with an optical biosensor [26]. In contrast, ITC measurements of FGF2 binding to heparin determined an affinity ~10 fold lower [84].

Therefore, there must be some other difference between the surface and solution measurements that accounts for these discrepancies. One possible contribution might be from the secondary binding sites for heparin that exist in many FGFs. Originally discovered in FGF2 [61,85,86] and then subsequently confirmed in FGF2 by proteomics [87]. A recent study has demonstrated their existence in a number of other FGFs, including FGF1 [88].

These secondary binding sites are of much lower affinity than the canonical binding site [61]. With oligosaccharides immobilised on a surface, engagement of the sugar by the cannonical binding site of the FGF would prevent any interaction of the lower affinity secondary binding sites. Only one face of the oligosaccharide is likely to be available for protien binding because of steric hindrance by the underlying surface, particualrly as sugars seem to lie down on [38]. In contrast, in a solution assay using

heparin, which is a considerably longer polymer, the secondary bidning sites may play a role and so contribute to the lower affinity, which would be the average of the cannonical binding site and one or more of the secondary binding sites.

Therefore, there may be some fundamental difference between the surface and solution measurements that needs resolving.

CHAPTER 5

Functionalization NPs with an oligosaccharide

5.0 Functionalizing NPs with an oligosaccharide

5.1 Introduction

Gold nanoparticles have very high extinction coefficients and they do not bleach. The result is that they are very interesting probes for imaging biological molecules. Since direct coupling of oligosaccharides to peptides was not effective, in this chapter the functionalisation of gold nanoparticles with the oligosaccharide-maleimide (Chapter 3) is explored. To react a maleimide-sugar with the nanoparticles, it is necessary to place a thiol on the nanoparticle ligand shell. However, thiols incorporated directly into the ligands of the nanoparticle would, during the initial ligand shell formation step, bind to the gold surface and so be unavailable for reaction with the sugar-maleimide. Moreover, if a ligand with a thiol at each extremity was used, this would lie down on the gold surface and would represent a major defect in the ligand shell, compromising the stabilty of the nanoparticles. Therefore, a new ligand shell for nanoparticles was designed, which would allow the addition of a thiol in a step subsequent to the formation of a ligand shell.

To provide a benchmark, the mixed matrix ligand shell [72], which consists of alkane thiol ethylene glycols (SH-PEG) and a peptidol (CVVVT(ol)), was used in stability tests. Dithiothreitol (DTT) was used to probe nanoparticle stability, because it is a small, uncharged dithiol. Thus, if there were defects in the ligand shell, DTT would replace the ligands on the gold nanoparticle in a ligand-exchange reaction. In the presence of electrolytes, DTT does not impart colloidal stability to nanoparticles and they will aggregate, which causes a redshift of their absorbance and the loss of

the characteristic plasmon band at ~520 nm. Thus, DTT-mediated ligand exchange provides a rapid and effective means of testing the integrity of a nanoparticle ligand shell [71].

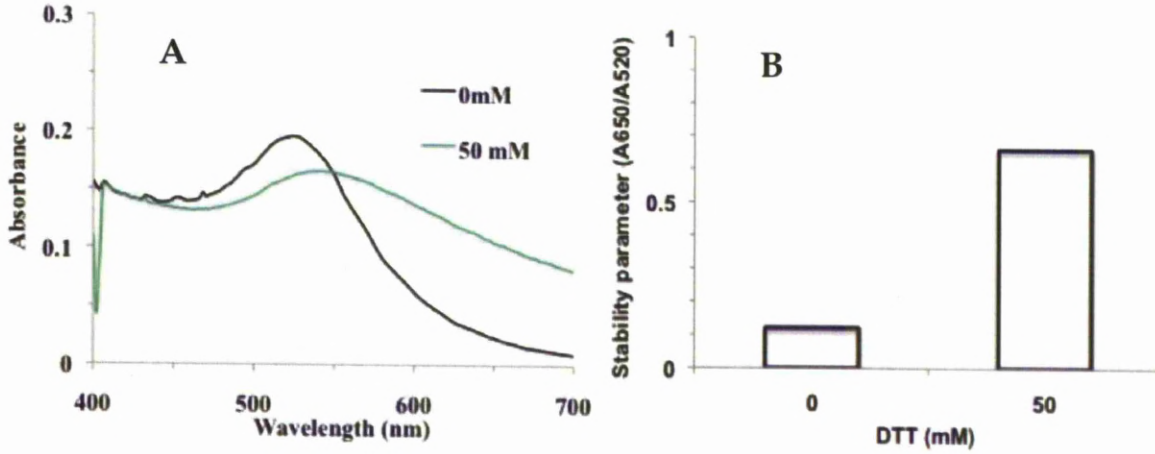

Figure 5.1: Calculation of a stability parameter for gold nanoparticles.

8.6 nm diameter gold nanoparticles were capped with a mixed-matrix ligand shell. The nanoparticles were then subject to incubation for 48 in 0.5 M NaCl in the presence and absence of DTT. The absorbance spectrum (A) was then used to calculate a stability parameter, the ratio of absorbance at 650 nm to that at 520 nm, corresponding to the plasmon band. A stability parameter of over 0.2 indicates aggregation of the nanoparticles.

Figure 5.2 shows the stability of mixed matrix stabilised ligand gold nanoparticles after incubation in 0.5 M NaCl in the presence and absence of DTT. As found previously by others [71,72], the mixed matrix nanoparticles are stable in 0.5 M NaCl. This is demonstrated by the typical plasmon band at 520 nm and an absence of absorbtion at longer wavelengths (Fig. 5.1 A). In contrast, in the presence of DTT, after 48 h there is a redshift in the plasmon band and an increase in absorbtion at longer wavelengths (Fig. 5.1A). To allow the analysis of multiple spectra of nanoparticles, a stability parameter is calculated, as the ratio of absorbtion at 650 nm to that at the plasmon band, 520 nm for this size of nanoparticles. The stability parameter clearly increases when the nanoparticles aggregate (Fig. 5.1B). The concentration dependence of DTT-induced ligand exchange was then determined, by acquiring uv-vis spectra for mixed-matrix nanoparticles incubated with different concentrations of DTT for various times (Fig. 5.2). The mixed-matrix nanoparticles were stable for up to 21 h in 50 mM DTT. However, at longer times (48 h), there was evidence for ligand exchange occurring from around 15 mM DTT.

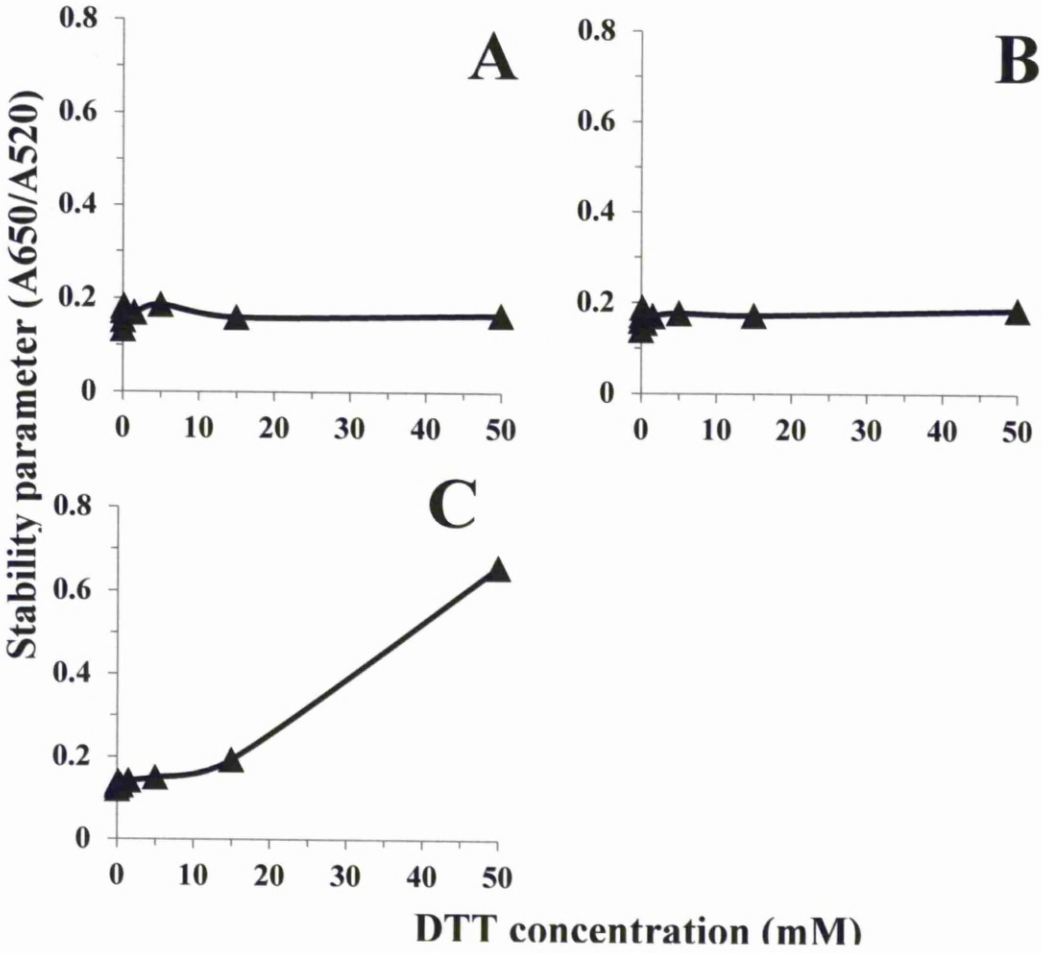

Figure 5.2: DTT-induced ligand exchange of mixed matrix stabilised gold nanoparticles.

DTT was added to mixed matrix stabilised gold nanoparticles in the presence of 0.5 M NaCl and the UV-vis spectra between from 400-700 nm were recorded at various times. The stability parameter was calculated as the ratio of absorbances 650 nm/520 nm. If this falls below 0.2, the nanoparticles are considered to be stable.Absorbance (650nm/520nm) of matrix ligand shell for different incubation intervals (A) 3 h, (B) 21 h, (C) 48 h incubation in DTT.

5.2 Design of a new ligand shell for nanoparticles

The same experiment was then repeated with disulphide alkane thiol ethylene glycol ligands (Fig. 5.3A). Disulphides have a high affinity for gold, like thiols, but they will not react with maleimide. Thus, by using a shell assembled from disulphide ligands, some of these could incorporate a terminal maleimide function (Fig. 5.3B), which could eventually be converted to a thiol using, for example, DTT.

Initial experiments used the ligands with a disulphide bond at 2 mM, exactly as for the mix-matrix ligands [72]. However, it was observed that the solution went cloudy, which was surmised to be the result of the hydrphobicity of the ligands. Since each ligand had two ethylene glycol terminated alkyl chains, there were, on a molar basis, twice as many of these units as used in the mix matrix. Therefore, because nanoparticle stability depends on ligand packing, it was decided that reducing the concentration of the disulphide ligands to 1 mM would not affect the stability of the ligand shell. When 1 mM disulphide ligand was added, the nanoparticle solution remained clear and pink. These nanoparticles could be separated on Sephadex G25 from excess ligands, citrate and residual Au^{+} ions remaining from synthesis just as effectively as the mix matrix nanoparticles (Section 2.6.5). This indicated that they were likely to be highly stable. The stability of the nanoparticles was then assessed by the DTT ligand exchange test.

To allow different experiments to be compared, the stability parameter was normalised to that of gold nanoparticles in the absence of DTT (Fig. 5.4). The results show that for short times (1 h to 4 h) the nanoparticles were stable at all concentrations of DTT. However, at longer times there was clear evidence for

nanoparticle aggregation at higher concentrations of DTT. After 24 h incubation in 20 mM DTT the nanoparticles were clearly aggregated, since the stability parameter was above 2. Interestingly, at low concentrations of DTT (1 mM and 3 mM) there was a slight increase in the stability parameter and then this declined to a value of 1 at 5 mM DTT. This effect was reproducible, but it probably does not indicate ligand exchange by DTT. Instead, because the nanoparticles have maleimide groups, the lower concentrations of DTT may simply cause small oligomers of nanoparticles to form. In this case the coupling of the plasmons will cause a slight redshift of the plasmon band, sufficient to account for the transient increase in stability parameter. Transmission electron microscopy would have to be used to determine whether this was the correct explanation.

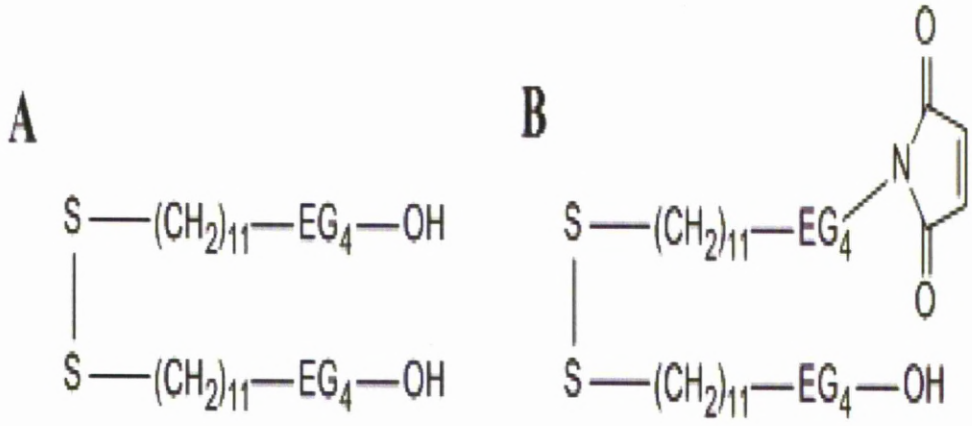

Figure 5.3: The disulphide ligands.

(A) PEG-dihydroxy ligand that linked to the Au nanoparticles via a disulphide bind; (B) PEG-Maleimide ligand, which can be used as a linkage between Au nanoparticles and other molecules via the maleimide function group.

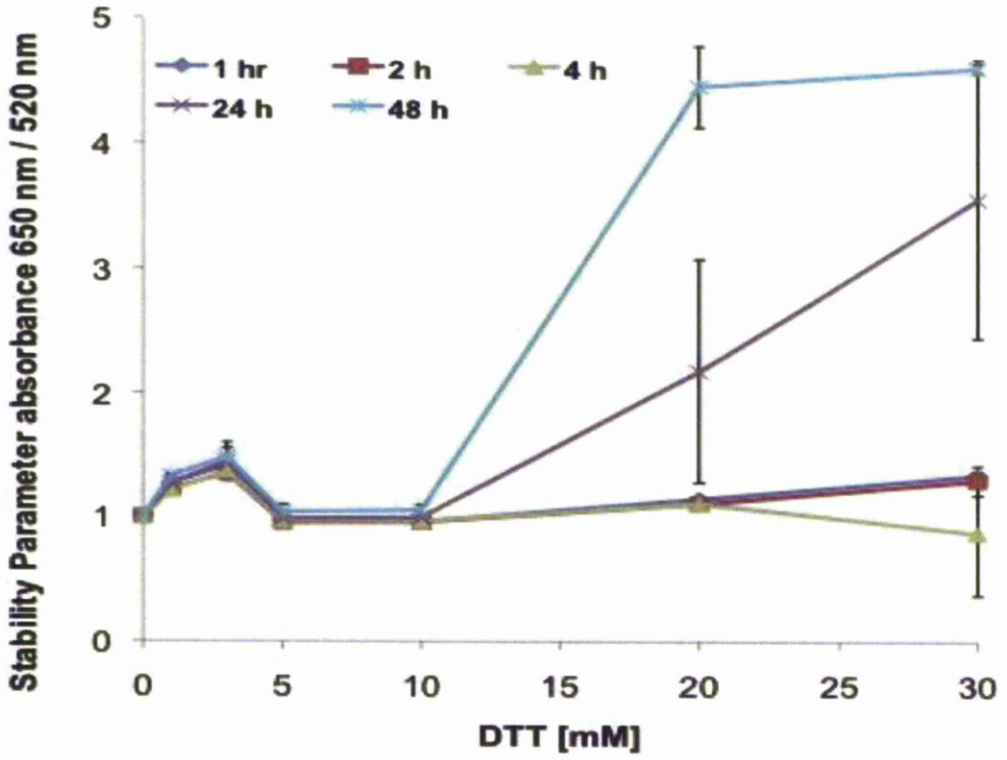

Figure 5.4: Stability of gold nanoparticles with a disulphide ligand shell in the presence of DTT.

The same protocol for the assembly of the mix-matrix ligand shell was followed, except that disulphide ligands were used. A fraction of the ligands (0.5 %, mole/mole) contained a terminal maleimide goup. DTT was added to the disulphide ligand stabilised gold nanoparticles in the presence of 0.5 M NaCl and the UV-vis spectra between from 400-700 nm were recorded at various times. The stability parameter was calculated as the ratio of absorbance 650 nm/520 nm and then normalised to the stability parameter of the nanoparticles in the absence of DTT. A stability parameter of 1 equates to stable nanoparticles, but value above 2 are indicative of nanoparticle aggregation. Values are the mean±standard deviation of triplicate samples.

5.3 Synthesis of a heparin-derived oligosaccharide-nanoparticle conjugate

The disulphide capped nanoparticles were nearly as resistant to DTT-induced ligand exchange as the mixed matrix nanoparticles (Figs 5.1, 5.2 and 5.4). In particular, they could be incubated in the presence of 5 mM DTT for several hours without compromising their stability. Therefore, the maleimide functions on these nanoparticles were converted to a thiol by incubation with 1 mM DTT, after which excess DTT was removed by gel filtration on Sephadex G25. The resulting nanoparticles were then incubated with the maleimide-DP6 (Chapter 3) for 1 h. To determine whether the oligosaccharide had coupled to the nanoparticles, these were then subject to anion-exchange chromatogrpahy on a microcolumn of DEAE-Sepharose. Nanoparticles with a disulphide-PEG ligand shell (disulphide PEG n=0) did not bind to the DEAE column, as expected, since there are no charged groups present in the ligand shell (Fig. 5.3). Similarly, nanoparticles with the disulphide-PEG ligand shell, where maleimide groups had been converted to thiols through reaction with DTT (disulphide PEG + SH) also failed to bind to the column (Fig. 5.5). In contrast, nanoparticles with a thiol group were reacted with the maleimide-DP6, the nanoparticles bound to the DEAE Sepharose (disulphide PEG + DP6), supported by the strong red colour of the column. These nanoparticles could be eluted with 1 M NaCl.

The present data show clearly that the disulphide PEG ligands are a reasonable alternative to the mixed matrix, since they impart good stability to gold nanoparticles. Moreover, because these nanoparticles are so stable, it is possible to react terminal maleimide goups with DTT and so install a thiol on the outside of the

nanoparticle. This thiol is able to react with the maleimide-DP6. Thus, the work presented in this chapter provides a clear means of coupling oligosaccharides to gold nanoparticles. Since there are powerful techniques for the detection of single gold nanoparticles using photothermal microscopy and electron microscopy, this advance opens up the possibility of doing single molecule experiments with oligosaccharides.

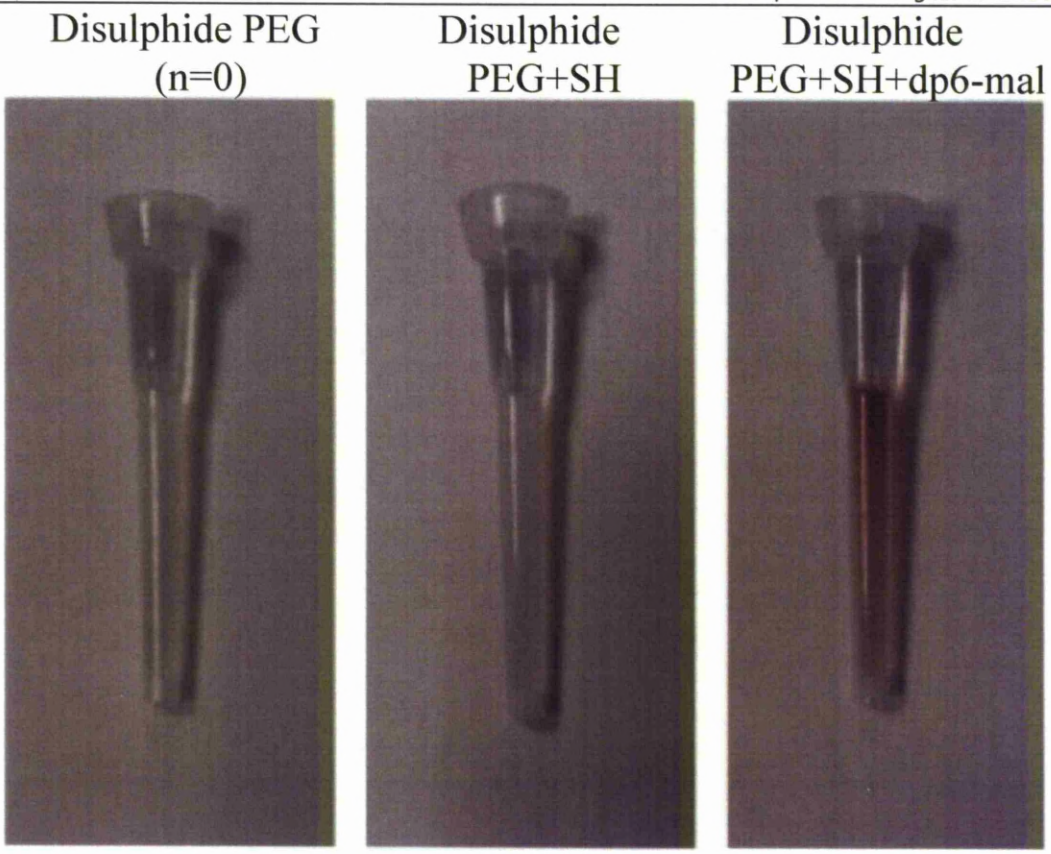

Figure 5.5: Chromatography of disulphide ligand capped nanoparticles on DEAE Sepharose.

Nanoparticles capped with disulphide ligands were loaded onto a mini column of DEAE Sepharose in a white pipette tip. After loading and washing in PBS the columns were photographed. Disulphide PEG (n=0), nanoparticles with a disulphide PEG ligand shell; Disulphide PEG + SH, nanoparticles with a disulphide PEG ligand shell where maleimide group were converted to thiols by reaction with DTT; Disulphide PEG + dp6 same nanoparticles afer reaction with the maleimide-DP6. Red colour indicates the presence of nanoparticles.

5.4 Discussion

To couple maleimide-functionalised oligosaccharides (Chapter 3) to nanoparticles required the design and testing of a new ligand shell. As summarised in Section 5.1, because thiols have such a high affinity for gold, it was not possible to use ligands with a thiol at each extremity, since such ligands would lie down on the gold. Disulphides have essentially the same affinity for gold as thiols, but do not react with maleimide. Thus, the interaction of thiols with gold proceeds through a thiolate anion (S^-), due to the dissociation of the S-H bond. Similarly, interaction of disulphides with gold results in the S-S bond breaking and formation of two thiolate anions [89-92]. It is important to note that this occurs in the course of the interaction of the sulfur with the gold atoms on the surface, so there are never any free thiolate anions able to react with an entity in solution. For these reasons, is was clear that the use of disulphide ligands would provide a protecting group on the sulfurs and prevent their reaction with the maleimide on the terminal ethylene glycol unit of the ligand. What was less clear was whether disulphide ligands would provide good stabilisation of the nanoparticles. This is because these ligands are bulkier than those of the mix matrix and so may not pack as effectively in the self-assembled monolayer.

Nanoparticles with a disulphide-PEG ligand shell were found to be resistant to non-specific binding to Sephadex G25 and DEAE Sepharose, similar to the mix matrix stabilised nanoparticles. This was indicative of a reasonably defect free ligand shell [72]. The ligand exchange experiments with DTT provided further evidence that the disulphide-PEG ligand shell imparted excellent stability to the nanoparticles. Moreover, because these nanoparticles were so stable in the presence of DTT, it was possible to react terminal maleimide goups with DTT and so install a thiol on the

outside of the nanoparticle. The lack of defects in the ligand shell is further evidenced by the observation that such thiol groups remained exposed to solvent and reacted with a maleimide-DP6, rather than burrowing through the ligand shell to bind with the underlying gold surface in what might be considered an intramolecular reaction.

In conclusion, the work presented in this chapter provides a new ligand shell for gold nanoparticles which enables direct coupling to thiols and so in a two step reaction to oligosaccharides with a maleimide at the reducing terminus. Since there are powerful techniques for the detection of single gold nanoparticles using photothermal microscopy and electron microscopy, this advance opens up the possibility of doing single molecule experiments with oligosaccharides.

CHAPTER 6

General Discussion

6.0 General Discussion

In Chapter 4, it was noted that biosensor surfaces that had been reacted previously with sugars *via* their reducing ends directly onto the surface, tended to lie down, which is presumably a consequence of non-specific interactions between the body of the sugar and the surface. To ensure that the sugar termini are attaching appropriately, it would be desirable to have a single, common reacting species, which could be applied to any sugar (GAG) structures, without suffering differential reactivity. Unfortunately, the reducing ends of HS oligosaccharides, if freed from a polysaccharide or proteoglycan, do not possess this quality. Significant differences in reactivity have been noted. For example, reducing end units consisting of N-sulfated glucosamine may not only react to different extents but, *via* distinct mechanisms from, say, N-acetyl glucosamine; the latter having the capability of forming an oxasoline ring [51,93]. To meet these two challenges the possibility of developing standardised pre-treatments to circumvent differential reactivity on the one hand and avoid the sugars lying down on the surface, on the other, alternative approaches are required.

To this end a variety of approaches to reacting the reducing end of oligosaccharides in the test tube, rather than directly onto a surface were explored. The work with peptides (Section 3.3) showed that the poor reactivity of the reducing end precludes useful reaction with species that cannot be dissolved at high concentration. Thus, a strategy to produce a reactive reducing end must use a species that can be dissolved at sufficiently high concentration to drive the reaction; MBPH is an example of one such species, which also provides a chromophore, albeit weak. The derivatisation of thiol-functionalised Analight chips with the maleimide-oligosaccharide had two aims. First, to provide evidence for the reactivity of the maleimide-oligosaccharide,

which was achieved (Section 4.3). Second, to provide an alternative to the direct reaction of sugars to biosensors surfaces [38] for the characterisation of protein-HS interactions. The level of maleimide-oligosaccharide immobilised was far lower than expected and the blocking of non-specific binding with CHO-PEG not as effective as published [38]. Despite this, the power of DPI was amply demonstrated by the analyses it allowed. In particular, the measurement of mass and thickness of bound species showed that although the signal from non-specific binding in the control channel was similar to that in the maleimide-oligosaccharide channel, the origins of the signals were different. In the control channel it was due to non-specific binding to the underlying surface, whereas in the maleimide-oligosaccharide surface, much of the signal was due to specific interactions of the FGFs with the immobilised oligosaccharide (Section 4.3). The importance of this analysis is that it demonstrated not just that the maleimide-oligosaccharide was indeed thiol-reactive, but that it retained its expected protein-binding activity and so could be used to produce other tools, such as oligosaccharide functionalised gold nanoparticles. However, due to the low level of immobilisation of maleimide-oligosaccharide, it was felt that the thickness measurements did not preclude some contribution in this channel from non-specific binding of the FGF to the underlying surface. For this reason, the binding parameters and the stoichiometry of the FGF:oligosaccharide interaction were not analysed.

The nanoparticle work described in this thesis provides new tools with which to explore the function of HS. However, there are several issues that need to be addressed before sugar-nanoparticles can be used to dissect at the single molecule level the assembly of protein-HS complexes *in vitro* and in living cells. The first issues relates to the stability of the disulphide-PEG capped nanoparticles. These

nanoparticles do not bind non-specifically to Sephadex G25 or to DEAE Sepharose. In previous work [72], a more extensive series of low pressure chromatography matrices were used to screen for non-specific binding to optimise ligand shell assembly conditions. The rationale was that these matrices present functional groups commonly found on biomolecules. In addition, while the disulphide-PEG capped nanoparticles are resistant to ligand exchange with DTT, they are perhaps not as resistant as certain formulations of the mixed-matrices [71]. Therefore, the stability of the disulphide capped nanoparticles needs to be explored further.

The first step would be to vary synthesis conditions and use the DTT ligand-exchange assay as a screen for ligand shell stability. The protocol used in the present work simply took that used for mixed-matrices, but there is no reason why these should be optimal for the disulphide-PEG ligands. Thus, these experiments would focus on the concentration of ligand, the length of time allowed for ligand shell assembly and the timing of the addition of electrolytes, which helps drive the assembly of the ligand shell, but may also reduce the solubility of the disulphide-PEG ligands, which, because they have a disulphide and two alkyl chains, are less soluble in water than the corresponding thiol ligands. With thiols, it appears that the mixture of ligands (thiol-alkyl-PEG and peptidol) imparts better stability than thiol-alkyl-PEG alone [71]. Thus, another route to explore is whether a mixture of disulphide-PEG and disulphide peptidols would produce a more robust ligand shell. The disulphide ligand capped nanoparticles showing the highest resistance to DDT ligand exchange would be subject to non-specific binding tests on Sephadex G25, DEAE- and CM-Sepharose. Non-specific binding to living cells would be measured for the best performing nanoparticles with a photothermal microscope and by

electron microscopy [33]. In this way, the most stable disulphide capped nanoparticles would be identified.

Alongside this work, transferring the disulphide ligand shell to quantum dots would be of interest. Quantum dots are excellent fluorescent labels and so can be used with all standard microscopes. A thesis project in the laboratory (Katie Wilson, in preparation) has achieved this for thiol ligands. As for gold nanoparticles, a disulphide ligand shell would allow a maleimide function to be introduced onto the quantum dots, which would give access to more possibilities for coupling to biomoleucles, including sugars. This would allow far more applications of oligosaccharide-nanoparticles, because the measurement of fluorescence is widely available, e.g., fluorescence activated cell sorting, and fluorescence microscopy. These are discussed at the end of this chapter.

The slight decrease in stability observed with the disulphide-PEG capped nanoparticles functionalised with maleimide at low concentrations of DTT needs to be followed up. In the first instance, TEM may reveal whether there are significant dimers/oligomers of nanoparticles formed under these conditions. Although the present methods provides for control of the stoichiometry of functionalisation of nanoparticles [74], this was not implemented, because the initial aim was to demonstrate the functionalisation of nanoparticles with an oligosaccharide. It is possible that there will be a slight loss of stability related to cross-linking nanoparticles with DTT *via* their maleimide groups; if there is more than one maleimide *per* nanoparticle, cross-linking may be favoured at specific DTT concentrations. Therefore, the implementation of stoichiometric functionalisation of the nanoparticles, necessary to making single molecule measurements, may also

resolve the issue of the loss of stability of the nanoparticles when they are incubated with low concentrations of DTT.

It has been demonstrated that if 10% of nanoparticles from a synthesis carry a ligand with a specific function, then these nanoparticles can only possess one such function each [74]. Previous work has used functions that lend themselves to reversible affinity chromatography (6 x his tags and nickel nitrilotriacetic acid) [33,72,74]. In these examples, a ligand carrying the function is added at different mole percentages of total ligand and then by affinity chromatography, the conditions under which 10% of the nanoparticles are functionalised (so bind to the affinity column) are identified. These nanoparticles are recovered from the affinity column and used. While the titration of maleimide functionalised disulphide-PEG ligand in a disulphide-PEG ligand shell is possible, to establish the percentage of functionalised nanoparticles will require the reaction of the maleimide. Two approaches could be taken in this respect. In the first, a small sample of the functionalised nanoparticles could be reacted with a hexahistidine peptide terminated with a cysteine residue. Chromatography on a nickel-nitrilotriacetic acid column would then be used to identify the nanoparticle preparation containing 10% functionalised nanoparticles, as described [74]. The remainder of these nanoparticles would then be reacted with DTT and maleimide-oligosaccharide to provide mono-functionalised nanoparticles. Alternatively, the nanoparticles could be reacted with DTT and then with maleimide-oligosaccharide. Chromatography on DEAE-Sepharose would determine which nanoparticle preparation contained 10% nanoparticles functionalised with oligosaccharide. The disadvantage of the latter approach is that would consume more oligosaccharide.

An important application of the maleimide functionalised nanoparticles would be to react with mercury derivatised oligosaccharides, which is described below. Following the lyase treatment of HS by heparitinases, the non-reducing termini of freshly released oligosaccharides contain a unique 4,5-unsaturated uronate derivative. Importantly, residues, (formerly either D-Glc A or L-Ido A), are both transformed into the same unsaturated derivative. Consequently, the only difference that can exist in these non-reducing termini is whether they bear a 2-O-sulfate or not. A drawback of this approach is that it is not possible to establish the former identity of the unit, but a significant advantage is that it opens-up the possibility of creating entirely homogeneous non-reducing termini for subsequent reactions. Any remaining 2-O-sulfate groups can be removed conveniently by the endosulfatase enzyme, 2-O-sulfatase, which has found use in HS sequencing strategies [94] [7].

Once the non-reducing ends have been rendered identical in this manner, they will then be available to react with mercury (Hg^{2+} ions) through addition across the 4,5, unsaturated bond, employing a process [50] that is a modification of that used conventionally to remove the unsaturated terminal sugar unit [95]. This reacts the double bond with the acidic mercury (II) chloride to ensure formation of the stable mercury adduct and avoids peeling, which proceeds under more basic conditions.

The mercury-derivatised sugar would then be available to react with thiol groups, for which there is a very high affinity [96], and which is the principal origin of the high toxicity of mercury. This raises the interesting possibility of exploiting libraries of oligosaccharides, whether from natural HS libraries, heparin or chemically

derivatised heparins (which are all susceptible to degradation with heparitinase enzymes) [52] modified *via* the non-reducing end with mercury derivatisation, to generate a series of tools with which to study structure-function relationships but, equally, it offers the possibility of bespoke derivatised surfaces, nanoparticles, and glycoconjugates. In the former cases, the thiol derivatised surfaces and nanoparticles, which are described in this thesis, could form a starting point, with a series of sized oligosaccharides derived from systematically modified heparin. These would then allow a range of interactions, for example, the network of FGF signalling proteins, to be studied and analysed. In the latter case, a new line of investigation, in which (for example) proteins/peptides with known exposed thiol groups (cysteine side chain) or, in which one had been introduced, could be derivatised to form novel proteoglycan analogues. These may serve as convenient vehicles by which to introduce the protein or GAG moiety into experimental systems, or serve as well-defined tools with which to investigate ligand-receptor specificity and stoichiometry. They offer the possibility of oligosaccharides possessing identical end-groups and would provide a means to produce extensive libraries of nanoparticle-oligosaccharide conjugates.

The combination of libraries of oligosaccharides conjugated to gold nanoparticles and quantum dots would open up further exciting avenues of research. Stoichiometric (1:1) oligosaccharide:gold nanoparticle conjugates can be detected quantitatively by electron microscopy and by photothermal microscopy. This would enable experiments that aimed to dissect the stoichiometry of ligand-receptor-HS co-receptor complexes, such as those formed with FGFs. Cell lacking sulfated HS, e.g., by treatment with heparinases and/or chlorate [33,97] will form a functional signalling complex in the presence of an exogenous heparin-derived oligosaccharide. Thus, using nanoparticle labelled oligosaccharide and FGF ligand would enable the

assembly of FGF signalling complexes to be quantified in time and in terms of the stoichiometry of the complex in living cells. To enable muliplex, different sized nanoparticles could be used, e.g., 5 nm and 12 nm diameter. This would allow discrimination in the electron microscope. In the photothermal microscope this strategy would not work and a combination of gold and silver nanoparticles, which absorb at different wavelengths and so can be discriminated, would be necessary. Oligosaccharide-quantum dots conjugates would complement such experiments. Thus, photothermal tracking of nanoparticles provides a very high resolution, e.g,, pointing accuracy of 13 nm [33], but low coverage. That is on any individual cell, only a few dozens of complexes events would be tracked in a day. In contrast, fluorescence techniques, including those with single quantum dot resolution acquire information over then entire cell, though at lower resolution. Together, the two approaches would resolve the stoichiometry of the signalling complex and its dynamics. Of particular interest may be the long-running controversies over historical data that indicate that both the FGF ligand [35,98] may be translocated to the nucleus following receptor-mediated endocytosis. Live cell imaging of quantum dot conjugates would not be prone to artefacts associated with cell breakage and fixation, which were used to collect the original data.

Finally, the sensitivity of detection of nanoparticle is exceptional, for example, 100 pM is readily detected by eye. The interaction with cellular HS of a number of bacterial and viral pathogens is integral to their infectivity. Therefore, an oligosaccharide of suitable structure, able to identify one or more pathogens conjugated to a nanoparticle might provide a cheap, field deployable assay for some human and livestock pathogens. Since it is detectable by the naked eye and the probe

is stable (the oligosaccharide-nanoparticle conjugate does not require refrigeration) such materials may have applications in preventative healthcare in the least developed countries.

References

1. Azmi, N. S., and Fernig, D. G. (eds) (2013). Heparan sulfate surfaces to probe the functions of the master regulator of the extracellular space. Chapter 16, Pan Stanford Publishing Pte, Singapore.
2. King, N., Westbrook, M. J., Young, S. L., Kuo, A., Abedin, M., Chapman, J., Fairclough, S., Hellsten, U., Isogai, Y., Letunic, I., Marr, M., Pincus, D., Putnam, N., Rokas, A., Wright, K. J., Zuzow, R., Dirks, W., Good, M., Goodstein, D., Lemons, D., Li, W., Lyons, J. B., Morris, A., Nichols, S., Richter, D. J., Salamov, A., Sequencing, J. G., Bork, P., Lim, W. A., Manning, G., Miller, W. T., McGinnis, W., Shapiro, H., Tjian, R., Grigoriev, I. V., and Rokhsar, D. (2008). The genome of the choanoflagellate Monosiga brevicollis and the origin of metazoans, *Nature*, **451**, pp. 783-788.
3. Ori, A., Wilkinson, M. C., and Fernig, D. G. (2011). A systems biology approach for the investigation of the heparin/heparan sulfate interactome, *J Biol Chem*, **286**, pp. 19892-19904.
4. Ori, A., Wilkinson, M. C., and Fernig, D. G. (2010). A systems biology approach for the investigation of the heparin/heparan sulfate interactome. , *J. Biol. Chem. (submitted)*, pp.
5. Ori, A., Wilkinson, M. C., and Fernig, D. G. (2008). The heparanome and regulation of cell function: structures, functions and challenges, *Front Biosci*, **13**, pp. 4309-4338.
6. Capila, I., and Linhardt, R. J. (2002). Heparin-protein interactions, *Angew Chem Int Ed Engl*, **41**, pp. 391-412.
7. Drummond, K. J., Yates, E. A., and Turnbull, J. E. (2001). Electrophoretic sequencing of heparin/heparan sulfate oligosaccharides using a highly sensitive fluorescent end label, *Proteomics*, **1**, pp. 304-310.
8. Lyon, M., Deakin, J. A., and Gallagher, J. T. (1994). Liver heparan sulfate structure. A novel molecular design, *J Biol Chem*, **269**, pp. 11208-11215.
9. Ferro, D. R., Provasoli, A., Ragazzi, M., Casu, B., Torri, G., Bossennec, V., Perly, B., Sinay, P., Petitou, M., and Choay, J. (1990). Conformer populations of L-iduronic acid residues in glycosaminoglycan sequences, *Carbohydr Res*, **195**, pp. 157-167.
10. Turnbull, J. E., and Gallagher, J. T. (1991). Sequence analysis of heparan sulphate indicates defined location of N-sulphated glucosamine and iduronate 2-sulphate residues proximal to the protein-linkage region, *Biochem J*, **277 (Pt 2)**, pp. 297-303.
11. Murphy, K. J., Merry, C. L., Lyon, M., Thompson, J. E., Roberts, I. S., and Gallagher, J. T. (2004). A new model for the domain structure of heparan sulfate based on the novel specificity of K5 lyase, *J Biol Chem*, **279**, pp. 27239-27245.
12. Busse, M., Feta, A., Presto, J., Wilen, M., Gronning, M., Kjellen, L., and Kusche-Gullberg, M. (2007). Contribution of EXT1, EXT2, and EXTL3 to heparan sulfate chain elongation, *J Biol Chem*, **282**, pp. 32802-32810.
13. Esko, J. D., and Zhang, L. (1996). Influence of core protein sequence on glycosaminoglycan assembly, *Curr Opin Struct Biol*, **6**, pp. 663-670.
14. Kusche-Gullberg, M., and Kjellen, L. (2003). Sulfotransferases in glycosaminoglycan biosynthesis, *Curr Opin Struct Biol*, **13**, pp. 605-611.
15. Gorsi, B., and Stringer, S. E. (2007). Tinkering with heparan sulfate sulfation to steer development, *Trends Cell Biol*, **17**, pp. 173-177.
16. Lamanna, W. C., Kalus, I., Padva, M., Baldwin, R. J., Merry, C. L., and Dierks, T. (2007). The heparanome--the enigma of encoding and decoding heparan sulfate sulfation, *J Biotechnol*, **129**, pp. 290-307.
17. Turnbull, J. E., and Gallagher, J. T. (1990). Molecular organization of heparan sulphate from human skin fibroblasts, *Biochem J*, **265**, pp. 715-724.
18. Turnbull, J., Powell, A., and Guimond, S. (2001). Heparan sulfate: decoding a dynamic multifunctional cell regulator, *Trends Cell Biol*, **11**, pp. 75-82.
19. Vanpouille, C., Deligny, A., Delehedde, M., Denys, A., Melchior, A., Lienard, X., Lyon, M., Mazurier, J., Fernig, D. G., and Allain, F. (2007). The heparin/heparan sulfate sequence that interacts with cyclophilin B contains a 3-O-sulfated N-unsubstituted glucosamine residue, *J Biol Chem*, **282**, pp. 24416-24429.
20. Rudd, T. R., Hughes, A., Holman, J., de Oliveira Ferreira, E., Cavalcante Pilotto Domingues, R. M., and Yates, E. A. (2012). Heparan sulphate, its derivatives and analogues share

structural characteristics that can be exploited, particularly in inhibiting microbial attachment, *Brazilian Journal of Medical and Biological Research*, **45**, pp. 386-391.

21. Yamada, S., Yamane, Y., Tsuda, H., Yoshida, K., and Sugahara, K. (1998). A major common trisulfated hexasaccharide core sequence, hexuronic acid(2-sulfate)-glucosamine(N-sulfate)-iduronic acid-N-acetylglucosamine-glucuronic acid-glucosamine(N-sulfate), isolated from the low sulfated irregular region of porcine intestinal heparin, *Journal of Biological Chemistry*, **273**, pp. 1863-1871.
22. Mulloy, B., and Forster, M. J. (2000). Conformation and dynamics of heparin and heparan sulfate, *Glycobiology*, **10**, pp. 1147-1156.
23. Ernst, E. (1998). Shark cartilage for cancer?, *Lancet*, **351**, pp. 298.
24. Yayon, A., Klagsbrun, M., Esko, J. D., Leder, P., and Ornitz, D. M. (1991). Cell surface, heparin-like molecules are required for binding of basic fibroblast growth factor to its high affinity receptor, *Cell*, **64**, pp. 841-848.
25. Turnbull, J. E., Fernig, D. G., Ke, Y., Wilkinson, M. C., and Gallagher, J. T. (1992). Identification of the basic fibroblast growth factor binding sequence in fibroblast heparan sulfate, *J Biol Chem*, **267**, pp. 10337-10341.
26. Delehedde, M., Lyon, M., Gallagher, J. T., Rudland, P. S., and Fernig, D. G. (2002). Fibroblast growth factor-2 binds to small heparin-derived oligosaccharides and stimulates a sustained phosphorylation of p42/44 mitogen-activated protein kinase and proliferation of rat mammary fibroblasts, *Biochem. J.*, **366**, pp. 235-244.
27. Guimond, S., Maccarana, M., Olwin, B. B., Lindahl, U., and Rapraeger, A. C. (1993). Activating and inhibitory heparin sequences for FGF-2 (basic FGF). Distinct requirements for FGF-1, FGF-2, and FGF-4, *J Biol Chem*, **268**, pp. 23906-23914.
28. Delehedde, M., Lyon, M., Vidyasagar, R., McDonnell, T. J., and Fernig, D. G. (2002). HGF/SF binds to small heparin-derived oligosaccharides and stimulates the proliferation of human HaCaT keratinocytes., *J. Biol. Chem.*, **277**, pp. 12456-12462.
29. Robinson, C. J., Mulloy, B., Gallagher, J. T., and Stringer, S. E. (2006). VEGF165-binding sites within heparan sulfate encompass two highly sulfated domains and can be liberated by K5 lyase, *J Biol Chem*, **281**, pp. 1731-1740.
30. Uniewicz, K. A., and Fernig, D. G. (2008). Neuropilins: a versatile partner of extracellular molecules that regulate development and disease, *Front Biosci*, **13**, pp. 4339-4360.
31. Izvolsky, K. I., Shoykhet, D., Yang, Y., Yu, Q., Nugent, M. A., and Cardoso, W. V. (2003). Heparan sulfate-FGF10 interactions during lung morphogenesis, *Dev Biol*, **258**, pp. 185-200.
32. Yan, D., and Lin, X. (2009). Shaping morphogen gradients by proteoglycans, *Cold Spring Harb Perspect Biol*, **1**, pp. a002493.
33. Duchesne, L., Octeau, V., Bearon, R. N., Beckett, A., Prior, I. A., Lounis, B., and Fernig, D. G. (2012). Transport of fibroblast growth factor2 in the pericellular matrix is controlled by the spatial distribution of its binding sites in heparan sulfate, *PLOS Biology 10.*, pp. e100136.
34. Rudd, T. R., Uniewicz, K. A., Ori, A., Guimond, S. E., Skidmore, M. A., Gaudesi, D., Xu, R., Turnbull, J. E., Guerrini, M., Torri, G., Siligardi, G., Wilkinson, M. C., Fernig, D. G., and Yates, E. A. (2010). Comparable stabilisation, structural changes and activities can be induced in FGF by a variety of HS and non-GAG analogues: implications for sequence-activity relationships, *Org Biomol Chem*, **8**, pp. 5390-5397.
35. Fernig, D. G., and Gallagher, J. T. (1994). Fibroblast growth factors and their receptors: an information network controlling tissue growth, morphogenesis and repair, *Prog Growth Factor Res*, **5**, pp. 353-377.
36. Ornitz, D. M., and Itoh, N. (2001). Fibroblast growth factors, *Genome Biol*, **2**, pp. REVIEWS3005.
37. Schlessinger, J., Plotnikov, A. N., Ibrahimi, O. A., Eliseenkova, A. V., Yeh, B. K., Yayon, A., Linhardt, R. J., and Mohammadi, M. (2000). Crystal structure of a ternary FGF-FGFR-heparin complex reveals a dual role for heparin in FGFR binding and dimerization, *Mol Cell*, **6**, pp. 743-750.
38. Popplewell, J. F., Swann, M. J., Ahmed, Y., Turnbull, J. E., and Fernig, D. G. (2009). Fabrication of carbohydrate surfaces by using nonderivatised oligosaccharides, and their application to measuring the assembly of sugar-protein complexes, *Chembiochem*, **10**, pp. 1218-1226.

39. Powell, A. K., Yates, E. A., Fernig, D. G., and Turnbull, J. E. (2004). Interactions of heparin/heparan sulfate with proteins: appraisal of structural factors and experimental approaches, *Glycobiology*, **14**, pp. 17R-30R.
40. Iduron. http://www.iduron.co.uk/.
41. Rahmoune, H., Gallagher, J. T., Rudland, P. S., and Fernig, D. G. (1998). Interaction of heparan sulphate from mammary cells with extracellular regulatory proteins. Acidic and fibroblast growth factor: regulation of the activity of bFGF by high and low affinity binding sites in heparan sulphate, *J. Biol. Chem.*, **273**, pp. 7303-7310.
42. Luo, Y., Ye, S., Kan, M., and McKeehan, W. L. (2006). Structural specificity in a FGF7-affinity purified heparin octasaccharide required for formation of a complex with FGF7 and FGFR2IIIb, *J Cell Biochem*, **97**, pp. 1241-1258.
43 Luo, Y., Ye, S., Kan, M., and McKeehan, W. L. (2006). Control of fibroblast growth factor (FGF) 7- and FGF1-induced mitogenesis and downstream signaling by distinct heparin octasaccharide motifs, *J Biol Chem*, **281**, pp. 21052-21061.
44. Travers, A., and Drew, H. (1997). DNA recognition and nucleosome organization, *Biopolymers*, **44**, pp. 423-433.
45. Rudland, P. S., Leinster, S. J., Winstanley, J., Green, B., Atkinson, M., and Zakhour, H. D. (1993). Immunocytochemical identification of cell types in benign and malignant breast diseases: variations in cell markers accompany the malignant state, *J Histochem Cytochem*, **41**, pp. 543-553.
46. Thompson, S. M., Fernig, D. G., Jesudason, E. C., Losty, P. D., van de Westerlo, E. M., van Kuppevelt, T. H., and Turnbull, J. E. (2009). Heparan sulfate phage display antibodies identify distinct epitopes with complex binding characteristics: insights into protein binding specificities, *J Biol Chem*, **284**, pp. 35621-35631.
47. Chung, I., Akita, R., Vandlen, R., Toomre, D., Schlessinger, J., and Mellman, I. (2010). Spatial control of EGF receptor activation by reversible dimerization on living cells, *Nature*, **464**, pp. 783-787.
48. Berciaud, S., Cognet, L., Blab, G. A., and Lounis, B. (2004). Photothermal heterodyne imaging of individual nonfluorescent nanoclusters and nanocrystals, *Phys Rev Lett*, **93**, pp. 257402.
49. Skidmore, M. A., Patey, S. J., Thanh, N. T., Fernig, D. G., Turnbull, J. E., and Yates, E. A. (2004). Attachment of glycosaminoglycan oligosaccharides to thiol-derivatised gold surfaces, *Chem Commun (Camb)*, pp. 2700-2701.
50. Yates, E. A., Jones, M. O., Clarke, C. E., Powell, A. K., Johnson, S. R., Porch, A., Edwards, P. P., and Turnbull, J. E. (2003). Microwave enhanced reaction of carbohydrates with amino-derivatised labels and glass surfaces, *Journal of Materials Chemistry*, **13**, pp. 2061-2063.
51. Powell, A. K., Ahmed, Y. A., Yates, E. A., and Turnbull, J. E. (2010). Generating heparan sulfate saccharide libraries for glycomics applications, *Nat Protoc*, **5**, pp. 821-833.
52. Wang, D., Liu, S., Trummer, B. J., Deng, C., and Wang, A. (2002). Carbohydrate microarrays for the recognition of cross-reactive molecular markers of microbes and host cells, *Nat Biotechnol*, **20**, pp. 275-281.
53. Willats, W. G., Rasmussen, S. E., Kristensen, T., Mikkelsen, J. D., and Knox, J. P. (2002). Sugar-coated microarrays: a novel slide surface for the high-throughput analysis of glycans, *Proteomics*, **2**, pp. 1666-1671.
54. Rudd, T. R., Skidmore, M. A., Guimond, S. E., Guerrini, M., Cosentino, C., Edge, R., Brown, A., Clarke, D. T., Torri, G., Turnbull, J. E., Nichols, R. J., Fernig, D. G., and Yates, E. A. (2008). Site-specific interactions of copper(II) ions with heparin revealed with complementary (SRCD, NMR, FTIR and EPR) spectroscopic techniques, *Carbohydr Res*, **343**, pp. 2184-2193.
55. Rudd, T. R., Guimond, S. E., Skidmore, M. A., Duchesne, L., Guerrini, M., Torri, G., Cosentino, C., Brown, A., Clarke, D. T., Turnbull, J. E., Fernig, D. G., and Yates, E. A. (2007). Influence of substitution pattern and cation binding on conformation and activity in heparin derivatives, *Glycobiology*, **17**, pp. 983-993.
56. Ling, L., Dombrowski, C., Foong, K. M., Haupt, L. M., Stein, G. S., Nurcombe, V., van Wijnen, A. J., and Cool, S. M. (2010). Synergism between Wnt3a and heparin enhances osteogenesis via a phosphoinositide 3-kinase/Akt/RUNX2 pathway, *J Biol Chem*, **285**, pp. 26233-26244.
57. Osmond, R. I., Kett, W. C., Skett, S. E., and Coombe, D. R. (2002). Protein-heparin interactions measured by BIAcore 2000 are affected by the method of heparin immobilization, *Anal Biochem*, **310**, pp. 199-207.

58. Duchesne, L., Tissot, B., Rudd, T. R., Dell, A., and Fernig, D. G. (2006). N-glycosylation of fibroblast growth factor receptor 1 regulates ligand and heparan sulfate co-receptor binding, *J Biol Chem.*, **281**, pp. 27178-27189.
59. Rahmoune, H., Gallagher, J. T., Rudland, P. S., and Fernig, D. G. (1998). Hepatocyte growth factor/scatter factor has distinct classes of binding site in heparan sulfate from mammary cells, *Biochemistry*, **37**, pp. 6003-6008.
60. Kinsella, L., Chen, H. L., Smith, J. A., Rudland, P. S., and Fernig, D. G. (1998). Interactions of putative heparin-binding domains of basic fibroblast growth factor and its receptor, FGFR-1, with heparin using synthetic peptides, *Glycoconj J*, **15**, pp. 419-422.
61. Lyon, M., Deakin, J. A., Rahmoune, H., Fernig, D. G., Nakamura, T., and Gallagher, J. T. (1998). Hepatocyte growth factor/scatter factor binds with high affinity to dermatan sulfate, *J Biol Chem*, **273**, pp. 271-278.
62. Moulard, M., Lortat-Jacob, H., Mondor, I., Roca, G., Wyatt, R., Sodroski, J., Zhao, L., Olson, W., Kwong, P. D., and Sattentau, Q. J. (2000). Selective interactions of polyanions with basic surfaces on human immunodeficiency virus type 1 gp120, *J Virol*, **74**, pp. 1948-1960.
63. Knox, S., Merry, C., Stringer, S., Melrose, J., and Whitelock, J. (2002). Not all perlecans are created equal: interactions with fibroblast growth factor (FGF) 2 and FGF receptors, *J Biol Chem*, **277**, pp. 14657-14665.
64. Kesimer, M., and Sheehan, J. K. (2008). Analyzing the functions of large glycoconjugates through the dissipative properties of their absorbed layers using the gel-forming mucin MUC5B as an example, *Glycobiology*, **18**, pp. 463-472.
65. Biehle, S. J., Carrozzella, J., Shukla, R., Popplewell, J., Swann, M., Freeman, N., and Clark, J. F. (2004). Apolipoprotein E isoprotein-specific interactions with tissue plasminogen activator, *Biochim Biophys Acta*, **1689**, pp. 244-251.
66. Cross, G. H., Reeves, A. A., Brand, S., Popplewell, J. F., Peel, L. L., Swann, M. J., and Freeman, N. J. (2003). A new quantitative optical biosensor for protein characterisation, *Biosens Bioelectron*, **19**, pp. 383-390.
67. Cross, G. H., Ren, Y. T., and Freeman, N. J. (1999). Young's fringes from vertically integrated slab waveguides: Applications to humidity sensing, *J Appl Phys*, **86**, pp. 6483-6488.
68. Levy, R. (2006). Peptide-capped gold nanoparticles: towards artificial proteins, *Chembiochem*, **7**, pp. 1141-1145.
69. Shaw, C., Fenig, D. G., and Levy, R. (2011). Gold nanoparticles as advanced building blocks for nanoscale self-assembled systems, *J. Mat Chem.* , **21**, pp. 12181 – 12187.
70. Chen, X., Qoutah, W. W., Free, P., Hobley, J., Fernig, D. G., and Paramelle, D. (2012). Features of thiolated ligands promoting resistance to ligand exchange in self-assembled monolayers on gold nanoparticles, *Aust. J. Chem*, **65**, pp. 266-274.
71. Duchesne, L., Gentili, D., Comes-Franchini, M., and Fernig, D. G. (2008). Robust ligand shells for biological applications of gold nanoparticles, *Langmuir*, **24**, pp. 13572-13580.
72. Levy, R., Thanh, N. T., Doty, R. C., Hussain, I., Nichols, R. J., Schiffrin, D. J., Brust, M., and Fernig, D. G. (2004). Rational and combinatorial design of peptide capping ligands for gold nanoparticles, *J Am Chem Soc*, **126**, pp. 10076-10084.
73. Levy, R., Wang, Z., Duchesne, L., Doty, R. C., Cooper, A. I., Brust, M., and Fernig, D. G. (2006). A generic approach to monofunctionalized protein-like gold nanoparticles based on immobilized metal ion affinity chromatography, *Chembiochem*, **7**, pp. 592-594.
74. Free, P., Paramelle, D., Bosman, M., Hobley, J., and Fernig, D. G. (2012). Synthesis of silver nanoparticles with monovalently functionalized self-assembled monolayers, *Aust. J. Chem*, **65**, pp. 275-282.
75. Octeau, V., Cognet, L., Duchesne, L., Lasne, D., Schaeffer, N., Fernig, D. G., and Lounis, B. (2009). Photothermal absorption correlation spectroscopy (PhACS), *ACS Nano*, **3**, pp. 345-350.
76. Huang, X., and El-Sayed, M. A. (2010). Gold nanoparticles: Optical properties and implementations in cancer diagnosis and photothermal therapy, *Journal of Advanced Research*, **1**, pp. 13-28.
77. Hirsch, L. R., Gobin, A. M., Lowery, A. R., Tam, F., Drezek, R. A., Halas, N. J., and West, J. L. (2006). Metal nanoshells, *Ann Biomed Eng*, **34**, pp. 15-22.
78. Zhi, Z. L., Powell, A. K., and Turnbull, J. E. (2006). Fabrication of carbohydrate microarrays on gold surfaces: direct attachment of nonderivatized oligosaccharides to hydrazide-modified self-assembled monolayers, *Anal Chem*, **78**, pp. 4786-4793.

79. Pellegrini, L., Burke, D. F., Von Delft, F., Mulloy, B., and Blundell, T. L. (2000). Crystal structure of ®broblast growth factor receptor ectodomain bound to ligand and heparin, *Nature*, **407**, pp. 1029-1034.
80. Guimond, S., and Turnbull, J. E. (1999). Fibroblast growth factor receptor signalling is dictated by specific heparan sulphate saccharides, *Current Biology*, **9**, pp. 1343-1346.
81. Chamow, S. M., Kogan, T. P., Peers, D. H., Hastings, R. C., Byrn, A., and Ashkenazi, A. (1992). Conjugation of Soluble CD4 without Loss of Biological Activity via a Novel Carbohydrate-directed Cross-linking Reagent**267**, pp. 15916-15922.
82. Swann, M. J., Peel, L. L., Carrington, S., and Freeman, N. J. (2004). Dual-polarization interferometry: an analytical technique to measure changes in protein structure in real time, to determine the stoichiometry of binding events, and to differentiate between specific and nonspecific interactions, *Anal Biochem*, **329**, pp. 190-198.
83. Thompson, L. D., Pantoliano, M. W., and Springer, B. A. (1994). Energetic characterization of the basic fibroblast growth factor-heparin interaction: identification of the heparin binding domain, *Biochemistry*, **33**, pp. 3831-3840.
84. Baird, A., Schubert, D., Ling, N., and Guillemin, R. (1988). Receptor- and heparin-binding domains of basic fibroblast growth factor, *Proc Natl Acad Sci U S A*, **85**, pp. 2324-2328.
85. Seno, M., Sasada, R., Kurokawa, T., and Igarashi, K. (1990). Carboxyl-terminal structure of basic fibroblast growth factor significantly contributes to its affinity for heparin, *Eur J Biochem*, **188**, pp. 239-245.
86. Ori, A., Free, P., Courty, J., Wilkinson, M. C., and Fernig, D. G. (2009). Identification of heparin-binding sites in proteins by selective labeling, *Mol Cell Proteomics*, **8**, pp. 2256-2265.
87. Xu, R., Ori, A., Rudd, T. R., Uniewicz, K. A., Ahmed, Y. A., Guimond, S. E., Skidmore, M. A., Siligardi, G., Yates, E. A., and Fernig, D. G. (2012). Diversification of the Structural Determinants of Fibroblast Growth Factor-Heparin Interactions: Implications for Binding Specificity *J Biol Chem*, **287**, pp. 40061-40073.
88. Di Felice, R., Selloni, A., and Molinari, E. (2003). DFT study of cysteine adsorption on Au(111), *J. Phys. Chem. B*, **107**, pp. 1151-1156.
89. Gronbeck, H., Curioni, A., and Andreoni, W. (2000). Thiols and disulfides on the Au(111) surface: The headgroup-gold interaction, *J. Am. Chem. Soc.*, **122**, pp. 3839-3842.
90. Hager, G., and Brolo, A. G. (2003). Adsorption/desorption behaviour of cysteine and cystine in neutral and basic media: electrochemical evidence for differing thiol and disulfide adsorption to a Au(111) single crystal electrode, *J. Electroanal. Chem.*, **550**, pp. 291-301.
91. LeParc, R., Smith, C. I., Cuquerella, M. C., Williams, R. L., Fernig, D. G., Edwards, C., Martin, D. S., and Weightman, P. (2006). Reflection anisotropy spectroscopy study of the adsorption of sulfur-containing amino acids at the Au(110)/electrolyte interface, *Langmuir*, **22**, pp. 3413-3420.
92. Rudd, T., Skidmore, M. A., and Yates, E. A. (2005). Surface-Based Studies of Heparin/Heparan Sulfate-Protein Interactions: Considerations for Surface Immobilisation of HS/Heparin Saccharides and Monitoring Their Interactions with Binding Proteins, *Chemistry and Biology of Heparin and Heparan Sulfate*, pp. 345-366.
93. Turnbull, J. E., Hopwood, J. J., and Gallagher, J. T. (1999). A strategy for rapid sequencing of heparan sulfate and heparin saccharides, *Proc Natl Acad Sci U S A*, **96**, pp. 2698-2703.
94. Ludwigs, U., Elgavish, A., Esko, J. D., Meezan, E., and Roden, L. (1987). Reaction of unsaturated uronic acid residues with mercuric salts. Cleavage of the hyaluronic acid disaccharide 2-acetamido-2-deoxy-3-O-(beta-D-gluco-4-enepyranosyluronic acid)-D-glucose, *Biochem J*, **245**, pp. 795-804.
95. Clarkson, T. W., and Magos, L. (2006). The toxicology of mercury and its chemical compounds, *Crit Rev Toxicol*, **36**, pp. 609-662.
96. Zhu, H., Duchesne, L., Rudland, P. S., and Fernig, D. G. (2010). The heparan sulfate co-receptor and the concentration of fibroblast growth factor-2 independently elicit different signalling patterns from the fibroblast growth factor receptor, *Cell Commun Signal*, **8**, pp. 14.
97. Fedarko, N. S., and Conrad, H. E. (1986). A unique heparan sulfate in the nuclei of hepatocytes: structural changes with the growth state of the cells, *J Cell Biol*, **102**, pp. 587-599.

APPENDIX

Chemicals/Material

The chemicals listed below were used in this study. The reagents used were of analytical grade.

Chemicals/Biochemicals	Brand
Heparin	Celsus Laboratories, Cincinnati, USA
CALNN	Sigma-Genosys Ltd(Haverhill, UK)
PEGylated alkanethiol, HS-EC11-EG4	ProChimia Surfaces, Sopot, Poland).
CVVVT-ol	PeptideSynthetics, Fereham, UK
(GGGTVVC-amide)	Anaspec Inc, San Jose, USA
CALNNGGC-OH	Bachem, Bubendorf, Switzerland.
Na_2HPO_4	Poole, UK
NaH_2PO4	Poole, UK
NaCl	Sigma Aldrich, Stenheim, Germany
Etanol 95%	Hamburgh Chemical GmBH
Hydrochloric acid	Analar, Lutterworth, England
Acetic acid	Analar, Lutterworth, England
Ethanol	Fisher Scientific, Loughborough, UK
Formamide	Sigma Aldrich, Stenheim, Germany
MPBH	Thermo Scientific, Rockford, U.S.A
HPLC grade water	Fisher Scientific, Leicestershire, UK
BMPH	Thermo Scientific, Rockford, U.S.A
PEG-CHO	RappPolymereGmbH,Tubingen,Germany)

FGF-2	Lab B, UOL, Liverpool, UK
Tween-20	Sigma Aldrich, Dorset, UK
Cysteamine	Fluka, Steinheim, Switzerland
EDC	Fluka, Steinheim, Switzerland
DEAE Sepharose	Invitrogen Paisley, UK

Equipments	**Supplier**
Balance	Sartorius, Surrey, UK
Electronic Balance, AND ER-120A	Sartorius, Surrey, UK
Bench Top microcentrifuge	Eppendorf, Cambridge, UK
HPLC 1100(High Perfomance Liquid Chromatography)	Agilent, Warrington, UK
Minisort SRP 15, PTFE membrane 0.45 μm	Sartorius, Surrey, UK
Sephadex G10 column	GE Healthcare, Buckinghamshire, UK
Hitrap™ QHP column	GE Healthcare, Buckinghamshire, UK
Analight® Bio200	Farfield Group, Crewe. UK
Sephadex G25 superfine column	Sigma Aldrich, Dorset, UK
Nanosep centrifugal ultrafiltration devices	PALL Corp., Portsmouth, UK